EFFECT OF STRUCTURAL STIFFNESS ON THE RESPONSE OF PORTAL FRAMES TO GROUNDWATER EXTRACTION-INDUCED GROUND MOVEMENTS

Fabianus Lheurreux Mcterror Gomachab

EFFECT OF STRUCTURAL STIFFNESS ON THE RESPONSE OF PORTAL FRAMES TO GROUNDWATER EXTRACTION-INDUCED GROUND MOVEMENTS

Fabianus Lheurreux Mcterror Gomachab

A dissertation in partial fulfilment of the requirements for the degree of

MASTER OF ENGINEERING (STRUCTURAL ENGINEERING)

in the

Department of Civil Engineering
Faculty of Engineering, Built Environment and Information Technology

University of Pretoria

2017

SUMMARY

EFFECT OF STRUCTURAL STIFFNESS ON THE RESPONSE OF PORTAL FRAMES TO GROUNDWATER EXTRACTION-INDUCED GROUND MOVEMENTS

Fabianus Lheurreux Mcterror Gomachab

Supervisor: Professor S.W. Jacobsz

Co-Supervisor: Professor E.P. Kearsley

Department: Civil Engineering

University: University of Pretoria

Degree: Master of Engineering (Structural Engineering)

Civil structures are founded on or within soil. Understanding the interaction of a structure with the soil it is founded on or within is vital for designing and constructing structures that will be safe and functional for the required design life. Structures are, furthermore, designed to meet acceptable limiting requirements to achieve the standards of safety and functionality. If, however, the interaction between a structure and founding soil is altered by an external stimulus such as ground movements it can have detrimental effects on the structure that can jeopardise the safety and functionality of the structure.

Extraction of groundwater from aquifers causes a reduction in the interstitial pore-water pressure of the aquifer. The reduction in pore-water pressure, in turn, results in an increase in the effective stresses acting on the soil skeleton inducing settlement. Pore-water pressure reduction induced by groundwater extraction, however, is not uniform throughout the aquifer which results in a non-uniform increase in effective stresses resulting in differential settlement of the soil. The magnitude of settlement is greatest closest to the point of extraction, decreasing with increased distance away from the extraction point. Groundwater extraction also increases the seepage forces acting on the soil skeleton resulting in horizontal ground movements.

Structures founded within the zone of influence will be affected by the vertical and horizontal ground movements induced by the groundwater extraction. The interaction relationship between the structure and the founding soil will, therefore, be altered resulting in a change in the manner in which the structure resists and transmits loading as well as additional loading being imposed onto the structure. The structure will respond to the altered interaction by deforming. The deformation of the structure, however, needs to remain within acceptable limits. The stiffness resulting from the material and geometrical properties of the structure will have an effect on the response of the structure and the resultant distortion.

The response of structures to groundwater extraction-induced ground movements was investigated by means of geotechnical centrifuge models. Four single storey two-bay portal frames instrumented with strain gauges and linear variable differential transducers were used to represent a structure with varying stiffness, rigid and flexible slabs and columns founded within the zone of influence. The groundwater extraction was modelled with a simulated aquifer constructed in a centrifuge strongbox where the surface settlement was measured with linear variable differential transducers and the ground movements tracked by means of digital image correlation. The pore-water pressure was measured with piezometers while the extraction well water level was monitored with a pressure meter.

The study found that the resultant ground movements can be successfully modelled in a geotechnical centrifuge at elevated gravitational fields. The modelling results corroborate the response of the aquifer response previously found through numerical and analytical modelling as well as monitoring and inspection of real aquifers during groundwater extraction. The main conclusions show that as the pore-water pressure reduced non-uniformly, the soil settlement increased non-uniformly throughout the aquifer while the increased seepage forces also induced a component of horizontal ground movement.

The conclusions deduced from the response of the portal frames, show that rigid frames with a high global stiffness, rigid slabs and columns, deform by rigid body rotation to the imposed differential settlement. Flexible frames depict greater localised deformation concentrated to bays where deformation is imposed. Frames where the vertical stiffness is greater than the horizontal, rigid slabs and flexible columns, show a greater bending type deformation whereas frames with a greater horizontal stiffness, flexible slab and rigid columns, undergo a vertical shear type deformation in response to the imposed differential settlement.

DECLARATION

I, the undersigned hereby declare that:

- I understand what plagiarism is and I am aware of the University's policy in this regard;
- The work contained in this thesis is my own original work;
- I did not refer to work of current or previous students, lecture notes, handbooks, or any other study material without proper referencing;
- Where other peoples work has been used this has been properly acknowledged and referenced;
- I have not allowed anyone to copy any part of my thesis;
- I have not previously in its entirety or in part submitted this thesis at any university for a degree.

Signature of student:

Name of student: Fabianus Lheurreux Mcterror Gomachab

Student number: 12109984

Date: 2018/02/16

ACKNOWLEDGEMENTS

This dissertation would not have been possible without the help, assistance and support of a number of people. I would like to bestow my heartfelt gratitude towards the following people:

1. My supervisors, Prof Jacobsz and Prof Kearsley, for undertaking this project with me and for the guidance, insight, support and direction you gave throughout.
2. The laboratory staff and technicians: Mr Scholtz, Mr Mostert, Mr Van Staden, Mr Jansen and Mr Nkadimeng for their assistance in all laboratory-related matters and the assistance and company during the long hours of preparation for testing.
3. *Aurecon Namibia* for the financial assistance and opportunity to undertake this project.
4. Mr L Van Staden, Mrs R Linde and Mr F Carstens for the unending support and motivation, not just during 2017, but throughout my studies.
5. My good friend, Peter Mlilwana, for the support, advice and the time spent proofreading this dissertation. I wish you all the success in pursuing your master's and beyond.
6. My mother, Fabiola Tsamases, grandmother, Lena Gomachas, my siblings, the extended Gomacha family and my partner, Gezina with the /Hoxobe family for the patience, understanding, support and motivation throughout my studies.

Table of Contents

List of Figures

List of Tables

1 INTRODUCTION

1.1 BACKGROUND

Civil structures are founded on or within soil. Soil-structure interaction, which is the term for the interaction process between the founding soil and a structure, dictates the behaviour of a structure founded on soil and the response of the soil to the loading applied by the structure. Understanding the interaction between the structure and the founding soil is important for designing and constructing structures that will be safe and functional for the required design life.

Surface structures and possible founding soil improvements should be designed according to codes of practice and generally accepted guidelines to meet acceptable limiting requirements resulting in structures that are safe and functional. Structural engineers should design structures that can withstand and accommodate allowable deflection and deformation while remaining serviceable. Foundation and geotechnical engineers should design foundations and assess the founding soil so that the required settlement limits are not exceeded and foundation systems do not fail. Under normal serviceability conditions, the soil and structure will interact with minimal deviation from the limits it was designed for. Not only overloading and variation in loading from that which a structure was designed for, but also processes that induce excessive ground movement such as tunnelling and/or groundwater extraction can, however, change the soil-structure interaction. Civil engineers generally have a well-researched and experience-based understanding of the behaviour of structures due to variation in structural loading such as structures founded on problem soils (expansive clays or collapsible soils) and ground movement due to tunnelling and deep excavations. The aim of this research is to obtain a general understanding of the behaviour of framed structures undergoing differential settlement induced by groundwater extraction.

Groundwater is the second most abundant source of fresh water in the world and the largest source of water used for human consumption (Cashman and Preene, 2013). Groundwater is viewed as a valuable resource by hydrologists for its importance in the greater hydrological cycle and uses as potable water whereas, in the construction industry, groundwater presents problems that would not be present in its absence. Both industries tap into aquifers to extract or control groundwater. Extracting groundwater causes a reduction in the pore-water pressures within an aquifer due to the lowering of the water table. Effective stresses of the soil increase due to the reduced pore-water pressures. Terzaghi's principle (Terzaghi, 1943) of effective stresses stipulates that the total pressure is a sum of the effective stresses on the soil skeleton and the pore-water pressure of the interstitial pore water. Variation in the pore-water pressure without a variation in the total stress will result in a numerically equal increase in the effective stresses. Vertical compression of the soil skeleton is driven by the increase in inter-granular effective stresses and the rearrangement of the granular material. The rearrangement of the granular particles is

further facilitated by the seepage forces exerted on the soil particles. Increased seepage forces caused by pumping increases the vertical settlement of the soil layer but also induces horizontal ground movement.

Due to the shape of a dewatering cone around abstraction boreholes, the reduction in pore-water pressure is not uniform throughout the aquifer and therefore the soil settlement is also not uniform. The zone of influence for the pore-water pressure reduction and soil settlement propagates away from the point of extraction with diminishing influence further from the extraction point. The two influence zones may coincide depending on the soil properties and aquifer type which dictate the rate of consolidation. The settlement influence may also lag the pore-water pressure influence, resulting in settlement occurring after the extraction process has concluded. Foundations founded within the settlement zone of influence will be affected by the ground movement.

One of the main causes of structural damage and/or failure is excessive differential settlement of the foundations (Díaz and Tomás, 2016). The behaviour of a structure is dictated by geometrical and material properties, the relative soil-structural stiffness and the interaction between the soil and structure. Therefore, groundwater extraction induced ground movements may have an impact on the behaviour of structures. The response of a structure will be governed by the amount of vertical and horizontal ground movement, the amount of differential soil settlement and the subsequent differential foundation settlement, which will be a function of the global structural stiffness, the relative stiffness between structural elements and the interconnection of the structural elements.

Structures are designed to transfer loads from the point of application to the point of dissipation, which is the foundations. The foundations act as adapters that spread out the load so that it is less than the limiting bearing capacity of the soil and therefore the load can be resisted safely by the bearing soil. Differential settlement and angular distortion of foundations may alter this pattern of load transfer, commonly known as load paths. Load path changes may result in load and stress redistribution and/or amplification of stresses within a structure which could result in structural damage, loss of functionality and ultimately failure due to the structure resisting and thus transferring the applied loads in a manner it was not designed to.

1.2 OBJECTIVE OF STUDY

The objective of this study was to determine the behaviour of two-bay single storey portal frames, founded on soil undergoing differential settlement and horizontal strain due to groundwater extraction resulting from non-uniform dewatering, i.e. a sloping water table. The soil settlement was induced by changes in pore-water pressure and the subsequent effective soil stress changes due to groundwater

extraction. The behaviour of structures, founded within the zone of influence, will be affected by the induced ground movement. In this study, the following relationships were investigated:

- The effect of water extraction on the pore-water pressure change;
- The effect of pore-water pressure change on soil settlement;
- The effect of soil settlement on portal frame deformation;
- The effect of structural deformation on strain development in the structure;
- The effect of frame stiffness on the load and moment redistribution or amplification in the structure.

1.3 SCOPE OF STUDY

The aim of the study was to utilise physical modelling, in the form of centrifuge modelling, to investigate the response of structures to groundwater extraction-induced ground movement. The 1:30 scale models were tested at 30 g. The study was limited to physical modelling with finite element modelling as well as hand calculations used in preliminary investigations and result comparison and verification. Full-scale modelling was not considered for the study although elements from literature were incorporated.

A homogenous plane strain unconfined (phreatic) aquifer with modified silica sand soil confined in a centrifuge strongbox was modelled to investigate the groundwater extraction induced ground movement. The silica sand was modified by adding 10 % vermiculite by mass to the sand. The aquifer was dewatered from one side only from an extraction well spanning the full width of the aquifer. The groundwater extraction induced ground movement was measured using linear variable differential transducers (LVDTs) on the soil surface to measure the soil settlement and digital image correlation (DIC) to track the ground movements.

Four plane strain single storey two-bay aluminium portal frames were used to model the response of structures founded within the zone of influence of groundwater extraction. The portal frames varied in slab and column thicknesses, which resulted in different stiffnesses for the frames. The portal frames were instrumented with strain gauges and LVDTs.

The interaction at the soil-foundation interface and the interaction of the foundation system (frame footing and founding soil) were not considered for this study. The portal frames were loaded by deadweight to impose the desired load magnitude. Complex and pattern loading were not considered in this study.

1.4 METHODOLOGY

Before any modelling began, a review of literature was conducted to obtain knowledge on the topics of groundwater extraction, soil consolidation and settlement, structural behaviour and damage, as well as soil-structure interaction.

An experimental procedure was developed to guide the experiments conducted for the study. Initially, preliminary tests such as compressibility and grading analysis were conducted on the soil. This was followed by making and/or testing, and calibrating the instrumentation that was used for the study. Preliminary finite element modelling was conducted to investigate the behaviour of the frames used in this study. After all the preliminary testing and numerical modelling were concluded, centrifuge modelling proceeded.

The physical modelling was conducted in a geotechnical centrifuge accelerated to 30 g corresponding to the model scale of 1:30. A centrifuge strong box was used to confine the models. Initially, the soil was placed in the strong box with the aluminium portal frames founded within the soil. Piezometers were used to measure the pore-pressure variation within the soil. The resulting soil settlement was measured by means of LVDTs and the movement the soil mass, determined by means of DIC. The response of the structural frames to the ground movement was investigated with strain gauges glued to the frames and LVDTs installed in line with the walls of the frame.

To investigate the effect of groundwater extraction on the soil settlement referred to as groundwater extraction-soil interaction (GSI) the tests were initially conducted without the structural frames. The model was set up to investigate the soil response with piezometers installed in the soil and LVDTs in line with the piezometers. DIC was, furthermore, used to investigate the vertical and horizontal ground movement of the soil. Once the soil behaviour was established, the groundwater extraction-soil-structure interaction (GSSI) was investigated by conducting the centrifuge tests with the soil and the various portal frames.

The influence of the local and global stiffnesses of the portal frames was determined by measuring the strain changes in the frames. Strain gauges were placed at the positions of initial maximum hogging and sagging as well where maximum change in bending moments was expected on the columns. The strain changes in the frame were expected to give an indication of the local behaviour of the frame. The global behaviour was investigated by means of the variation in load within the columns. The global behaviour, when comparing the initial and final loads of the columns, was expected to give an indication of any variation in load paths of the frame. The soil-structure interaction was investigated by comparing the free-field/greenfield soil settlement (soil settlement in the absence of structural loading) measured in the

GSSI tests and the frame vertical soil settlement.

Finally, the data and results obtained from the tests were analysed. A discussion and analysis of the results are presented in this report as well as the conclusions reached for each of the stipulated objectives.

1.5 ORGANISATION OF THE REPORT

The report is organised to contain the following chapters and appendices.

- Chapter 1, **Introduction**, serves as the introduction to the report. This chapter contains a brief discussion of the topic and motivation for the study. The chapter, furthermore, presents a detailed outline of the objectives of the study, the scope of the study and the methodology implemented to achieve the study objectives.
- Chapter 2, **Literature Review**, contains a summary of the literature study. The literature review serves as a review and summary of the available literature pertaining to the relevant literature on the topic considered.
- Chapter 3, **Research Methodology**, is a summary of the experimental procedure followed to achieve the research objectives. The chapter contains details of the materials utilised, the models designed and developed and tests conducted and instrumentation used.
- Chapter 4, **Result Discussion and Analysis**, contains a review of the results obtained from the tests conducted. It, furthermore, contains the experimental result discussion and analysis of the results.
- Chapter 5, **Conclusion and Recommendations**, contains the conclusions reached for the research objectives. Finally, recommendations for future research and implementation of processes learned during the study are presented.

2 LITERATURE REVIEW

2.1 INTRODUCTION

This literature review serves as a summary of the available knowledge on the methods and factors contributing to groundwater extraction, the resulting soil settlement and the consequent effects of this phenomenon on infrastructure response, behaviour, and subsequent damage due to settlement. The review starts with an assessment of groundwater, focusing on types of groundwater bearing soils, soil properties and methods, and systems used for groundwater extraction. Attention is also drawn to soil settlement due to groundwater extraction and load induced settlement of foundations. The study focusses on the behaviour and damage of structures founded on soils undergoing settlement, therefore, attention is drawn to investigations on the behaviour, damage and failure of structures. The review concludes with a study of soil-structure interaction focusing on structural response due to soil-structure interaction.

2.2 GROUNDWATER WITHDRAWAL

For groundwater withdrawal to be achieved in an economical, efficient, environmentally friendly manner and with minimal detrimental consequences, a thorough knowledge and understanding of groundwater and groundwater bearing soil strata must be established. This section aims to summarise the available literature on the topic.

> *"It is more than mere coincidence that most failures have been due to the unanticipated action of water, because the behaviour of water depends, more than anything else, on minor geological details that are unknown." Karl Terzaghi, 1943*

2.2.1 Groundwater and Water Bearing Soils

Soil and rock are made up of mineral particles that are in contact with each other. The soil and rock are two-phase or three-phase materials. A volume of the material contains voids, which are either widely distributed in the form of pores or locally concentrated as fissures or fractures. A two-phase volume of soil would be completely dry and the voids filled with air or completely saturated where water fills the voids. Partially saturated soil is a three-phase material comprising of soil, water and air. The pore-water pressure is measured relative to atmospheric pressure. The pressure at which the pore-water pressure is atmospheric is defined as the phreatic surface or the water table. Below the water table the pores, fractures, and fissures are fully saturated (Fang, 1991; Knappett and Craig, 2012; Cashman and Preene, 2013).

Groundwater is continuously in motion as it forms part of the greater hydrological cycle. The flow through soil is inter-granular, flowing through the interconnected pores under a hydraulic gradient which is known as seepage. Groundwater flow is generally slow, in the absence of pumping or other human activities, ranging from a few meters per day in high-permeability soils to a few millimetres a year in low-permeability soils. The permeability (k, the coefficient of permeability) of the soil is a critical parameter for the assessment of how water flows through soil and rock. Cashman and Preene (2013), define permeability as, "the measure of the ease or otherwise with which the groundwater can flow through the pores of a given soil mass." It is dependent on the average size and connectivity of the pores, which is in turn related to the distribution of the particle sizes, particle shape, and soil structure. The typical values for k for different types of soil are presented in Table 2.1.

Table 2-1: Coefficient of permeability (m/s) (adapted from (Knappett and Craig, 2012))

1	10^{-1}	10^{-2}	10^{-3}	10^{-4}	10^{-5}	10^{-6}	10^{-7}	10^{-8}	10^{-9}	10^{-10}
			Desiccated and fissured clays							
Clean gravels		Clean sands and sand-gravel mixtures			Very fine sands, silts and clay-silt laminate			Unfissured clays and clay-silts (>20% clay)		

Below the water table pore-water may be static, with hydrostatic pore pressure, or seep through the soil under a hydraulic gradient. Bernoulli's theory is applicable to pore water, however, due to the small seepage velocities, the velocity head is neglected (Knappett and Craig, 2012) as indicated in Equation 2-1.

$$h = \frac{u}{\gamma_w} + z \qquad \text{Equation 2-1}$$

Where:

h = total hydraulic head (m)

u = pore-water pressure (kPa)

z = elevation head (m)

γ_w = the unit weight of water (9.81 kN/m^3)

Above the water table, the soil can remain saturated with the pore-water held in place by the capillary tension. The maximum negative pressure, u_c, can be estimated by Equation 2-2 (Knappett and Craig, 2012):

$$u_c \approx -\frac{4T_s}{eD} \qquad \text{Equation 2-2}$$

Where:

u_c = maximum negative pore pressure (kPa)

T_s = the surface tension of pore fluid (kN/m)

e = void ratio

D = pore size (m)

The total hydraulic head is important as it governs groundwater flow. Groundwater flows from a high total hydraulic head to a low total hydraulic head. Furthermore, the modern understanding of groundwater flow in one dimension is in accordance with Darcy's empirical law as indicated in Equation 2-3 (Knappett and Craig, 2012):

$$\mathrm{Q} = kA\left(\frac{dh}{l}\right) \; or \; kAi \qquad \text{Equation 2-3}$$

Where:

Q = volumetric flow of water per unit time (m^3/s)

A = the cross-sectional area through which the water flows (m^2)

l = the length of the flow path between the upstream and downstream ends (m)

dh = the difference in total hydraulic head between the upstream and downstream ends (m)

k = the permeability of the porous media through which the water flows (m/s)

i = hydraulic gradient

Darcy's law gives an indication of the key factors affecting groundwater flow which is vital for understanding how groundwater may be manipulated by groundwater lowering and extracting systems (Knappett and Craig, 2012; Cashman and Preene, 2013):

- An increase in the permeability will increase the flow rate, with all other parameters constant,
- An increase in the cross-sectional area will increase the flow and finally,
- An increase in the hydraulic gradient will increase the flow.

The behaviour and flow of groundwater in soil are important in assessing groundwater abstraction and dewatering systems. In addition, to fully comprehend the behaviour of groundwater, one must assess the geological water-bearing soil strata (Cashman and Preene, 2013). The Construction Industry Research and Information Association Report C515 present the following definitions for the strata types as presented by Preene et al., (2000):

- Aquifer – Soil or rock forming a stratum, group of strata, or part or stratum that is water-bearing.
- Aquiclude – Soil or rock forming a stratum, group of strata, or part or stratum of very low permeability, which acts as a barrier to groundwater flow.
- Aquitard – Soil or rock forming a stratum, group of strata, or part or stratum of intermediate to low permeability, which yields only small groundwater flow.

Aquifers are the water-bearing strata and groundwater withdrawal is conventionally carried out in this formation. Aquifers can be unconfined where the aquifer formation starts at the natural ground level (NGL), whereas confined aquifers are overlain by aquicludes. In unconfined aquifers or phreatic aquifers, the voids are fully saturated and the pore pressures hydrostatic below the water table. A piezometer installed into the saturated part of the aquifer will show a water level at the level of the water table. If water is pumped from the aquifer, the water table will be lowered locally around the point of extraction to form a drawdown curve. The thickness of the aquifer will be reduced, as the effective stresses will be increased due to a decrease in pore-pressures in line with the drawdown curve (Cashman and Preene, 2013).

During pumping, the behaviour of confined aquifers is different from that of unconfined aquifers. In contrast to an unconfined aquifer, a confined aquifer is fully saturated as a saturated zone may exist in the confining aquiclude, known as piezometric level, the level to which water will rise in a piezometer installed in the formation (Cashman and Preene, 2013). If a confined aquifer is pumped, the piezometric level will be lowered to form a drawdown curve. Provided the piezometric level is not drawn down below the aquifer level, the aquifer will remain saturated. The aquifer yields water by compression, reduction in pore space, and consolidation as the excess pore-pressures are dissipated. In artesian aquifers, the pore-pressures are high enough with the piezometric level above the NGL, that the aquifer can yield water without it being pumped (Cashman and Preene, 2013).

The presence of aquitards presents challenges of its own, as the intermediate permeability results in water flowing out of the aquitard and into the aquifer contributing to the aquifer yield. Groundwater will continue flowing out of the aquitard until the pore-pressures have equilibrated which results in delayed consolidation settlements, as indicated in Figure 2-1. (Knappett and Craig, 2012; Cashman and Preene, 2013)

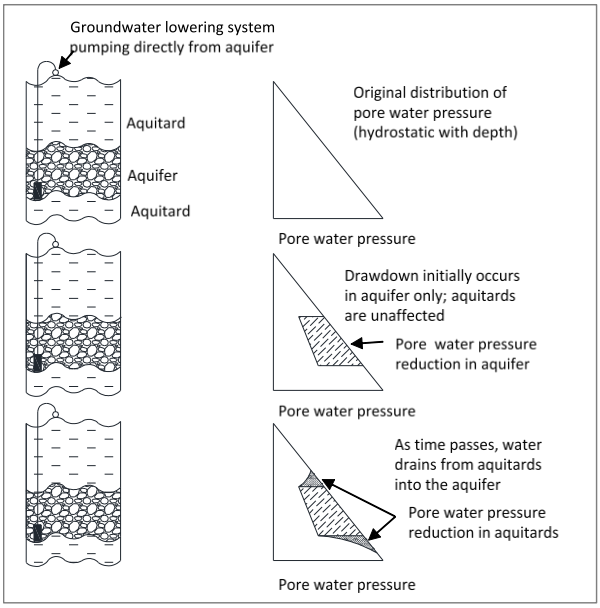

Figure 2-1: Response of aquitards to groundwater withdrawal (adapted from Cashman and Preene, 2013)

When water is pumped from an aquifer, the water level in the pumping well drops and water will flow from the aquifer towards the well. The water level drop in the aquifer will decrease away from the extraction point, forming the drawdown curve. The distance from the point of extraction to where the drawdown curve levels out to the original piezometric level, is the distance of influence. The distance of influence increases with pumping time until it reaches a quasi-steady state. The distance of influence gives an indication of the cone of depression and how far the zone of significant settlements will extend with time. The two most commonly used methods to determine the radial distance of influence for radial flow, R_o, are the empirical formula developed by Weber and the time-dependent formula described by Cooper and Jacob as shown in equation 2-4 and 2-5 respectively as presented by Cashman and Preene (2013).

$$R_o = Cs\sqrt{k} \qquad \text{Equation 2-4}$$

$$R_o = \sqrt{\frac{2.2kDt}{S}} \qquad \text{Equation 2-5}$$

Where:

s = drawdown (m)

k = soil permeability (m/s)

C = empirical factor, equal to 3000

D = aquifer thickness (m)

t = time since pumping began (s)

S = aquifer storage coefficient

The distance of influence for horizontal plane flow, Lo, can be determined using Equation 2-6 according to Powrie and Preene as presented by Cashman and Preene (2013):

$$L_o = \sqrt{\frac{12kDt}{S}} \qquad \text{Equation 2-6}$$

Where the variables have the same definition as defined above.

2.2.2 Groundwater Withdrawal Methods and Systems

The design of dewatering and groundwater extraction systems should be aimed at developing a workable and economical solution to groundwater related problems. Fang (1991) list the following purposes for dewatering systems:

- Intercepting and lowering the water table
- Improvement of the stability of slopes
- Preventing bottom of excavations from heaving
- Improve density and compaction characteristics of soils in the bottoms of excavations
- Reduction of the water content of soils in borrow areas
- Reducing the earth pressures on temporary supports and sheeting

Cashman and Preene (2013) indicate two main philosophical views for the design of groundwater systems, namely: the theoretical approach and the empirical approach. The theoretical approach views the design problem as a seepage calculation problem. It implies that the major challenge is estimating the discharge flow and the design of the equipment is a secondary problem. In contrast, the empirical method focuses on designing and selecting the appropriate well type, spacing and pump size for the prevailing geological conditions. Cashman and Preene (2013) continue to list the following key factors, together with those proposed by Gambolati and Teatini (2015) that need to be incorporated into the systems:

- Aquifer types and properties
- Aquifer depth and thickness
- Aquifer compaction and ground displacement
- Presence of aquitards and aquicludes
- Distance of influence and aquifer boundaries
- Initial groundwater level and pore-pressure profile
- Presence of compressible strata

- Modelling past and future events
- Mitigating environmental impacts

Cashman and Preene (2013) present the principal methods for groundwater control and most suitable methods given a combination of *k* and required drawdown. These are shown in Table 2.2 and Figure 2.2 respectively.

Table 2-2: Principle methods for groundwater control by pumping (Cashman and Preene, 2013)

Method	Typical Applications
Drainage pipes or ditches	Control of surface water runoff and shallow groundwater
Sump pumping	Shallow excavations in clean, coarse soils, for control of groundwater and surface water
Wellpoints	Generally shallow, open excavations in sandy gravels down to fine sands and possibly silty sands
Horizontal wellpoints	Generally shallow trench or pipeline excavations or large open excavations in sands and possibly silty sands
Deep wells with electric submersible pumps	Deep excavations in sandy gravels to fine sands and water-bearing fissured rocks
Deep wells with electric submersible pumps and vacuum	Deep excavations in silty fine sands, where drainage from the soil into the well may be slow
Shallow bored wells with suction pumps	Shallow excavations in sandy gravels to silty fine sands and water-bearing fissured rocks
Ejectors	Excavations in silty fine sands, silts, laminated or fissured clays in pore-water pressure control are required
Passive relief wells and sand drains	Relief of pore-water pressure in confined aquifers or sand lenses below the floor of the excavation to ensure basal stability
Collector wells	Tunnels or deep excavations in relatively permeable soils such as sands and gravel, where surface access does not allow the installation of many wells
Syphon drains	Long-term slope drainage and landslide stabilisation in low permeability soils
Artificial recharge	Soils of high moderate permeability and fissured rocks, in which lowering of groundwater must be controlled so that environmental effects can be mitigated
Electro-osmosis	Low-permeability soils and some peats

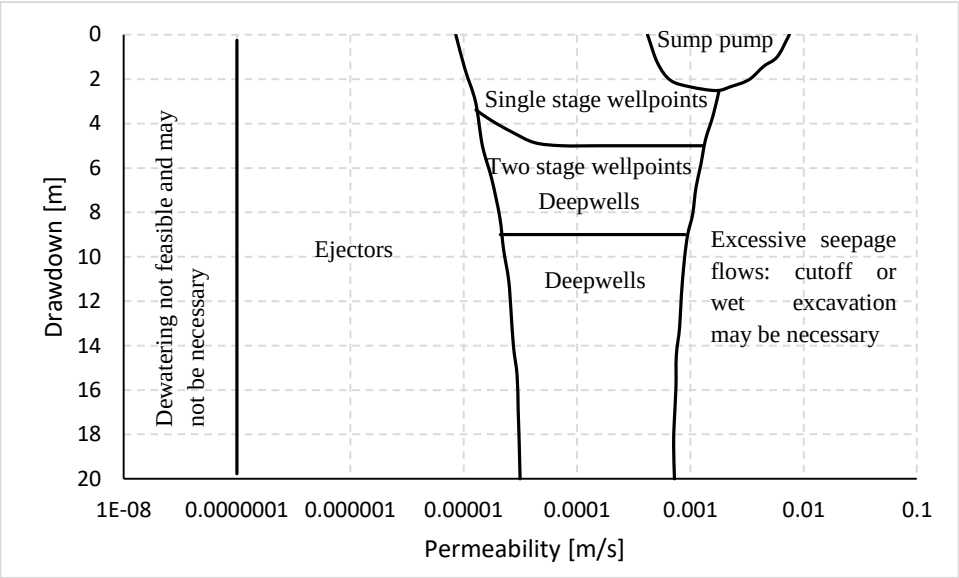

Figure 2-2: Range of application of pumped well groundwater control techniques (adapted from (Cashman and Preene, 2013))

2.2.3 Environmental Impacts of Groundwater Control

Groundwater control has the potential for causing adverse environmental impacts. These impacts may be localised to the control point or extend considerable distances away from the extraction point as groundwater forms part of the greater hydrological cycle. The consequences of adverse groundwater related environmental impacts are far-reaching, ranging from aquifer pollution to substantial ground settlement (Cashman and Preene, 2013). Preene and Brassington (2003) group these impacts into five main categories:

1. Pumping and abstraction from aquifers
2. Physical disturbance of aquifers creating pathways for groundwater flow
3. Physical disturbance creating barriers to groundwater flow
4. Discharges to groundwater
5. Discharges to surface water

Table 2.3 presents the temporary and permanent activities related to groundwater extraction, which forms part of this study:

Table 2-3: Potential environmental impacts from control activities (adapted from (Preene and Brassington, 2003))

Category	Potential Impacts	Duration	Relevant Activities
Pumping and abstraction	Ground settlement Derogation of individual sources Effect on aquifer groundwater levels Effect on aquifer groundwater quality Depletion of groundwater dependent features	Temporary	Dewatering of excavations and tunnels using wells, wellpoints, and sumps Drainage of shallow excavations or waterlogged land by gravity flow
		Permanent	Permanent drainage of basements, tunnels, and road and rail cuttings, both from pumping and from gravity flow

Furthermore, Gambolati and Teatini (2015) state that the major environmental consequence of groundwater pumping is anthropogenic land subsidence. In addition to land subsidence the authors also list (1) upheaval of ground surface due to the injection of water, (2) formation of earth fissures caused by groundwater pumping in subsiding basins, (3) the activation of pre-existing shallow faults, creating failure of the land surface and (4) inducing and triggering micro-seismic and seismic events because of changes in the natural effective and total stress regimes, (Gambolati and Teatini, 2015). The next section, therefore, focusses on water extraction induced land subsidence.

2.3 LAND SUBSIDENCE

Land subsidence is known to be one of the major anthropogenic consequences of fluid withdrawal. The area affected by fluid withdrawal-induced land subsidence can range from a localised area around the extraction point to affecting entire deltas and basins. Numerous authors have studied the relationship between groundwater withdrawal and consequent land subsidence i.e. (Majumder and Sundaram, 1991; Baú D et al., 2004; Roy and Robinson, 2009; Fahmi et al, 2015).

2.3.1 Consolidation Settlement and Mechanics of Soil Settlement

A volume of soil can be visualised as solid soil skeleton with interconnected voids filled with water and/or air. The solid soil skeleton and water are assumed to be incompressible for the loads commonly experienced in engineering practice, whereas air is deemed highly compressible. The volume of soil can be altered by rearrangement of soil particles by sliding and rolling in response to forces between particles. In dry or partially saturated soil, rearrangement of soil particles is facilitated by the compression of pore air, provided the soil structure is not at its densest. In fully saturated soil, a reduction in the volume is only possible if water can escape from the voids (Knappett and Craig, 2012).

Mitchell and Soga (2005), state that the problems involving volume change, deformation and strength require separate consideration of the stress that is carried by the grain assemblage and that carried by the fluid. Soil grains in contact can resist shear and normal stresses whereas the air and water can only resist normal stresses. Terzaghi (1943) presented his "Principle of Effective Stress", an intuitive relationship based on experimental data, for fully saturated soils that relate the following three stresses:

- The total normal stress, σ, on a plane within the soil mass
- The pore-water pressure, u, the pressure of the water filling the voids
- The effective normal stress, σ', representing the stress transmitted through the grain assemblage

Terzhagi (1943) proposed the relationship as indicated in Equation 2-7:

$$\sigma = \sigma' + u \qquad \text{Equation 2-7}$$

The principle of effective stress asserts that the effective stress, σ', controls the stress-strain, volume change and strength of soil, independent of the magnitude of the pore-pressure. The pore-pressure acts equally in all directions but is assumed not to compress the soil particles or cause the particles to press against each other. The initial magnitude of the pore-pressure is governed by the position of the water table and is called the static pore pressure, u_s. Any variation from u_s is called excess pore-pressure, u_e, with the pore-pressure at any point within the soil is the sum of the two. The u_e will result in a hydraulic gradient being established, resulting in seepage of pore-water towards a free-draining boundary of the soil layer. This drainage will continue until u_s is reached and all the excess pore-pressure has dissipated, a process known as dissipation, $u_e = 0$ and $u = u_s$. As the drainage takes place the effective stress on the soil particles increase and the soil particles can rearrange and take up new positions. The time required for the drainage to be complete is dependent on the permeability of the soil. This entire process is known as consolidation (Mitchell and Soga, 2005; Cashman and Preene, 2013).

The process of consolidation can be instigated by two distinct occurrences, namely: a local increase in pore-pressures and subsequent increase in the total head or a decrease in pore-pressure a distance away. Both processes will result in a hydraulic gradient being established, water draining towards the lower total head and consolidation ensuing. The first process would be due to an increase in total stress, u, locally, i.e. if a structure is founded on saturated clay. The second process would be due to pumping or groundwater lowering a certain distance away within a connected aquifer (Budhu and Adiyaman, 2010; Knappett and Craig, 2012). Furthermore, it is known that behaviour if soil is stress history dependent and therefore accurate knowledge of the past maximum consolidation pressure and compressibility characteristics of soil is needed for reliable prediction of the rate and total settlement of soil. The relations between soil void ratio, e, and effective stress depends on the stress history. If the present effective stress is the maximum the soil has been subjected to, the soil is said to be normally

consolidated. If the soil had been subjected to higher effective stresses in the past, the soil is said to be over-consolidated. The over-consolidation ratio (OCR), is the maximum effective stress the soil had ever been subjected to over the present effective stress (Mitchell and Soga, 2005; Knappett and Craig, 2012).

Figure 2.3 shows the void ratio vs effective stress relationships for soil. The $e - \sigma'$ curve shows soil that is initially compressed, uncompressed and recompressed. On the other hand, the $e - log(\sigma')$ relationship of normally consolidated soil is linear and called the virgin compression line. During compression along this line, soil mainly undergoes permanent deformation. The over-consolidated soil is represented by the expansion-recompression part of the $e - log(\sigma')$ graph. Deformations along this line of the graph are almost always recoverable (Knappett and Craig, 2012).

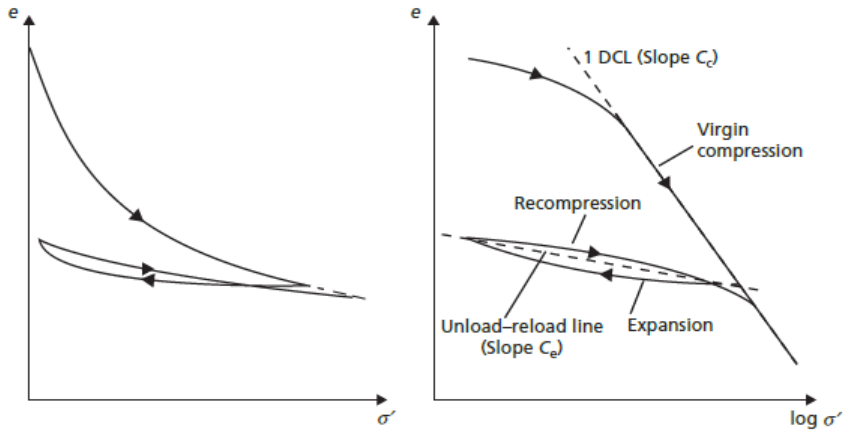

Figure 2-3: Void ratio-effective stress relationship (Knappett and Craig, 2012)

There are two prevailing theories for consolidation settlement, namely: Terzaghi's theory of one-dimensional consolidation and Biot's general theory of three-dimensional consolidation (Biot, 1941). Both theories make certain assumptions regarding the properties of soil. Terzaghi's (1943) assumptions are as follows:

1. The soil is homogeneous
2. The soil is saturated
3. The solid particles and water are incompressible
4. Compression and flow are one dimensional
5. Strains are small
6. Darcy's law is valid for all hydraulic gradients
7. The coefficient of permeability and the coefficient of volume compressibility remain constant throughout the process
8. There is a unique relationship, independent of time, between void ratio and effective stress

It is generally accepted that assumptions induce errors and discrepancies and Terzaghi's assumptions are no exception. There is evidence of deviation from Darcy's law at low and high hydraulic gradients (6) and the coefficient of permeability decreases with a decrease in the void ratio (7). Finally, experimental results show that the relationship between void ratio and effective stress is not independent of time due to secondary compression (8) (Knappett and Craig, 2012). Biot (1941) makes the following assumptions regarding the soil properties:

1. Isotropy of the material
2. Reversibility of stress-strain relations under final equilibrium conditions
3. Linearity of stress-strain relations
4. Small strains
5. The pore-water is incompressible
6. The water may contain air bubbles
7. The water flows through the porous skeleton according to Darcy's law

Like Terzaghi, the assumptions made by Biot are subject to criticism, especially the second and third assumption but for practical requirements, both theories have been found to be satisfactory, (Biot, 1941; Knappett and Craig, 2012).

Duncan (1993), studied the effects of consolidation on the design and construction of two modern construction projects together with the difficulties involved in determining the magnitudes and rates of consolidation settlement. The author lists further limitations of conventional analysis of consolidation settlement:

- Difficulties in evaluating pre-consolidation pressures
- Difficulties in selecting values of c_v (coefficient of consolidation) for consolidation rate calculations
- Difficulties in determining whether embedded sand layers will or will not provide internal drainage to consolidating clay layers
- Shortcomings in conventional consolidations theory

The author elaborates further on the shortcomings in the text and limitations of conventional analysis of consolidation settlement. The following section focusses on groundwater withdrawal, through dewatering, pumping and/or water table lowering induced settlement. The limitations of consolidation theories are also addressed further.

2.3.2 Groundwater Withdrawal-Induced Soil Settlement

Groundwater withdrawal-induced settlement is primarily studied by means of numerical models, mainly finite element (FE) and finite difference (FD) modelling. Lowering of water table within and aquifer results in a decrease in the pore-water pressure. It is evident from Terzaghi's effective stress relationship, which yields a self-equilibrating equation, that the resultant increase in effective stress should be numerically equal to the decrease in the pore-water pressure. A cone of depression on ground level propagates away from the point of extraction, because of the effective stress increase, consolidation settlement ensues. Numerous authors have used the concept of the self-equilibrating stresses, together with Terzaghi or Biot's consolidation theories and numerical modelling, to study the mechanics of land subsidence due to groundwater extraction, ensuing complications and subsequent consequences (Vasco et al, 2001; Shaqour and Hasan, 2008; Wang et al, 2015; Cui et al., 2016).

With the improvement in modern computing power, researchers now prefer implementing the three-dimensional theory of consolidation in studying the problem at hand. Gambolati and Teatini (2015) present the coupled and uncoupled formulations, originally presented by Biot (1941, 1955), of flow and stress in an isotropic porous median experiencing a groundwater flow field. The difference between the two formulations arises from the way the flow equation is incorporated into the solution. The initial equilibrium equations for a porous medium subjected to pore pressure variations in terms of displacement are presented as in Equation 2-8 to Equation 2-10:

$$G\nabla^2 u + (\lambda + G)\frac{\partial \epsilon}{\partial x} = \frac{\partial p}{\partial x} \qquad \text{Equation 2-8}$$

$$G\nabla^2 v + (\lambda + G)\frac{\partial \epsilon}{\partial y} = \frac{\partial p}{\partial y} \qquad \text{Equation 2-9}$$

$$G\nabla^2 w + (\lambda + G)\frac{\partial \epsilon}{\partial z} = \frac{\partial p}{\partial z} \qquad \text{Equation 2-10}$$

Where:

u, v, w = components of incremental position vector along x, y, z axis

∇^2 = Laplace operator

λ = Lame constant (vE/[(1-2v)(1+v)])

ϵ = $\epsilon_{xx} + \epsilon_{yy} + \epsilon_{zz}$, the volume strain or dilation

p = pore pressure

v = Poisons ratio of soil

E = Young's modulus of soil

G = Shear modulus of soil

The groundwater flow equation for the coupled formulation which makes it possible to solve for the flow and stress simultaneously is presented in Equation 2-11 (Gambolati and Teatini, 2015):

$$\frac{1}{\gamma}\nabla(K_{ij}\nabla) = n\beta\frac{\partial p}{\partial t} + \frac{\partial \epsilon}{\partial t} \qquad \text{Equation 2-11}$$

Where:

∇ = gradient operator

K_{ij} = hydraulic conductivity tensor

n = medium porosity

β = compressibility of water

γ = unit weight of water

The groundwater flow equation of the uncoupled formulation for the flow equation is solved independently for the pore pressure and the gradient of the pore pressure integrated into the equilibrium equation as a known quantity as presented in Equation 2-12 (Gambolati and Teatini, 2015):

$$\nabla\left(K_{ij}\frac{\nabla p}{\gamma}\right) = \gamma(n\beta + \alpha)\frac{\partial p}{\partial t} \qquad \text{Equation 2-12}$$

Where:

α = vertical compressibility of an isotropic soil [(1+v)(1-2v)]/[(1-v)E]

Furthermore, Budhu and Adiyaman (2010) presented a publication on the basic mechanics governing the changes in stress states due to groundwater pumping and compared results based on the mechanics of existing field data. The authors begin by presenting the groundwater subsidence and uplift (see Figure 2.4) due to the fluctuation of the water table. It is evident that the soil subsidence is made up of permanent, non-recoverable settlement, and elastic, recoverable settlement, like the void ratio-effective stress curve presented by Knappett and Craig (2012).

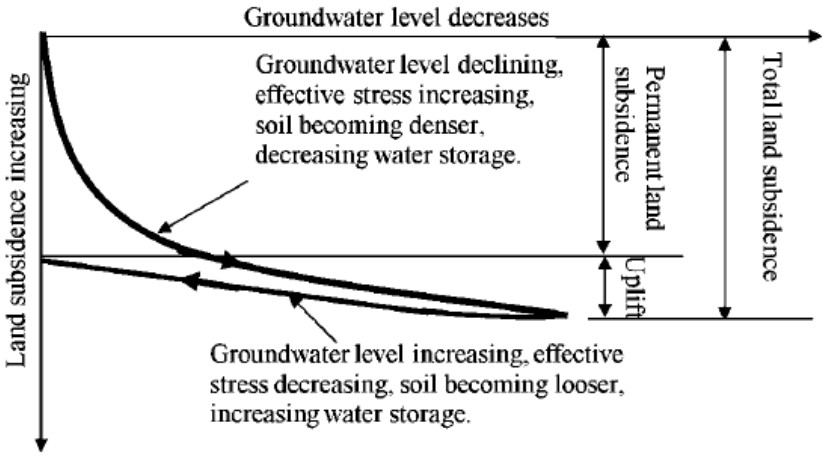

Figure 2-4: Illustration of effects of groundwater changes on land subsidence (Budhu and Adiyaman, 2010)

Fahmi et al. (2015) presented a void ratio-log(u̇) curve (see Figure 2.5) to show the nonlinear behaviour of soil under cyclic loading created by a fluctuation of the water table. The curve, based on results from FE modelling shows similar response for normally and over-consolidated soil as that presented by Knappett and Craig (2012) (see Figure 2.3). As stated by Duncan (1993) it is, therefore, important to know the stress history of soil, albeit difficult to estimate, as the immediate, total and rate of settlement will be influenced by the stress history and the ratio between immediate and total settlement is important. For over-consolidated clay, the ratio is observed to be about 0.6 while for normally consolidated clay it is generally less than 0.2 (Burland and Wroth, 1974).

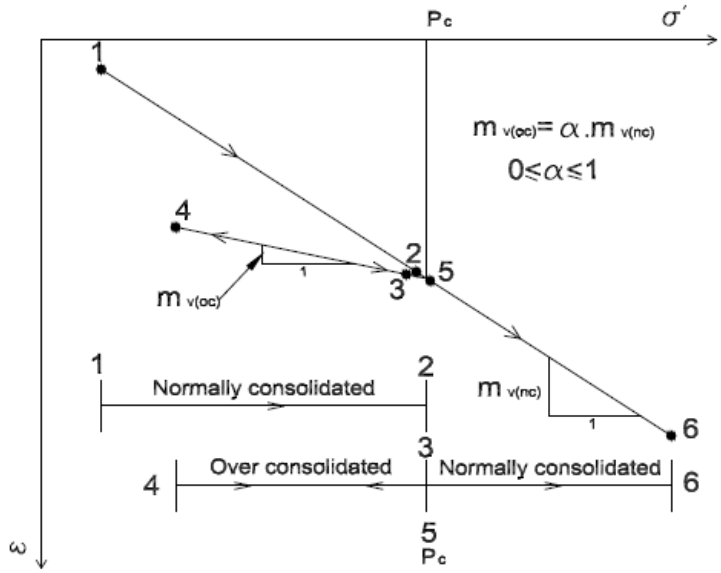

Figure 2-5: Simplified inelastic behaviour of soil under cyclic loading (Fahmi et al., 2015)

Budhu and Adiyaman (2010) deduced the effective stress increments on a volumetric soil element due to the lowering of the water table. The drop in head decrease with distance from the point of extraction until the maximum distance of influence, equivalent to Ro or Lo is reached. The distance of influence is also representative of the extent to which the cone of depression would propagate which is indicative of the differential settlement that results from lowering of the water table.

Figure 2.6, shows a volumetric soil element with the induced effective stress increase. The initial hydrostatic stresses (static pore pressures) are depicted by numbers, 1-2-3 and 4-5-6. The resultant hydrostatic stresses, due to the lowered water table are depicted by numbers, 3-7-8 and 5-9-10. The increase in effective stresses is subsequently determined from the difference between the initial and resultant hydrostatic stress states.

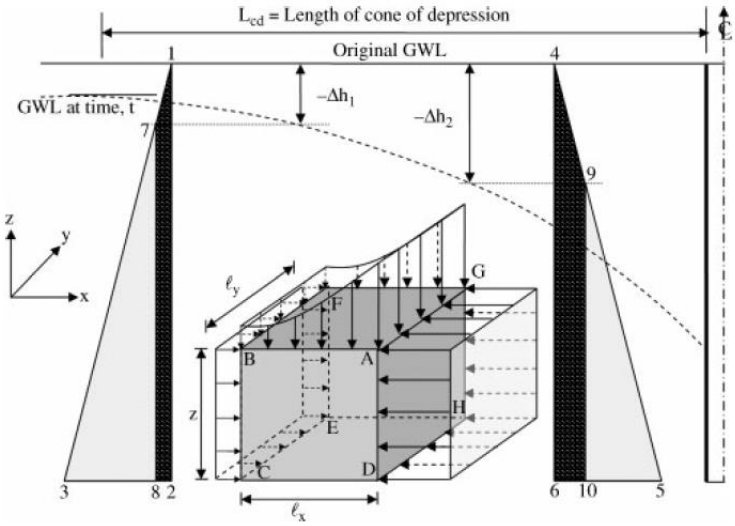

Figure 2-6: Stresses on a finite volume element (Budhu and Adiyaman, 2010)

The stresses on the volumetric element can be further decomposed into, isotropic effective stresses (Part 1) and vertical stresses increasing toward the point of water extraction, with uniform lateral compressive effective stress (Part 2). The first part of the effective stress state will induce isotropic compression of the volumetric element. The second effective stress state, on the other hand, would induce shearing on vertical micro-planes, with micro-rotation. Figure 2.7 depicts the stress states on a volumetric element with the contributing stress states.

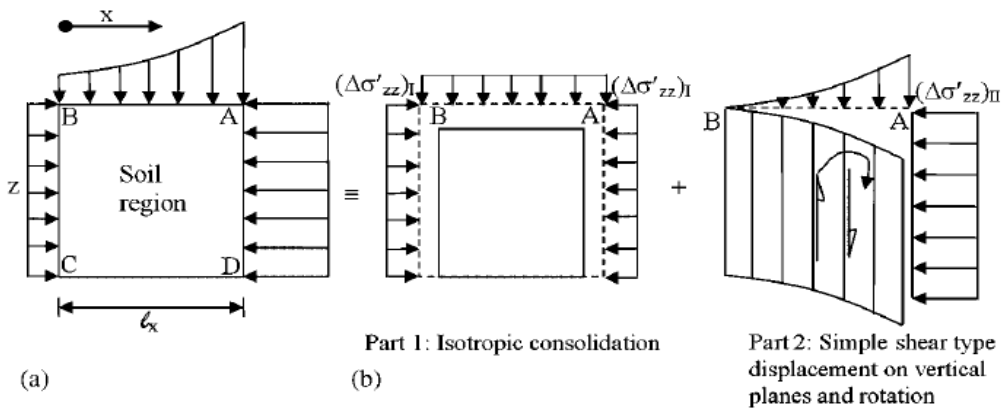

Figure 2-7: Stress changes imposed by groundwater decline in aquifers (Budhu and Adiyaman 2010)

Figure 2.8 shows the components of land subsidence due to groundwater extraction as presented by Budhu and Adiyaman (2010). Initially, soil settles due to isotropic consolidation induced by the isotropic effective stress (Part 1). Consolidation settlement due to part 2 loading ensues, accompanied by simple shearing and rotation. The settlement can take place individually or simultaneously depending on the method and the way extraction is conducted. The settlements can be superimposed to determine the total resultant settlement with time.

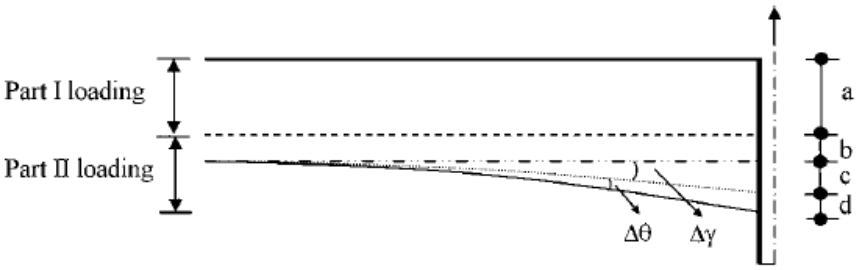

a = subsidence due to hydrostatic consolidation (compression, compaction)

b = subsidence due to consolidation settlement from simple shearing

c = subsidence due to simple shear on vertical plane

d = subsidence due rotation (when micro-rotation = macro-rotation)

Δθ = change in rotation

Δγ = change in simple shear strain

Figure 2-8: Components of land subsidence from groundwater pumping (Budhu and Adiyaman, 2010)

The limitations of consolidation theories identified by Duncan (1993) prompted further research. Yang et al. (2015) conducted a coupled FE study to analyse the effects of nonlinearity of hydraulic properties such as porosity and permeability of the soil. The author found that due to the groundwater withdrawal-induced subsidence the soil is compressed which results in decreased porosity and permeability. The decrease in permeability in regions around the area of extraction produces hydraulic gradient and seepage forces that may result in accelerated subsidence and increased horizontal ground movement.

Baú et al. (2004) conducted a parametric FE study investigating the influence of ground surface flow conditions on hydraulic drawdown and land subsidence due to subsurface fluid withdrawal. They found that the choice of boundary condition can affect land subsidence significantly. The assumption of an impermeable boundary leads to an overestimation of the subsidence, largely due to the larger pressure decline and larger horizontal pressure gradients occurring in the overburden.

Typical values for groundwater induced land subsidence can vary from a few millimetres to metres of ground settlement. The rate and total settlement are affected by (1) shallow burial depths of the pumped formations, (2) highly compressible deposits, (3) considerable pore pressure decline and (4) large thickness of the depressurised water-bearing strata, (Gambolati and Teatini, 2015). Figure 2.9 shows typical trends of vertical (△z) and horizontal (Ur) ground settlement with time as presented by Yang et al. (2014).

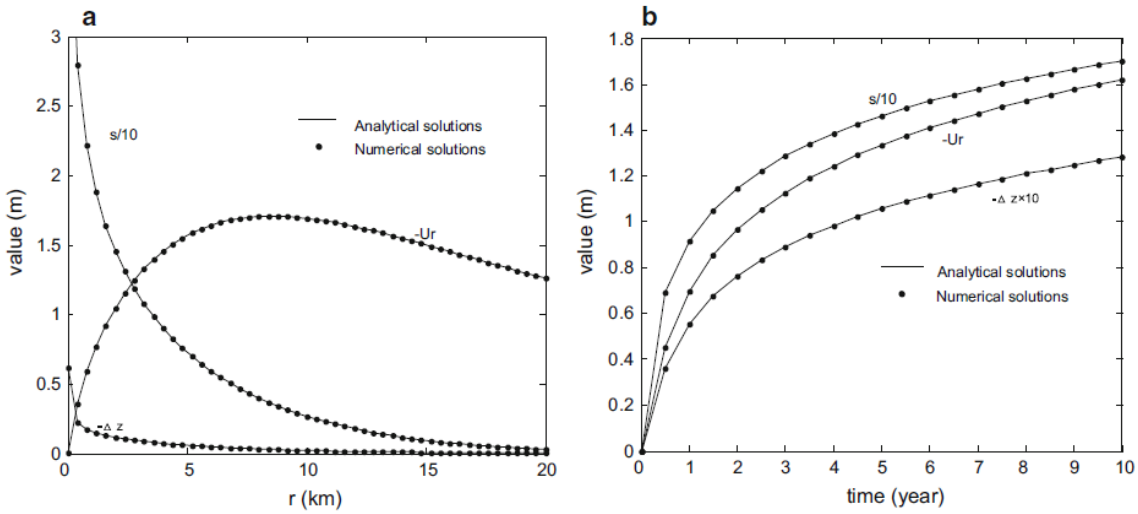

Figure 2-9: Spatial distribution and temporal change of drawdown, vertical displacement, and horizontal displacement (Yang et al., 2015)

2.3.3 Load and Soil Settlement Induced Foundation Settlement

The settlement of foundations and the geometric and material properties of structures will dictate the response of a structure to land subsidence. Therefore, although investigating foundation settlement is not aim of the study, a brief discussion on load and settlement induced foundation settlement is included. Foundations transmit structural loads safely to the bearing soil. To perform satisfactorily, foundations are designed to meet two principal performance criteria, presented graphically in Figure 2.10 (British Standards Institution., 2004; Knappett and Craig, 2012):

1. Provide sufficient bearing resistance to support applied loads, which represents Ultimate Limit States (ULS) criteria
2. Avoid excessive deformations which might lead to damage and loss of functionality of supported structure under load, which represents Serviceability Limits States (SLS) criteria.

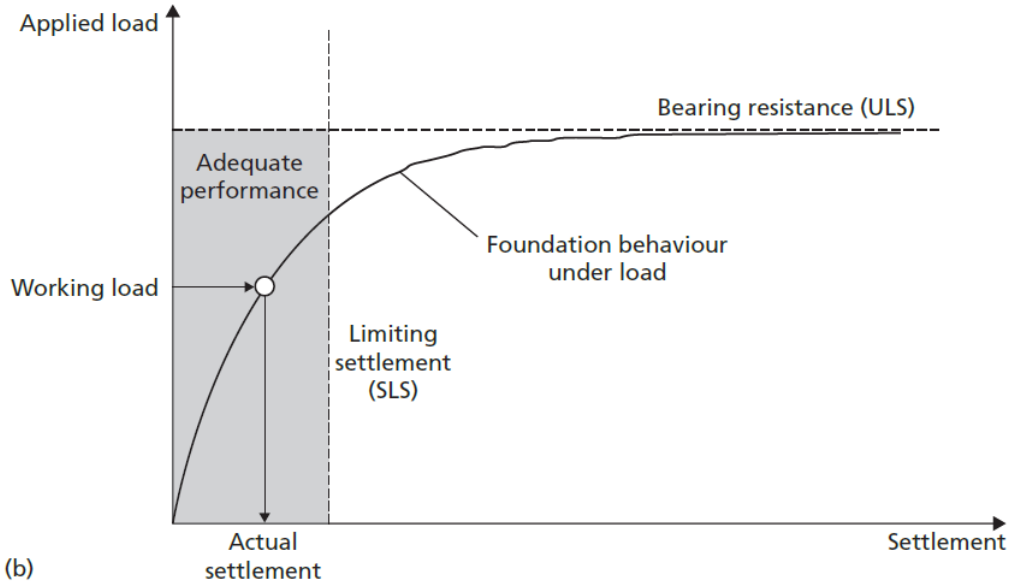

Figure 2-10: Foundation performance and limit state design (Knappett and Craig, 2012)

To estimate the suitability of foundation design, it is necessary to estimate the vertical displacement due to approximately steady loads transmitted from the structure. The typical time settlement history of a foundation is presented graphically in Figure 2.11. It is useful to determine the total settlement (S) as the sum of the three components indicated in Equation 2-13 (British Standards Institution., 2004; Fang, 1991). This settlement should be less than 50 mm (British Standards Institution., 2004).

$$S = S_i + S_c + S_s \qquad \text{Equation 2-13}$$

Where:

S = Total settlement

S_i = Immediate or distortion settlement

S_c = Consolidation settlement

S_s = Secondary settlement

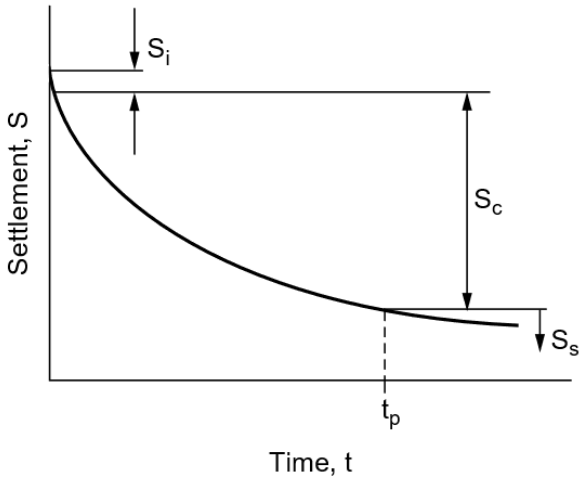

Figure 2-11: Typical time-settlement history of a foundation (Fang, 1991)

The total settlement as calculated using Equation 2-13 should, however, be evaluated in conjunction with parameters described in Section 2.4.1. The immediate component of settlement (S_i) happens concomitantly with load application, primarily because of distortion within the foundation soil structure. The remaining settlement results from the gradual expulsion of water from the voids and the simultaneous compression of the soil skeleton. The distinction between S_c and S_s is made based on the physical process which controls the time rate of settlement. Consolidation settlement refers mainly to primary consolidation, in which the time rate of settlement is controlled by the rate at which water can be expelled from the soil voids. The secondary compression settlement is dictated by the rate at which the soil skeleton itself compresses and yields (Fang, 1991).

The immediate settlement is generally not elastic although it is calculated using elastic theory. Knappett and Craig (2012) present Equation 2-14 for determining the immediate settlement (S_i), firstly for a semi-infinite, homogeneous, isotropic mass with linear stress-strain relationship.

$$S_i = \frac{qB}{E}(1 - v^2)I_s \qquad \text{Equation 2-14}$$

Where:

B = Lesser dimension in the case of a rectangular footing or the diameter for a circular footing

q = Uniform pressure below foundation

E = Young's modulus of the soil

I_s = Influence factor depending on the shape of the loaded area

v = Poisson's ratio

Values for the influence factors are presented in Table 2-4, for the centre, corner and average displacement under a flexible loaded area. Equation 2-15 indicates that the settlement is in direct proportion to both the pressure and width of the loaded area. The contact pressure between the loaded area and the supporting mass is uniform for the flexible loaded area. E, however, differs for clays and sands supporting the loaded area. In the case of clays, it is reasonable to assume that E is constant throughout the deposit and the settlement distribution in Figure 2-12(a) applies. For sands, however, E varies with confining pressure and therefore, will be greatest below the centre of the loaded area. Figure 2-12(b) depicts the resultant vertical settlement of a flexible footing on sand.

If the loaded area is rigid, infinitely stiff in bending, the displacement across the loaded area will be uniform, and its magnitude slightly less than the average displacement under a flexible area. The contact pressure distribution is also not uniform. Figure 2-13 presents the form of contact pressure distribution for a rigid footing with a circular area for sand (a) and clay (b) respectively.

Table 2-4: Influence factors for vertical displacement under flexible and rigid areas carrying uniform pressure (adapted from (Knappett and Craig, 2012))

Shape of area	I_s(flexible)			I_s(rigid)
	Centre	Corner	Average	Average
Sqaure (L/B=1)	1.12	0.56	0.95	0.82
Rectangle (L/B=2)	1.52	0.76	1.30	1.20
Rectangle (L/B=5)	2.10	1.05	1.83	1.70
Rectangle (L/B=10)	2.54	1.27	2.25	2.10
Rectangle (L/B=100)	4.01	2.01	3.69	3.47
Circle	1.00	0.64	0.85	0.79

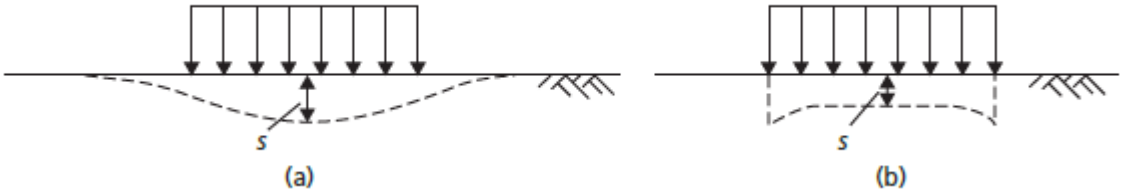

Figure 2-12: Distribution of vertical displacement beneath a flexible area: (a) clay and (b) sand (Knappett and Craig, 2012)

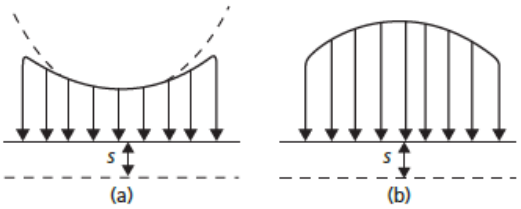

Figure 2-13: Contact stress distribution beneath a rigid area: (a) clay and (b) sand (Knappett and Craig, 2012)

For cases commonly encountered in practice, where the soil deposit is of limited thickness, i.e. underlain by bedrock, Equation 2-15 is proposed with the values for the coefficients μ_0 and μ_1 presented in Figure 2-14 (Knappet and Craig, 2012):

$$S_i = \mu_0 \mu_1 \frac{qB}{E} \qquad \text{Equation 2-15}$$

Where:

μ_0 = depends on the depth of embedment

μ_1 = depends on the layer thickness and shape of loaded area

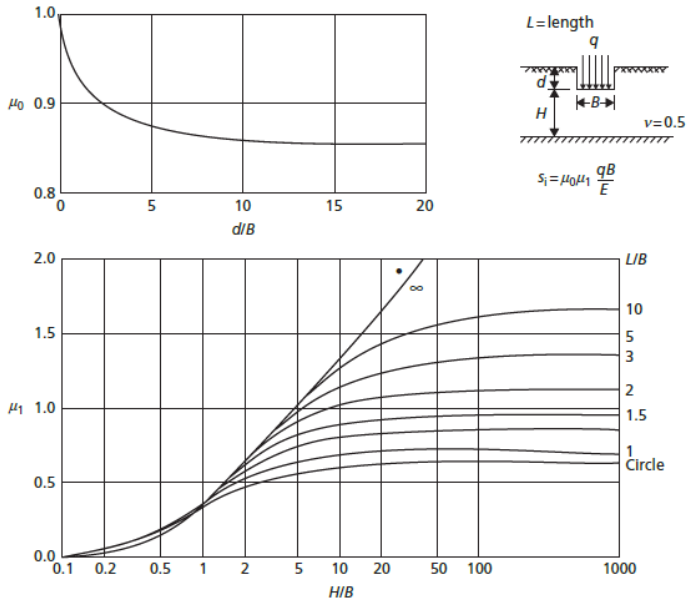

Figure 2-14: Coefficients μ_0 and μ_1 for vertical displacement (Knappett and Craig, 2012)

The values for the settlement calculations are dependent on E and v of soil in question. Due to the uncertainties in obtaining these parameters, values of vertical displacement calculated using the elastic theory are less reliable. These settlement calculations are however adequate for practical problems, provided that reliable values for the in-situ soil parameters are obtained (Knappett and Craig, 2012).

The compression settlement discussed deals mainly with load induced foundation settlement. The primary compression takes place due to an increase in total stress brought about by the applied foundation load. Groundwater withdrawal results in a decrease in the pore-water pressure which contributes to the primary consolidation settlement of the founding soil, therefore, the author theorises that the consolidation settlement should be the sum of water withdrawal and load induced consolidation as indicated in Equation 2-16:

$$S_c = S_{cl} + S_{cw} \qquad \text{Equation 2-16}$$

Where:

S_{cl} = foundation load induced consolidation settlement
S_{cw} = groundwater withdrawal induced consolidation settlement

The groundwater withdrawal-induced consolidation is of interest as the groundwater withdrawal profile will not be constant throughout. The resultant consolidation will be different for the various footings forming the foundation of the structure resulting in differential settlement of the structure. The following section, therefore, addresses the geometrical and material properties of structures that dictate the behaviour of structures due to differential settlement of the foundations.

2.4 STRUCTURAL BEHAVIOUR AND DAMAGE

From a structural engineer's point of view, a structure can be viewed as a transmitter element that safely transmits the load applied to it, from the point of application, through complex interactions, of the structural elements, slabs, beams, columns etc., to the foundations where it is resisted. Like foundations, the structure must transmit the applied loads without failing, to meet ULS criteria and without excessive deformation or cracking to meet SLS criteria (Mosley et al., 2012).

The behaviour of and damage to structures are summarised in the following point made by Wahls (1981) about buildings and settlement:

> *First, buildings should be expected to settle. Second, the differential settlement is more critical than total settlement. Third, structures and their foundations can be designed to minimise settlement. Finally, significant settlements can be tolerated without impairing the safety and function of many structures.*

2.4.1 Allowable Structural Deformation and Settlement

In assessing problems related to the settlement of structures, Bjerrum (1963) stated that engineers basically have two fundamental challenges. The first problem pertains to evaluating the allowable differential settlement a building can withstand and secondly, the prediction of what the expected total and differential settlement will be. In most buildings, it is the relative deflections that occur subsequent to application of finishes that cause damage. It should, however, be noted that it is impossible to design a building that will not show architectural damage in the form of cracks etc. Little (1969) estimated that the cost of preventing any sort of cracking could exceed 10 percent of the total building cost.

Skempton and Macdonald (1956) as well as Polshin and Tokar (1957), laid the groundwork for research pertaining to the allowable settlement of buildings while others including Meyerhof (1956), Bjerrum (1963), Little (1969), Grant et al (1974), Burland and Wroth (1974), Wahls (1994) and Charles and Skinner (2004) built on their work. Polshin and Tokar (1957) outlined an approach to define allowable differential settlement based on the assumption that the onset of visible cracking is associated with a critical tensile strain value, ϵ_{crit}. The value of ϵ_{crit} is not constant as it is dependent on several factors such as the function of a building and finishes. Acceptable strain values fall in the range of 0.05-0.1 % for brickwork and 0.03-0.05 % for reinforced concrete.

The problem associated with allowable settlements and soil structure interaction pertains to a bigger problem of serviceability and structural interaction. Numerous problems have hindered the progress made in researching the problem at hand. Burland and Wroth (1974) list the following:

1. Serviceability is subjective and depends both on the function of the building and the reaction of the users.
2. Buildings vary so much from one another, both in broad concept and in detail, that it is difficult to lay down general guidelines as to allowable movement.
3. Buildings, including foundations, seldom perform as designed because construction materials display different properties from those assumed in design. Moreover, a total analysis including the ground and the cladding would be impossibly complex and would still contain questionable assumptions.
4. As well as depending on loading and settlement, movements of buildings can be attributed to a number of factors such as creep, shrinkage, and temperature. There is as yet little quantitative understanding of these factors and there is a lack of careful measurements of the actual performance of buildings.

The complete description of the settlement of a structure requires many settlement points so that detailed contours and profiles of the foundation movement can be plotted (Terzaghi, 1935). Earlier work done on the topic of allowable settlement and damage was conducted by studying the settlement and damage of existing structures. Skempton and Macdonald (1956) studied settlement and damage observations on 98 buildings, 40 of which showed visible damage. The damage criterion used by the authors was based on the ratio (termed angular distortion) between differential settlement (δ) and the length between the two points (l) after eliminating the rigid body movement or tilt of the building. A study of allowable deformations and settlement by Polshin and Tokar (1957) yielded the following three criteria:

1. Slope – measured as the difference in settlement of two adjacent supports relative to the distance between them.
2. Relative deflection – comprising the ratio of deflection to the length of the defected part.
3. Average settlement under the building.
4. $S < S_{lim}$ – where S is the subsoil deformation determined by calculation and S_{lim}, the allowable ultimate soil deformation.

The authors also introduced an additional criterion in assessing allowable settlement for load-bearing walls, the ratio of the length (L) between panels, to the height (H). Table 2-5 shows the earlier limiting criteria presented by Skempton and Macdonald (1956), Polshin and Tokar (1957), Meyerhof (1956) and Bjerrum (1963).

Table 2-5: Limiting values from early research on allowable settlement

Author	Criteria	Limiting value	Notes
Skempton and Macdonald (1956)	Angular distortion (Frame buildings and load-bearing walls)	>= 1/1000	Avoid Settlement
		>= 1/500	Should be avoided
		>= 1/300	Cause cracking
		>= 1/150	Structural damage
Meyerhof (1956)	Angular distortion	> 1/1000	Load bearing walls
		> 1/500	Infilled frames
		> 1/250	Open Frames
Polshin and Tokar (1957)	Slopes (similar to angular distortion)	>= 1/500	Steel and concrete frame infilled structures
		>= 1/200	No infill or danger of damage to cladding
	Relative deflections (load bearing brickwork)*	L/H < 3, > 1/3300	Buildings on sand
		L/H > 5, > 1/2000	
		L/H < 3, > 1/2500	Buildings on clay
		L/H > 5, > 1/10000	
Bjerrum (1963)	Angular Distortion	> 1/750	Machines sensitive to settlement
		> 1/600	Danger for frames with diagonals
		<= 1/500	Building not cracking

*Maximum angular distortion of 1/1000 corresponds to a relative deflection of 1/2500.

The early research conducted on allowable settlement prompted Burland and Wroth (1974) to develop definitions and symbols for the description of ground and foundation movement. The following are the suggested definitions and symbols, widely adopted by various codes of practice such as the Eurocode 7: Geotechnical Design (British Standards Institution., 2004) and guidelines:

1. A change in length equal to δL over a length L gives rise to average strain $\epsilon = \delta L/L$. A shortening of $-\delta L$ over a length L gives rise to compressive strain $\epsilon = -\delta L/L$.
2. Settlement as indicated in, Figure 2-15(a), is denoted by the symbol ρ and implies that the displacement is downwards. If the displacement is upwards it is termed heave denoted by ρ_h.
3. Differential or relative settlement (or heave) denoted by $\delta\rho$ ($\delta\rho_h$). In Figure 2-15a the settlement of C relative to D is denoted by $\delta\rho_{CD}$ and is taken as positive. Settlement of D relative to C is denoted by $\delta\rho_{DC} = -\delta\rho_{CD}$. Maximum differential settlement is denoted by $\delta\rho_{max}$.
4. Rotation is denoted by θ as indicated in, Figure 2-15(a), and is used to describe the gradient of the straight line joining two reference points embedded in the foundation or ground.

5. Tilt is denoted by ω and normally describes the rigid body rotation of the whole superstructure or a well-defined part of it.

6. Relative rotation is denoted by β and describes the rotation of a straight line joining two points relative to the tilt, as indicated in Figure 2-15(b). This is identical to angular distortion defined by Skempton and Tokar (1957).

7. Angular Strain is denoted by α. It can be seen from Figure 2-15(c) that the angular strain at B is given by is given by Equation 2-17:

$$\alpha_B = \frac{\delta\rho_{BA}}{l_{AB}} + \frac{\delta\rho_{BC}}{l_{BC}} \qquad \text{Equation 2-17}$$

8. Relative deflection is denoted by Δ, as indicated in Figure 2-15(d) and is the maximum displacement relative to the straight line connecting two reference points at a distance L apart. Relative sag produces upward concavity for which Δ is positive.

9. Deflection ratio is denoted by Δ/L, Figure 2-15(d) with the same sign convention as in 8.

No attempt was made to define three-dimensional behaviour such as warping, however, the definitions are adequate to describe most types of in-plane deformation. Furthermore, the definitions relate to foundation and ground movement and description of the superstructure behaviour was not intended as standard terminology.

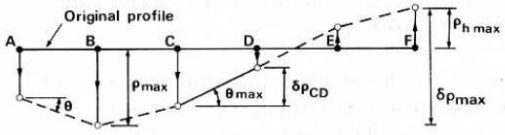

Figure 1a Definitions of settlement ρ, relative settlement $\delta\rho$ and rotation Θ

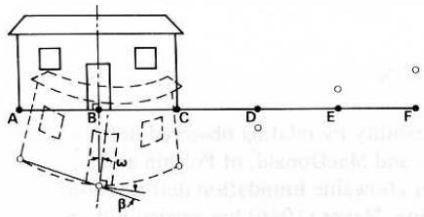

Figure 1b Definitions of tilt ω and relative rotation (angular distortion) β

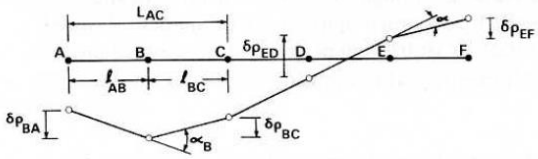

Figure 1c Definition of angular strain α

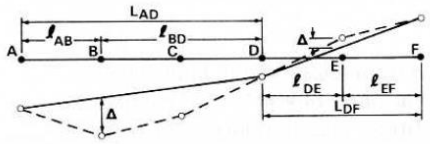

Figure 1d Definition of relative deflection (sag or hog) Δ and deflection ratio (sagging or hogging) Δ/L

Figure 2-15: Foundation deformation definitions and symbols (Burland and Wroth, 1974)

Charles and Skinner (2004) built on the work done by the preceding authors in their study of settlement and tilt of low-rise buildings. The authors stated that the significance of foundation movement is dependent on the magnitude of foundation movement that is tolerable for buildings and their occupiers and is a complex function of:

- The purpose of the building
- The ownership of the building
- The type of building superstructure
- The type of foundations
- The nature of the ground conditions

The authors also presented acceptable limits of values of tilt for different types of structures (see Table 2-6).

Table 2-6: Limiting values of tilt for different types of structures (adapted from (Charles and Skinner, 2004))

Structure or component	Tilt
Radar system	1/50000
Satellite antenna tower	1/6000
Machine operation: turbine	1/5000
Warehouse high racking	1/2000
Concrete tanks	1/500
Crane rails	1/333
Chimneys, towers	1/250
Stacking of goods	1/100
Floor drainage	1/100-150

Burland and Wroth (1974) noted that buildings become unserviceable before any risk of structural failure. Therefore, there was a need to move away from empirical deflection criteria and study fundamental causes of damage. The following section aims to establish the criteria and causes of structural damage due to ground movement.

2.4.2 Structural Damage

The preceding sections evaluated the allowable vertical settlement of foundations and the allowable deformations buildings can experience before structural damage is evident. Burland and Wroth (1974) continued their research on allowable settlement and evaluated the consequent damage to structures if set limits were exceeded. Since then, several other researchers have investigated ground-movement induced settlement, the most notable being Boscardin and Cording (1989), Boone (1996), Zhang and Ng (2004) and Son and Cording (2005).

Burland and Wroth (1974) in their study of structural damage, applied the concept of a critical strain to a simple structure such as a uniform, weightless, elastic beam of length (L), height (H) and unit thickness. The study of a simple beam helps to illustrate several important features even though real structures are a lot more complex. The aim was to calculate the strain in the beam and define a criterion for initial cracking. It was assumed that the deflected shape at the soffit of the beam is known and the two extreme modes of deformation namely: bending only and shear only were considered. For the bending only case, cracking will be initiated by direct tensile strain at the extreme fibre. For the shear only case, cracking will result from dithe agonal tensile strain. Although it is more realistic that both modes of deformation will take place simultaneously they will, initially, be considered separately. Figure 2-16 depicts the problem at hand.

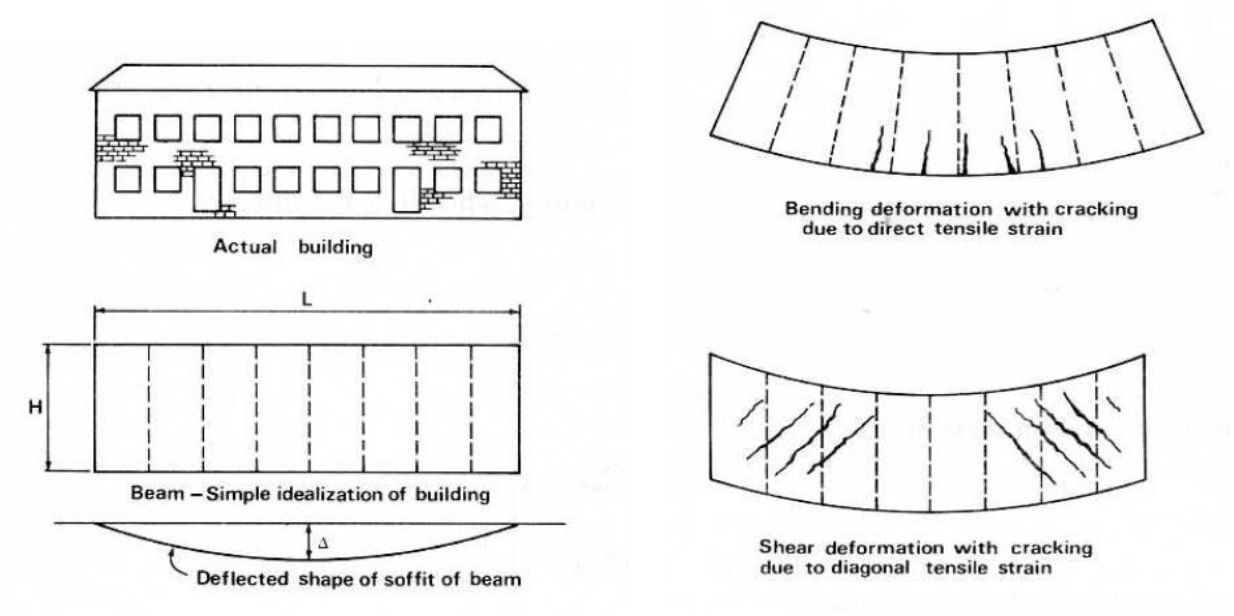

Figure 2-16: Simplified model for the determination of critical strain (Burland and Wroth, 1974)

After evaluating the modes of deformation individually, the authors evaluated the combined effects of bending and shear deformation. The expression presented by Timoshenko (1957) for the central deflection of a centrally loaded beam of unit thickness is used to determine the extreme fibre strain, $\epsilon_{b\,max}$, and maximum diagonal strain, $\epsilon_{d\,max}$ vs the deflection ratio. The extreme fibre strain can be calculated from Equation 2-18:

$$\frac{\Delta}{L} = (\frac{L}{12t} + \frac{3EI}{2yLGH})\epsilon_{b\,max} \qquad \text{Equation 2-18}$$

The maximum diagonal strain can be calculated from Equation 2-19:

$$\frac{\Delta}{L} = (1 + \frac{HL^2G}{18IH})\epsilon_{d\,max} \qquad \text{Equation 2-19}$$

Where:

E = Young's modulus
G = Shear modulus
t = In-plane thickness of the wall
y = Distance to the neutral axis
I = Second moment of inertial
L = Length of beam
I = Depth of beam

The relationships were plotted for v = 0.3 and E/G = 2.6, for a point and uniformly distributed load in Figure 2.17, and for various E/G values in Figure 2.18. It is evident from Figure 2.18 that the limiting value of $\frac{\Delta}{L\epsilon_{crit}}$ for diagonal strain is one. The limiting value for direct strain in bending decreases as L/H increases, reaching a minimum of 0.66 at L/H = 2.0, where after the limiting value increases gradually. Furthermore, it can be concluded that the relationship between ϵ_{max} and L/H is insensitive to the type of loading. Figure 2.18 indicates that the most desirable structure for minimising tensile strain for a given value of Δ/L is one that is relatively flexible in shear, i.e. large value of E/G. For a structure stiff in shear relative to its horizontal stiffness, the direct strain due to bending dominates.

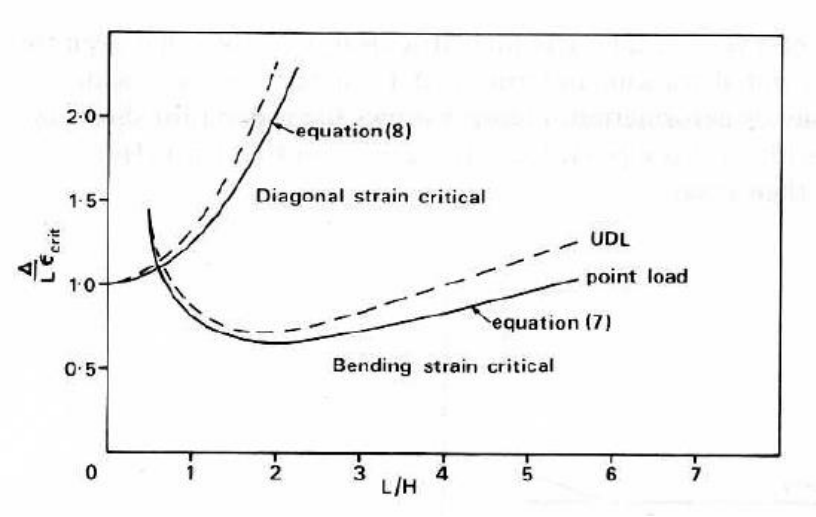

Figure 2-17: Relationship between $\frac{\Delta}{L\epsilon_{crit}}$ and L/H for rectangular beams deflecting due combined bending and shear - neutral axis in the middle (Burland and Wroth, 1974)

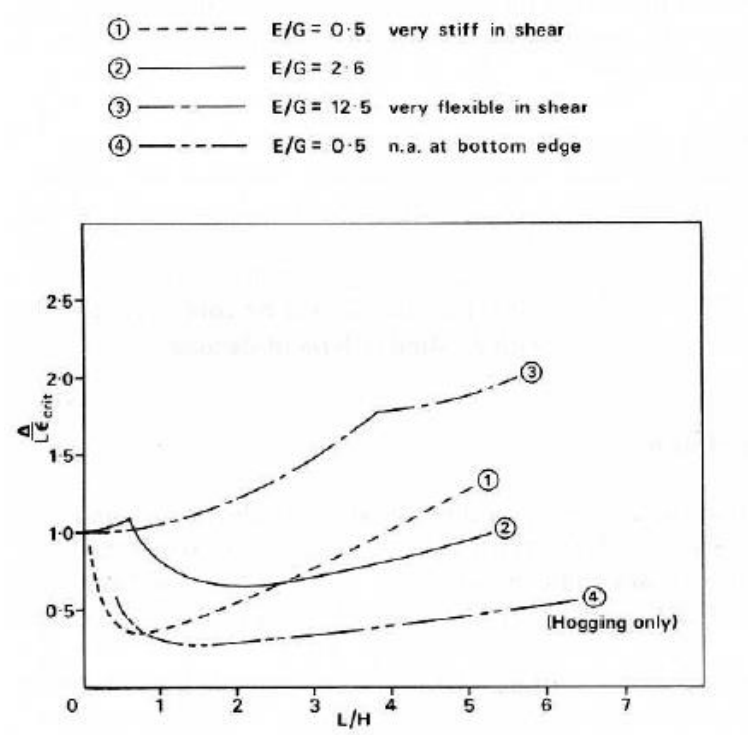

Figure 2-18: Relationship between $\frac{\Delta}{L\epsilon_{crit}}$ and L/H for rectangular beams deflecting due to combined bending and shear - neutral axis at the bottom (Burland and Wroth, 1974)

Boscardin and Cording (1989), recognised that buildings deforming due to ground movement, unlike buildings settling under own weight, has a substantial component of horizontal strain. Including the horizontal strain in the above formulation would, therefore, result in failure at smaller values of differential settlement and angular strain. The critical tensile strain was therefore modified as indicated in Equation 2-20 to have two components when the edge of the beam is in tension due to bending:

$$\epsilon_{crit} = \epsilon_{b\,max} + \epsilon_h \qquad \text{Equation 2-20}$$

Where:

$\epsilon_{b\,max}$ = Extreme fibre strain

ϵ_h = Horizontal strain at extreme fibre

For the case of diagonal tension with horizontal extension, the tensile strain, ϵ_θ, at any angle θ from the horizontal can be calculated using Equation 2-21:

$$\epsilon_\theta = \epsilon_h cos^2\theta + 2\epsilon_{d\,max} \cos\theta sin\theta \qquad \text{Equation 2-21}$$

The maximum value of $\epsilon_{\theta\,max}$ can expressed as indicated in Equation 2-22:

$$\epsilon_{crit} = \epsilon_{\theta\,max} = \epsilon_h cos^2\theta_{max} + 2\epsilon_{d\,max} \cos\theta_{max} sin\theta_{max} \qquad \text{Equation 2-22}$$

The values for $\epsilon_{b\,max}$ and $\epsilon_{d\,max}$ can then be replaced into the equations presented by Burland and Wroth (1974. It should, however, be noted that the determination of angular distortion (β) is different because of the addition of horizontal strain and it can be determined using Equation 2-23:

$$\beta = \frac{3\Delta}{L}\left[\frac{1 + 4\left(\frac{E}{G}\right)\left(\frac{H^2}{L^2}\right)}{1 + 6\left(\frac{E}{G}\right)\left(\frac{H^2}{L^2}\right)}\right] \qquad \text{Equation 2-23}$$

For typical values of L/H and E/G encountered in the field, β will vary between $2\Delta/L$ and $2.3\Delta/L$. Figure 2-19 shows the effect of E/G, for bending and shearing for a range of L/H.

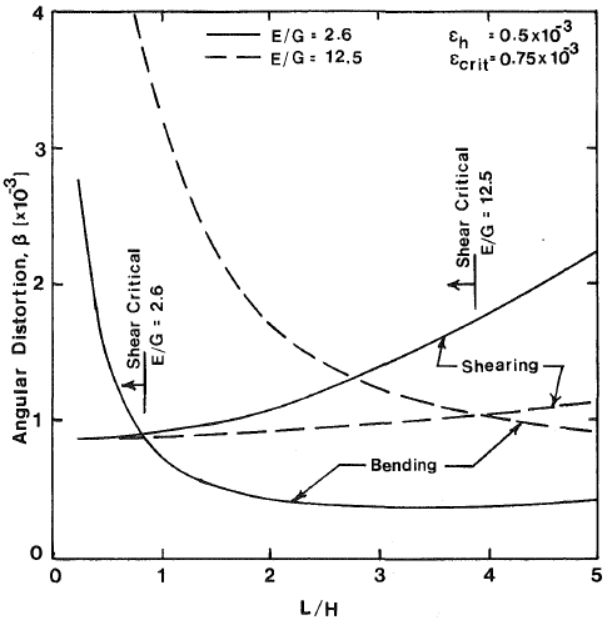

Figure 2-19: Effect of E/G ratio on a range of L/H where shearing is critical (Boscardin and Cording, 1989)

Burland et al. (1978) categorised building damage in the following categories:

- Aesthetic – affects only the appearance of the property (negligible to slight).
- Serviceability – cracking and distortion which impairs the weather tightness or other functions (moderate and severe).
- Stability – there is an unacceptable risk that some part of the structure will collapse unless preventative action is taken (very severe).

Table 2-7 presents the classification for visual damage based on the approximate crack width and ease of repair ranging from, negligible to very severe. It, however, only applies to masonry and blockwork. This criteria only relate to visual damage at a given time and it does not take into account its cause or possible progression.

Table 2-7: Classification of visual damage (Burland et al., 1978)

Class of Damage	Description of damage	Approximate width of cracks [mm]
Negligible to very slight	Hairline cracks	<0.1
Slight	Fine cracks easily treated during redecoration. Perhaps isolated slight fracture in building. Cracks in exterior brickwork visible upon close inspection	<1
Moderate	Cracks may require cutting out and patching, Recurrent cracks can be masked by suitable linings. Tuck-pointing and possibly replacement of a small amount of exterior brickwork may be required. Doors and windows sticking. Utility service may be interrupted. Weather-tightness often impaired.	5 to 15 - or several cracks >3 mm
Severe	Extensive repair removal and replacement of sections of walls, especially over doors and windows required. Windows and door frames distorted, floor slopes noticeably. Walls lean or bulge noticeably, some loss of bearing in beam. Utility service disrupted.	15 to 25 - depends on number of cracks
Very Severe	Major repair required involving partial or complete reconstruction. Beams lose bearing, walls lean badly and require shoring. Windows broken by distortion. Danger of instability.	Usually >25 - depends on number of cracks

Boscardin and Cording (1989) present a graph (see Figure 2-21), relating the visual damage to horizontal strain and angular distortion. The upper boundaries for damage are based on results for critical strain obtained from earlier research.

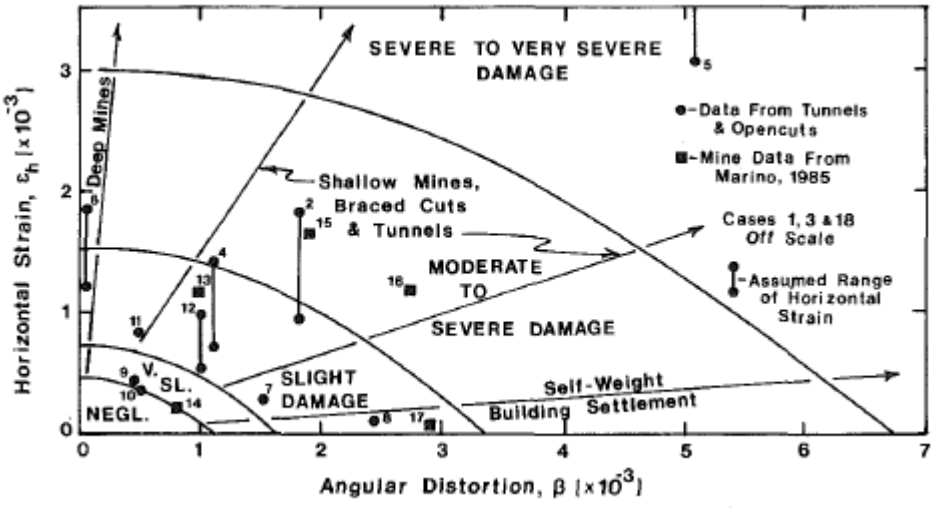

Figure 2-20: Relationship of damage to angular distortion and horizontal extension strain (Boscardin and Cording, 1989)

Charles and Skinner (2004) presented the expected damage in terms of settlement, distortion and tilt of foundations as follows:

- Uniform settlement – a building should not be adversely affected by uniform settlement, however, there could be problems with connection of services.
- Uniform Tilt – Tall structures could become unstable.
- Distortion without tilt – can cause serious damage to structures. For traditional brick and masonry structures, the damage will be much more severe where ground deformations give rise to upward bending. Cracking of walls is also dependent on factors such as length to height ratio of the wall.
- Distortion and tilt – will be dependent on the type of building but would entail a combination of the above problems.

The mitigation of structural damage and remedial action is also discussed by authors such as Charles and Skinner (2004), Son and Cording (2005) and Cashman and Preene (2013). The following are suggestions presented by the authors:

- Controlling construction procedures.
- Changing construction methods.
- Ensuring structural integrity.
- Increasing support stiffness.
- Improving the ground.
- Reinforcing foundation and structures.
- Avoidance of settlement.
- Re-levelling the building.
- Reduce the number of structures at risk.
- Selecting a different site.

Structural damage is a subjective area of research as criteria that would define damage to any structure would be difficult to determine. Structural behaviour and damage will not only be dictated by the geometric and material properties of the structure but will be highly dependent on the soil-structure interaction. With the allowable settlement, deformation and damage of structures determined, the following section will focus on the effects of soil-structure interaction on the settlement, deformation and damage to structures.

2.5 SOIL-STRUCTURE INTERACTION

The interaction between a structure and the soil it is founded on is a complex problem that starts with construction and continues throughout the design life of the structure. It is a combination of several different factors, none of which are linear, some of which are time-dependent. It would be impossible to consider these effects separately and then superimposing the results without introducing errors and approximations. Burland and Wroth (1974) presented the following factors that need to be considered for investigations of soil-structure interaction:

1. The immediate settlements caused by each increment of loads as the structure grows.
2. The long-term consolidation settlements (both primary and secondary) which overlap with the immediate settlements and of which a major proportion might occur during construction.
3. The changing stiffness of the structure as the building progresses.
4. The redistribution of loads and stresses within the structure due to differential settlement.

Several authors over the years investigated these effects simultaneously or individually while keeping in mind the approximations and errors introduced. Burland and Wroth (1974) with authors such as Jardine et al., (1986), Noorzaei et al., (1993), Noorzaei et al (1995), Breysse et al., (2005), Frantziskonis and Breysse, (2003), Smit (2010) and Mitropoulou et al., (2016) attempted to better understand the problems associated with soil-structure interaction and identified the salient features.

Furthermore, Noorzaei et al., (1993), postulated that the settlement, contact pressure and the bending moments in an elastic combined footing are affected by the structural stiffness, interconnection between columns and combined footings and the compressibility of the subsoil. The relative soil/structure stiffness is, therefore, an important parameter in assessing the soil-structure interaction. Potts and Addenbrooke (1997), defined a relative bending stiffness (ρ^*) of a building using Equation 2-24:

$$\rho^* = \frac{EI}{E_s H^4} \qquad \text{Equation 2-24}$$

Where:

E = Young's modulus of the structure

E_s = Young's Modulus of the founding soil

I = Second moment of inertia of the structure

H = Half the width of the superstructure in the plane of deformation

Potts and Addenbrook (1997) present two methods for the determination of the building bending stiffness. The first approach utilises the parallel axis theorem to define the structural stiffness about the neutral axis as shown in Equation 2-25:

$$(E_c I)_{stiffstruct} = E_c \sum_{1}^{n} (I_{slab} + A_{slab} h^2) \qquad \text{Equation 2-25}$$

Where:

E_c = Young's modulus of the concrete

I_{slab} = Second moment of area of the slab

A_{slab} = Cross sectional area of the slab

h = Height to the neutral axis of the building

Where n is the number of storeys. Since only a rigidly framed structure would deform in such a manner, this method is deemed to overestimate the bending stiffness of a structure. The alternative method for the determination of bending stiffness is obtained by summing the independent EI values for each slab. The formulation is presented as equation 2-26:

$$(E_c I)_{flexible} = E_c \sum_{1}^{n} I_{slab} \qquad \text{Equation 2-26}$$

Arapakou and Papadopoulos (2012) in their study of factors affecting differential settlement of framed structures define a relative rigidity factor (R) for a beam or foundation on elastic soil as indicated in Equation 2-27:

$$R = \frac{EJ}{E_s l^3} \qquad \text{Equation 2-27}$$

Where:

J = The moment of area for the foundation or slab

l = Span length of the frame or the width of the foundation.

Araparkou and Papadopoulos (2012) chose to use the moment of inertia as opposed to the second moment of area used by Potts and Adenbrooke (1997) to represent the geometrical properties of the structure. Son (2003) on the other hand, in contrast to the previous authors, chose to use shear stiffness for the structure instead of Young's modulus. He presented the relative soil-structure stiffness using Equation 2-28:

$$relative\ soil/structure\ shear\ stiffness\ = (\frac{E_{soil}L^2}{G_{build}Hb}) \qquad \text{Equation 2-28}$$

Where:

G_{build} = Elastic shear modulus of the building

L = Length of building portion subjected to ground movement

H = Height of the building

b = building wall thickness

It is evident from the three-different formulations of the relative stiffness that, relative stiffness could be dependent on the type of structure (frame or loadbearing brickwork) and the mode of deformation (shear or bending) that dictates. Furthermore, if the geometric properties of the structure are constant, it is evident that for all three formulations a decrease in structural stiffness will result in a decrease in the relative structure-soil stiffness. The opposite is true for the soil stiffness.

Son and Cording (2005, 2007, 2010) studied building damage due to excavation-induced ground movements. The study entailed the estimation of the behaviour of stiff and flexible structures on stiff and soft soil due to a free-field ground settlement simulating ground movement induced by excavations. They concluded that structures founded on stiff soils distorted more than structures founded on softer soils for the same free-field soil settlement. This was because of the soil modification by the structures on soft soils. Furthermore, stiffer structures distorted less, before cracking, than softer structure. After cracking, the stiffer structures responded in the same manner as flexible structures, due to a reduction in stiffness.

Smit and Clayton (2011) investigated the behaviour of modern flexible framed structures undergoing differential settlement. The magnitudes of column loads at ground level, for a 5x5 bay structure, was used as an indication of the structural behaviour. A concrete stiffness and a range of soil stiffnesses from 100 Pa to 1000 GPa, was used to determine the behaviour of the frame. Figure 2-21, shows that the column loads vary significantly throughout the soil stiffness range. For a softer soil, the corner and edge columns carry the largest load with the load decreasing for the edge and internal columns and increasing for the corner columns as the soil stiffens. The authors, furthermore, used ρ^* (see Equation 2-24) presented by Potts and Adenbrooke (1997) to determine three distinct zones of structural behaviour as follows (schematically presented in Figure 2-22):

- Zone 1, Flexible Structure: ρ^* typically less than $1x10^{-4}$. Structural loads can be considered without taking differential settlement into account.
- Zone 2, Intermediate Structure: ρ^*typically ranges from $1x10^{-4}$ to $1x10^{-1}$. The loads in the edge and corner columns increase and the loads in the internal columns decrease with an increase in the number of columns with an increase in ρ^*.
- Zone 3, Rigid Structure: ρ^* typically larger than $1x10^{-1}$. Structure is rigid in comparison to the soil. The loads, stresses and differential movements within the structure are constant and independent of the relative bending stiffness.

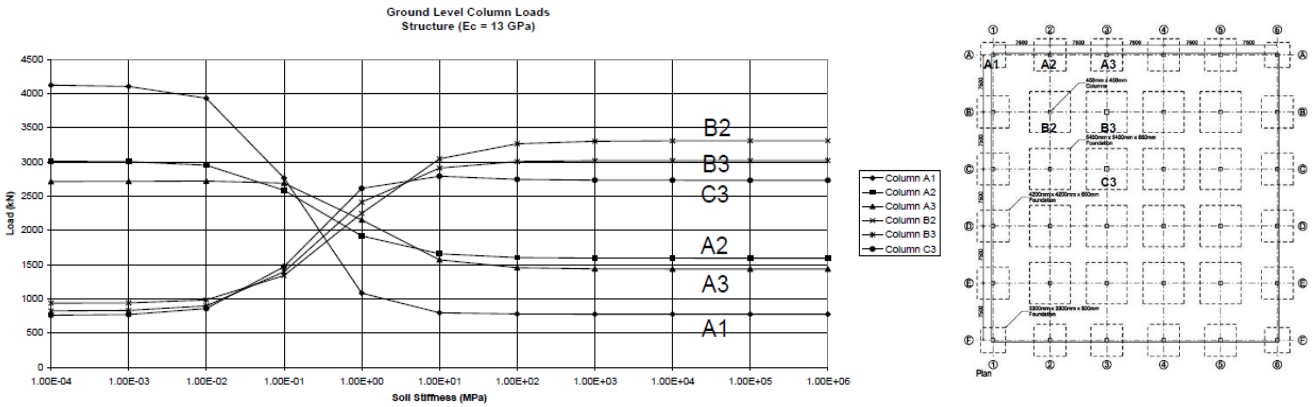

Figure 2-21: Ground level column loads (Smit and Clayton, 2011)

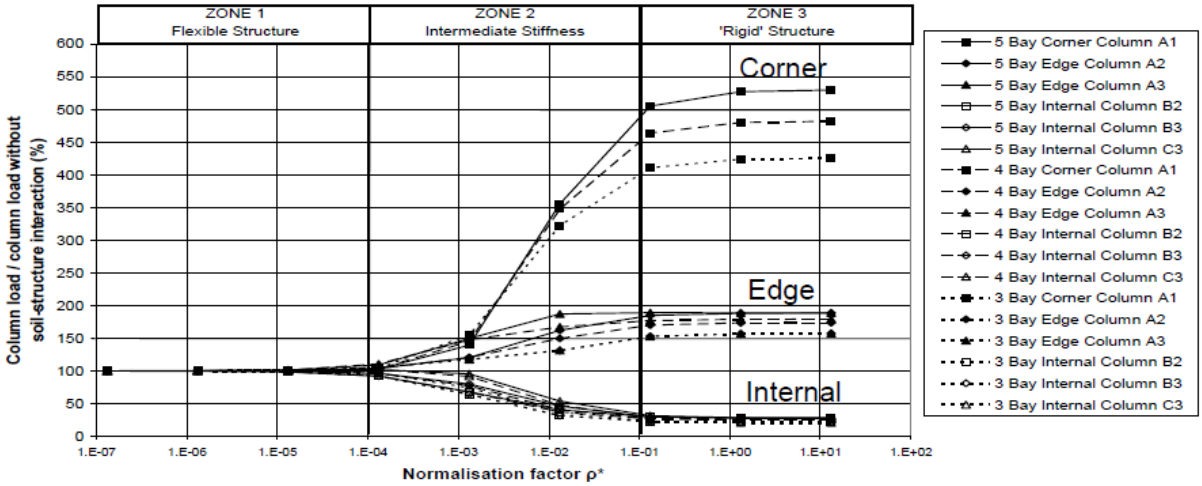

Figure 2-22: Structure normalisation (Smit and Clayton, 2011)

2.6 SUMMARY

A review of the relevant literature pertaining to the topics of groundwater, groundwater withdrawal and consequences, structural behaviour and damage, as well as soil-structure interaction, was carried out in this chapter. The following was deduced from the literature:

- Soil can be a two-phase or three-phase material and the static pressure in soil is dictated by the level of the water table or phreatic surface. The flow of water through soil is dictated by the presence of a hydraulic head and the porosity and permeability of the soil.
- Darcy's law gives an indication of the key factors affecting groundwater flow which are vital for understanding how groundwater can be manipulated by withdrawal systems. Knowledge of the prevailing geological water-bearing soil strata is important as the behaviour of groundwater flow and soil response will be governed by it. The zone of influence, the area of groundwater and propagation of the cone of depression will also be affected by the geological formations.
- The design of groundwater withdrawal systems should be aimed at developing a workable and economical solution. It should be purpose orientated and should optimise the well type, spacing and pump size for the prevailing geological conditions.
- Groundwater withdrawal can have major environmental consequences. Land subsidence is one of the major anthropogenic consequences of groundwater withdrawal, others including the formation of ground fissures and the activation of pre-existing shallow faults.
- Problems involving soil volume change, deformation and strength require separate consideration of stress that is carried by the soil grain assemblage and that carried by the water and fluid. The grain assemblage can resist shear and normal stresses whereas the fluid can only resist normal stresses.
- The principle of effective stress presented by Terzaghi states that the total normal stress on a soil assemblage is the sum of pore-water pressure and the effective normal stress on the grain assemblage. The principle of effective stress also asserts that the effective stress controls the stress-strain, behaviour volume change and strength of the soil.
- The process of consolidation is due to the dissipation of excess pore pressure induced by an increase in the pore pressure from its static state. The process continues until all the excess pore pressure has dissipated through the drainage of pore-water through a free-draining boundary of the soil formation. The process can be instigated by a load applied to a saturated volume of soil or the by groundwater withdrawal.

- Groundwater withdrawal-induced soil settlement induces a stress state on soil that results in differentially settling soil strata. The stress state comprises of isotropic consolidation and simple shear type displacement and rotation.
- Structures are founded on soil and induce stress in the soil formation, therefore load induced soil settlement was also considered. Foundations should be designed to limit structural stresses in the soil thus preventing excessive deformations and failure. The settlement of foundations is due to the sum of three components, namely: Immediate settlement, consolidation settlement and secondary settlement.
- Foundation structures must be able to transmit applied loads to the soil without excessive deformation and failure. The allowable deformation of structures is however subjective and dependent on various factors, such as the type and purpose of the building, occupants and the nature of the ground it is founded on.
- Although structural damage and failure are dependent on various factors, it is generally accepted that structures are deemed unserviceable long before structural failure occurs. Structural damage and failure are also generally associated with excessive movement of its foundations.
- Finally, soil-structure interaction is important in assessing the behaviour of a structure. The ultimate behaviour of a structure in service is dependent on the geometrical and material properties of the structure and the soil properties. The concept of relative structure soil stiffness is therefore vital in the assessment of structures.

Research pertaining to groundwater extraction induced ground movements is mainly limited to numerical and analytical models. There is a lack of knowledge pertaining to physical modelling of groundwater extraction induced ground movements and the behaviour of structures founded within the zone of influence of groundwater extraction. The latter parts of this chapter indicted the detrimental effects excessive ground movements can have on structures. Therefore, this study was undertaken to address these issues.

The following chapters present a centrifuge study and discussion of the results of the investigation of the above-mentioned phenomena.

3 RESEARCH METHODOLOGY

Anthropogenic land subsidence can be a critical consequence of groundwater extraction from aquifers as discussed in the literature review. Groundwater extraction from aquifers causes a reduction in the pore-water pressures within an aquifer and in the presence of compressible soils induces land subsidence. The extraction processes are, however, conducted from localised positions within an aquifer which causes the water table to lower differentially inducing differential soil settlement. These extraction processes, furthermore, increase the seepage thereby increasing the seepage forces acting on the soil particles and inducing horizontal ground movement within the aquifer. Groundwater extraction-induced ground movements are primarily investigated using numerical and analytical models for which certain assumptions are made which induce errors, albeit to a practically accepted degree. Discussions in the literature review, furthermore, showed the detrimental effects ground movements could have on structures founded within the zone of influence and that these structures can alter the ground movements induced by different stimuli. There is, however, a lack of information in quantifying the response of structures founded within the zone of influence and the alteration of ground movements induced by groundwater extraction. The complex relationships between the pore water, the soil and structures, in the form of portal frames, founded within the zone of influence during groundwater extraction prompted an investigation into these relationships using physical models in the form of small scale geotechnical centrifuge modelling. The centrifuge models were set-up to investigate the following relationships:

- Groundwater extraction and the differential drawdown of the water table
- Drawdown of the water table and pore-water response
- Pore water response and soil settlement
- Drawdown of the water table and ground movements
- Interaction between portal frames and induced ground movements
- Response of portal frames to induced ground movements

The centrifuge models comprised of silica sand modified with vermiculite confined in a centrifuge strongbox. Pressure transducers were used to measure the pore-water pressure, while linear variable differential transducers (LVDTs) were used to measure the soil settlement. Ground movements were tracked by means of digital image correlation (DIC). The induced ground movements were first investigated in the groundwater extraction-soil interaction tests (GSI). The soil-portal frame interaction and the response of four portal frames, with varying stiffness, to the ground movements, were investigated in the groundwater extraction-soil-structure interaction tests (GSSI). Figure 3-1 depicts the layout of the two centrifuge tests. The various components of the centrifuge tests are discussed in the following sections.

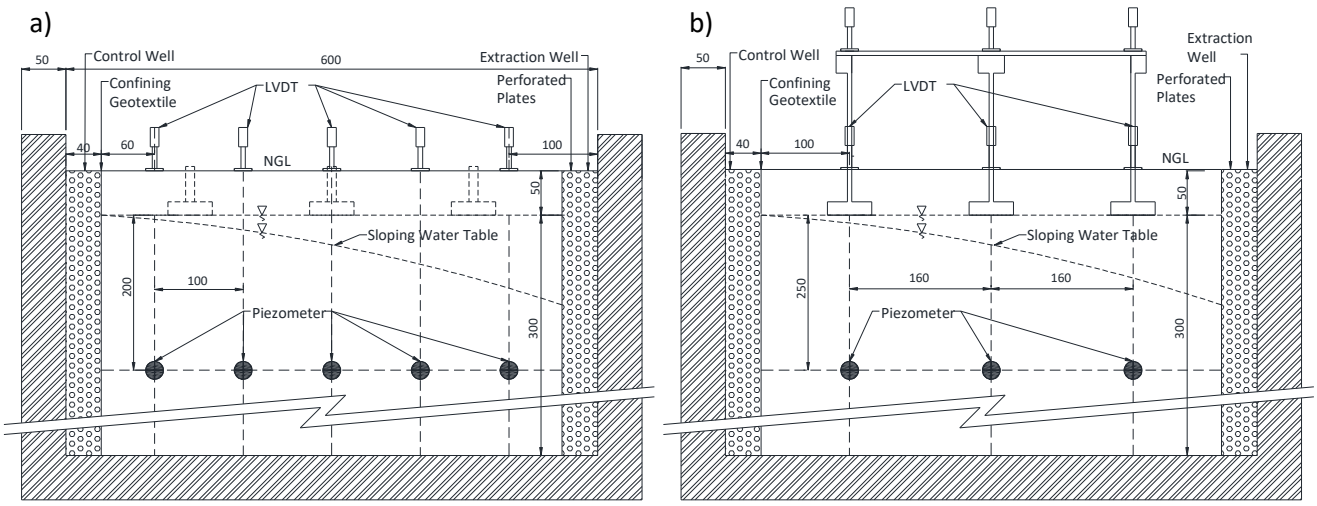

Figure 3-1: Schematic side view of centrifuge tests a) GSI Test, b) GSSI Test

3.1 GEOTECHNICAL CENTRIFUGE MODELLING

Centrifuge modelling is used to replicate the correct self-weight and stress-strain behaviour of soil and surface structures in scaled models to those of full-scale models/prototypes (Schofield, 1980; Taylor, 1995; Jacobsz, 2013; Ritter et al., 2017(a)). The kinematic, geometric, and dynamic relationships of the full-scale soil-structure interaction thus need to be replicated in the scaled model for the models to have the correct self-weight and stress-strain behaviour (Laefer et al., 2011). Geotechnical centrifuges are, therefore, used to elevate the gravitational field at which testing is conducted through centripetal acceleration of the models to replicate the correct self-weight and stress-strain behaviour.

3.1.1 Scaling Laws

The effect of increased gravitational acceleration on a model varies for various physical properties of a model. To obtain a required material property and/or geometrical requirement at an accelerated field, the appropriate scaling laws need to be applied. Table 3-1 shows the relevant scaling laws as presented by Jacobsz (2013). The testing for this study was conducted at a model acceleration of 30 g which corresponds to a model scale (n) of 30.

Table 3-1: Centrifuge scaling laws (Jacobsz, 2013)

Property	Scale Factor
Model Scale	n
Accelerations	n
Linear Dimensions	1/n
Stress	1
Strain	1
Density	1
Mass	$1/n^3$
Force	$1/n^2$
Bending Moment	$1/n^3$
Moment of Area	$1/n^4$
Time (consolidation)	$1/n^2$
Time (dynamic)	1/n
Time (creep)	1/n
Pore Fluid Velocity	n

3.1.2 University of Pretoria Geotechnical Centrifuge Facility

The experimental set-up preparation and testing were conducted at the University of Pretoria centrifuge facility, which is equipped with an Actidyn C67-4 centrifuge with a 0.8 m x 1.0 m x 1.3 m model platform/gondola (Jacobsz et al., (2014). The centrifuge arm radius, measured from the rotational axis to the gondola is 3 m. The centrifuge can support a payload of 1500 kg to an acceleration of 100 g or 950 kg to 130 g (Jacobsz et al., 2014). Figure 3-2 shows a photograph of the Actidyn C67-4 at the centrifuge laboratory (University of Pretoria, 2014).

A series of electric and fibre optic slip rings enable power and data systems to be supported, with fluid slip rings enabling air and water to be supplied to the centrifuge and centrifuge gondola during operation. These are all controlled remotely from the control computers situated in the centrifuge control room during operation of the centrifuge.

Figure 3-2: Geotechnical centrifuge at the University of Pretoria (University of Pretoria, 2014)

A strongbox with a window was used to confine the soil and water and to house the measuring instrumentation and structural frames. Two slotted partitioning plates, covered with a geotextile were used to create the extraction and control wells, 400 mm x 380 mm x 40 mm in size. A rigid steel plate, 520 mm x 350 mm x 5 mm, was also used to separate the box into soil investigation and structural investigation zones for the groundwater extraction-soil-structure interaction (GSSI) while the groundwater extraction-soil interaction (GSI) tests were conducted without the rigid plate.

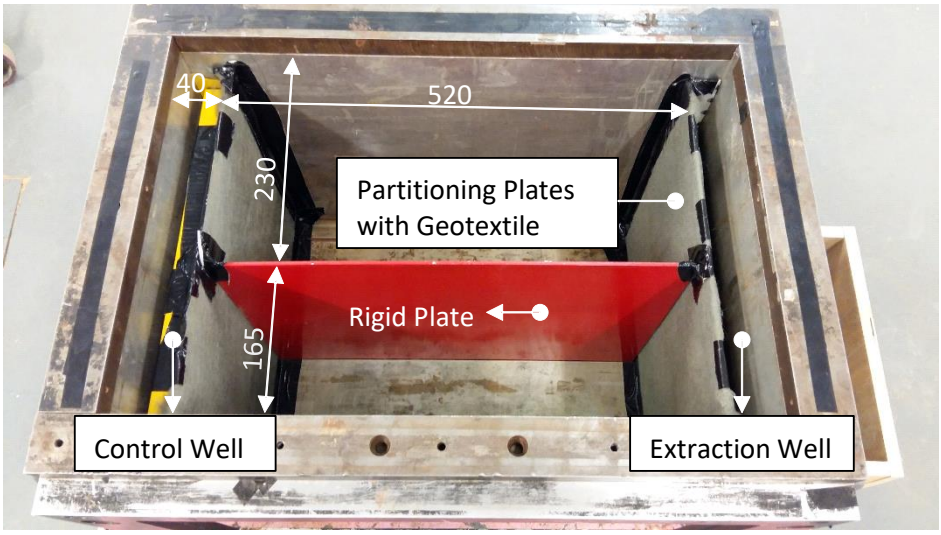

Figure 3-3: Centrifuge strongbox

3.2 EXPERIMENTAL MODEL

The centrifuge model set-up was designed to investigate the groundwater extraction induced ground movement and the response of the portal frames to the ground movements. The model comprised of modified silica sand confined in a strongbox with the initial water table at foundation founding level to model an unconfined aquifer. The water table was drawn down differentially to simulate a sloping water table in an aquifer as that created during groundwater extraction in aquifers. This section presents the materials and portal frames used during the centrifuge tests as well a description of the aquifer.

3.2.1 Modified Silica Sand

The geotechnical testing was conducted with modified fine silica sand obtained from a source near Cullinan, east of Pretoria. Archer (2014) determined the soil classification as poorly graded, slightly silty sand according to the Unified Soil Classification System (USCS) (ASTM Standard D2487, 2011). The particle size distribution (see Figure 3-4) was determined by sieve analysis and a Malvern Mastersizer 2000 apparatus (Archer, 2014). The physical properties of the Cullinan sand are also presented in Table 3-2 (Archer, 2014).

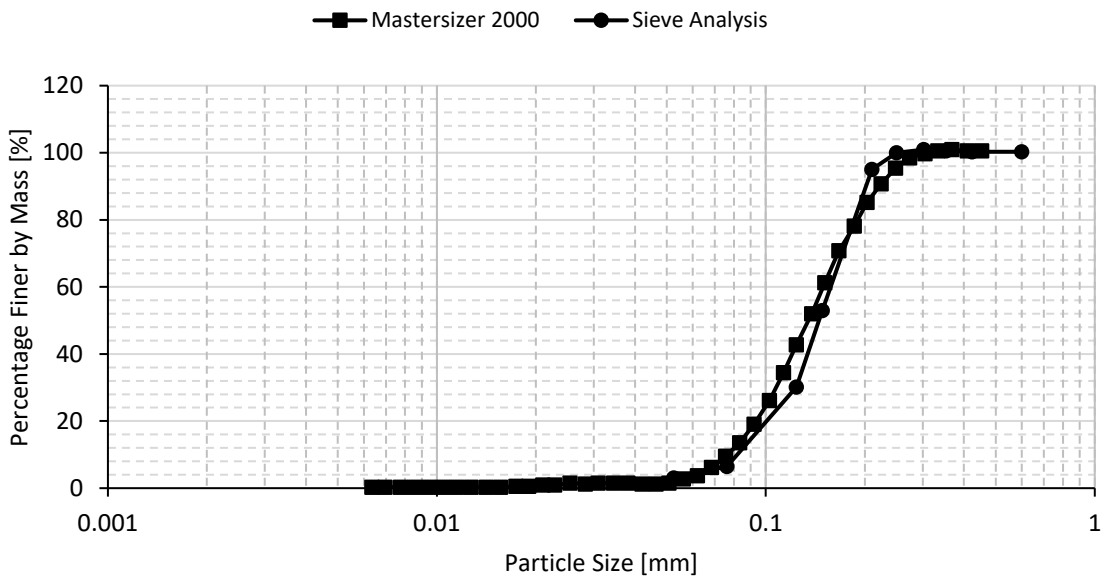

Figure 3-4: Particle size distribution of Cullinan sand (adapted from (Archer, 2014))

Table 3-2: Properties of Cullinan sand (Archer, 2014)

Property/Parameter	Value
D_{10} [mm]	0.077
D_{30} [mm]	0.108
D_{50} [mm]	0.135
D_{60} [mm]	0.150
Uniformity Coefficient, C_u	0.195
Max Dry Density (kg/m^3)	1669
Min Dry Density (kg/m^3)	1392
e_{max}	0.920
e_{min}	0.600
Specific Gravity	2.670
Particle Shape	Angular to sub-rounded
USCS Classification	SP

The Cullinan sand was modified by adding 10 % vermiculite by mass to increase the compressibility of the soil as it was desired to use a material that would undergo significant compression during dewatering. Three vermiculite percentages were considered, namely: 10, 20 and 30 % by mass. The compressibility of the soil, measured by the change in thickness of the samples under loading during the oedometer tests (see Figure 3-5), increased due to an increase in percentage vermiculite, but the permeability also increased. The soil permeability dictated the degree to which the water table could be controlled during centrifuge testing. Therefore, the lowest percentage vermiculite mixture was used, as it still resulted in an acceptable increase in compressibility while possessing sufficiently low permeability to differentially draw down the water table. The maximum and minimum dry density of the soil was determined according to the ASTM standard D4253-00 and ASTM standard D4254-91 as 1277 kg/m^3 and 1099 kg/m^3 respectively.

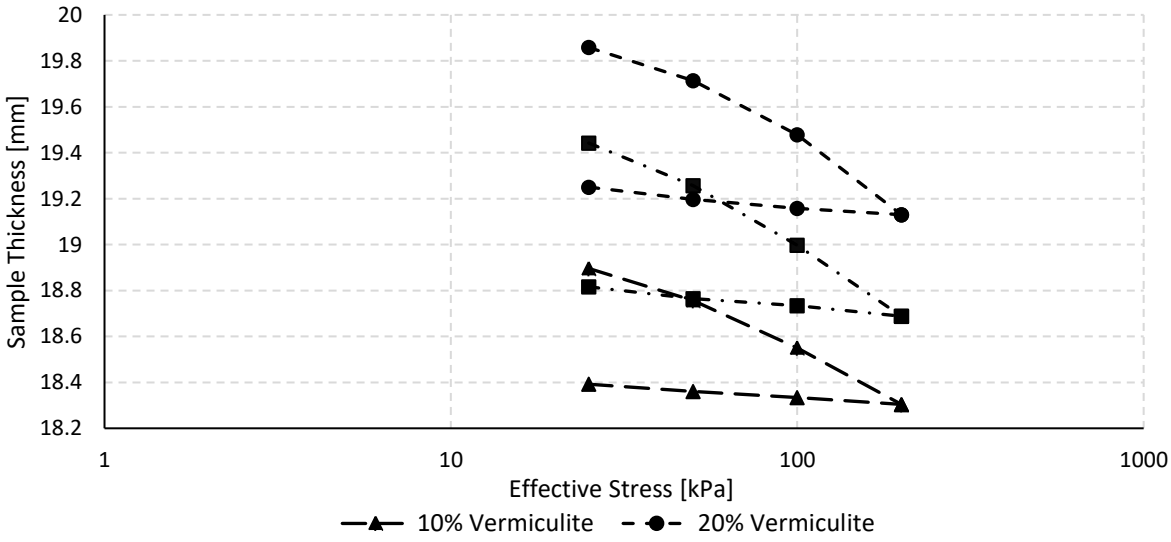

Figure 3-5: Oedometer soil compressibility results

3.2.2 Portal Frames

The soil structure interaction and the response of the portal frames to the imposed ground movements were investigated by assessing the response of plane strain two-bay single storey portal frames. Four frame configurations were considered with varying representative local and global structural stiffness. The local structural stiffness relates to the relative slab-column stiffness and the global structural stiffness relates to the overall structural stiffness. Two slab and column thicknesses of 5 and 10 mm were considered. By doubling the thickness, the second moment of inertia, I ($I = (bt^3/12)$), was increased 8 times with the width (b) of the members remaining constant. This relates to a slab/column of 10 mm having a bending stiffness (EI) 8 times greater than that of a slab/column of 5 mm.

Table 3-3 shows the model scale properties of the portal frames. The formulae presented by Potts and Addenbrook (1997) used to determine the bending stiffness of a building (Equation 2-25 and 2-26) do not yield representative structural stiffness values for the various frames configurations and loading conditions considered for the study. Therefore, the representative local and global stiffness values of the frames for the study were determined as indicated in Equations 3-1 and 3-2:

$$Local\ Stiffness/Relative\ factor = \frac{I_{Slab}}{I_{Column}} \qquad \text{Equation 3-1}$$

$$Global\ Stiffness = I_{slab} + \frac{I_{Column}}{N} \qquad \text{Equation 3-2}$$

Where:

I_{Column} = Moment of Inertia of column

I_{slab} = Moment of inertia of slab

N = Number columns

Table 3-3: Structural frame slab and column thickness

Structural Frame	Slab Thickness [mm]	Column Thickness [mm]	Frame Mass [kg]	Local Stiffness factor	Global Stiffness [mm^4]
Frame 1	10	10	5.030	1	27500
Frame 2	5	5	3.430	1	3437.5
Frame 3	5	10	4.450	0.125	15468.75
Frame 4	10	5	4.020	8	15468.75

Frames 1 and 2 have representative local stiffness of 1 while the representative global stiffness of Frame 1 was 8 times greater than Frame 2. Frames 3 and 4, on the other hand, had an equal representative global stiffness but Frame 3 had a representative local stiffness factor of 8 and Frame 4 a representative local stiffness factor of 0.125.

To achieve the required column and slab thickness, each of the structural frame columns were machined from a solid block of aluminium with a computer numerically controlled (CNC) milling machine. The column, footing and column head were milled as a single continuous piece. The plane strain portal frames see Figure 3-6 (a) Frame 1, (b) Frame 3, (c) Frame 4 and (d) Frame 2 were designed with column spacing, centreline to centreline, of 160 mm and the in-plane width equal to 165 mm. The columns were connected to the slab with 5 countersunk M5 screws spaced at 33.75 mm (see Figure 3-7). The slab-column connections were therefore assumed as fixed. The assumption was confirmed during strain measurement using strain gauges. The countersunk screws were configured such that the slabs and columns could be used interchangeably to create the four frames. The notation used hereafter when referring to the portal frames was based on the slab-column, Frame (slab-column), stiffness with a plus referring to rigid member and a minus referring to a flexible member i.e. Frame 1 = Frame (++) (see Figure 3-6).

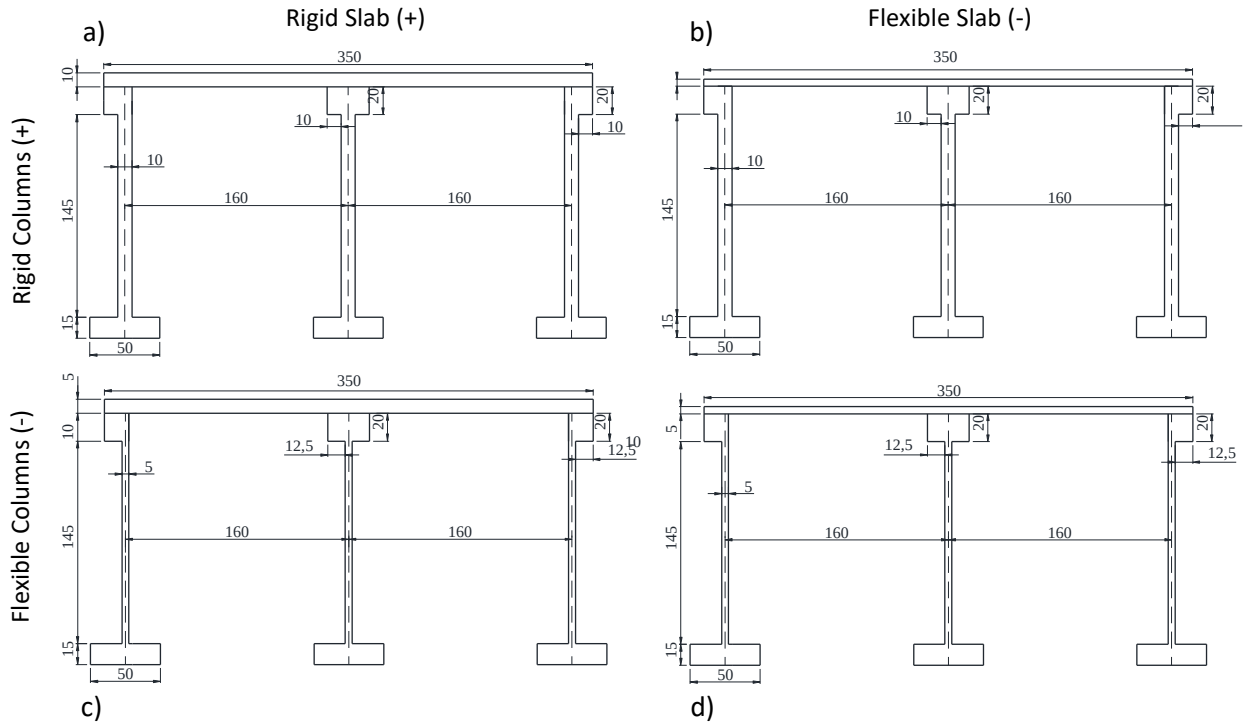

Figure 3-6: Structural frames

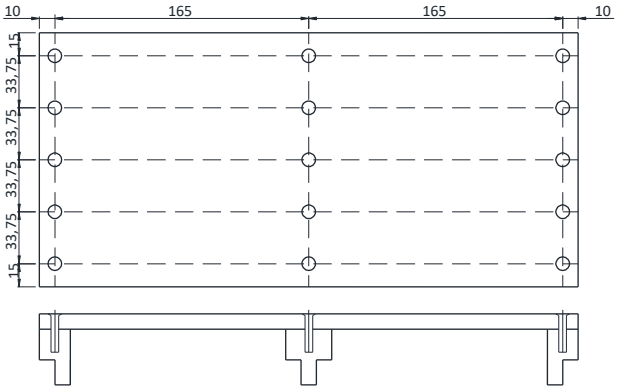

Figure 3-7: Slab-column connections

The portal frames were instrumented with HBM 3/350 LY13 strain gauges (HBM, 2017). The positioning of the strain gauges (see Figure 3-8) were determined with the aid of preliminary finite element analysis conducted on the portal frames. To fully capture the response of the structural frames and utilise the limited and localised measuring capability of the strain gauges effectively, three positions were identified to be instrumented and grouped as follows:

- Edge wall measurements – two-quarter bridges configured such that bending and axial strain could be determined from the resultant strain, gauges, 1 & 2 and 7 & 8 (see Figure 3-7).
- Column-Slab connection measurements – bending and axial strain at the connection, on the slab, measured with quarter bridges, gauges 3, 4, 5 and 6 (see Figure 3-7).
- Span measurements – bending strain at maximum mid-span measured with half bridges, gauge 9 and 10 (see Figure 3-7).

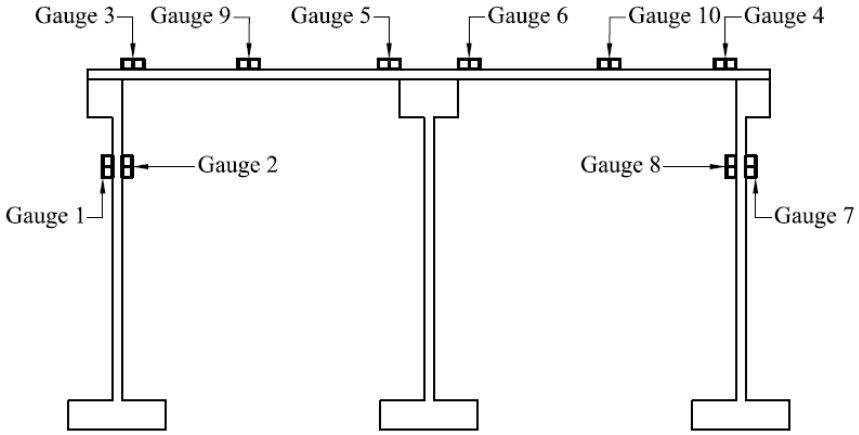

Figure 3-8: Strain gauge numbering and positioning

The frame slabs were loaded with a dead load corresponding to 15 kPa at 30 g. The structural frames were loaded with steel strips, 165 mm x 10 mm x 7 mm and with slots, 20 mm x 10 mm x 2 mm machined in-line with the strain gauges for the protection of the strain gauges. The average mass of the steel loading strips was 85 grams. Figure 3-9 shows the loading strips on the structural frame. The strip configuration allowed the strips to move independent of each other, therefore maintaining the load as the frame distorted, while also not influencing the stiffness of the frame.

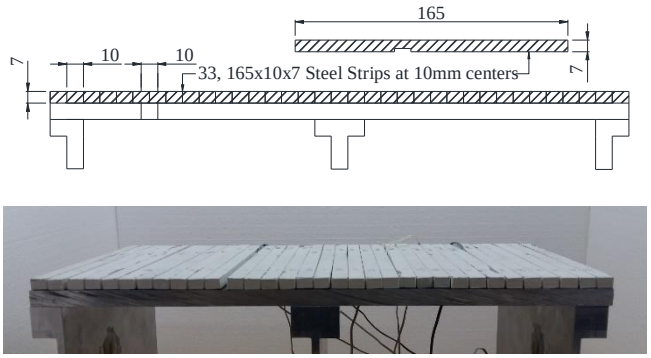

Figure 3-9: Frame loading

3.2.2.1 Effect of portal frame stiffness

FE modelling was used to investigate the effect the stiffness of the different column and slab thicknesses had on the response of the portal frames. The literature reviewed (see Section 2.5) showed that the load distribution and response of structures are dependent on the structural stiffness and the relative stiffness between the structural elements as well as the relative stiffness between the structure and the soil. The literature also showed that the determination of the stiffness of a structure is a difficult process and researchers such as Burland and Wroth (1974) and Smit and Clayton (2011) have used representative structural stiffness to differentiate between structures with varying geometrical and material properties and subsequently different responses. Therefore, no attempt was made to tie the response of the portal frames to a specific stiffness value in this study and the representative local and global stiffness values were used to differentiate between the portal frames.

Two different methods were used to investigate how the frame stiffness differed due to the different slab-column stiffness values and how this influenced their response. A FE model was set up where the structural elements were modelled with quadratic beam elements and the self-weight of the frames ignored so that only the response as a function of the stiffness was investigated.

For the first method, the two edge columns were fixed against rotation and translation at the foundation while a unit load was applied at the base of the central column. A representative vertical and horizontal stiffness was determined in the relevant direction by dividing the unit force by the resultant translation at that point, an approach similar to that utilised for spring stiffness (Kassimali, 2011). Figure 4-10

presents the resultant stiffness for the four portal frames as well as representative frames with varying column and slab stiffness of 7 and 8 mm to populate the graph. Two distinct zones can be identified from the graph divided by a line. All frames with a local/relative stiffness of one plot along the line with Frames (++) and (--) at the ends of this line. As the global stiffness of the frames increased the frames plot further along the line. The frames with a local stiffness factor greater than one, such as Frame (+-), plotted above the line as the vertical stiffness was much greater than the horizontal stiffness. The expected governing mode of deformation due to the imposed differential settlement of the foundations for these frames would, therefore, be a bending-type deformation. Frames with a local stiffness factor less than one, such as Frame (-+) plotted below the line as the horizontal stiffness was much greater than the vertical stiffness. The expected governing mode of deformation due to the imposed differential settlement of the foundations for these frames would, therefore, be a shear-type deformation.

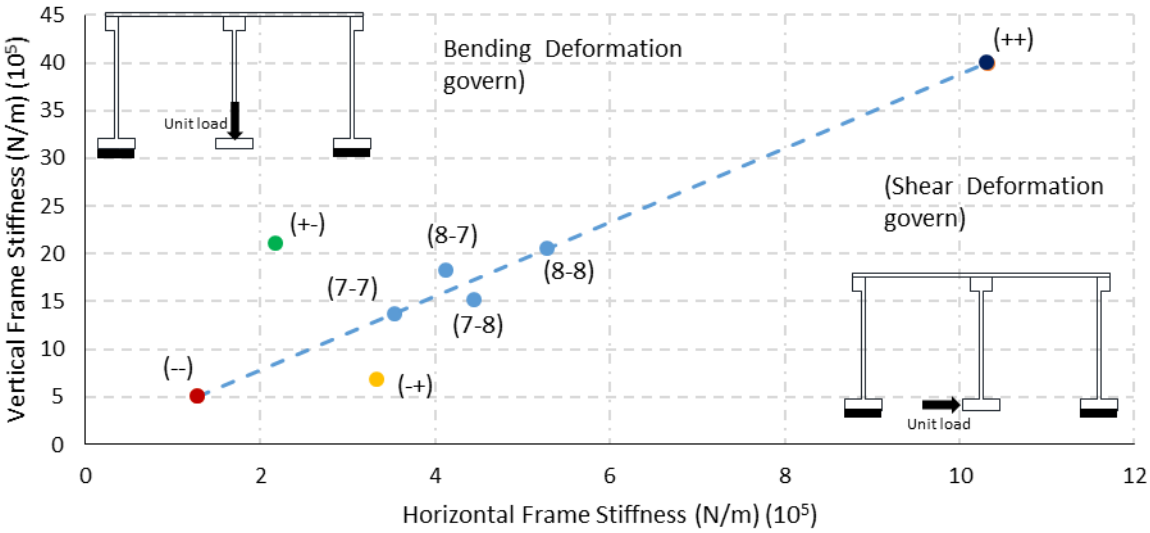

Figure 3-10: Vertical and horizontal frame stiffness

The second method was similar to that used by Smit and Clayton (2011). The columns were founded on spring elements with a specific stiffness and loaded with by a distributed load of 15 kPa. The stiffness of the springs were increased from a point where the structural stiffness was much greater than the stiffness of the supporting springs to a stiffness where the springs could be considered as completely rigid supports. Compressive column loads were taken as negative. Figure 3-11 shows the central and edge column loads of the four portal frames as the support stiffness varied. Three distinct zones of column loads were identified from the graph. In zone 1 there was no difference between the load in the edge and central columns for the frames as well as between the different frames. In this zone, the frames were much stiffer than the supporting springs. The response of the frames within this zone was similar to the response of the structures within Zone 1 identified by Smit and Clayton (2011) (see Section 2.5). As the support stiffness increased the loads within the central columns started to increase while decreasing for the edge columns (zone 2). Zone 3 started where column loads remained constant with

an increase in the support stiffness. The difference in load between the edge and central columns was greatest for Frame (+-) and the least for Frame (-+). This shows that increasing the local stiffness factor resulted in a greater difference in load between the edge and central columns. There was, however, no difference between the edge and central column loads for Frames (++) and (--) in zone 3 which shows that even though Frame (++) had rigid slab and columns that the distribution in column load was determined by the local stiffness factor which was 1 for both frames.

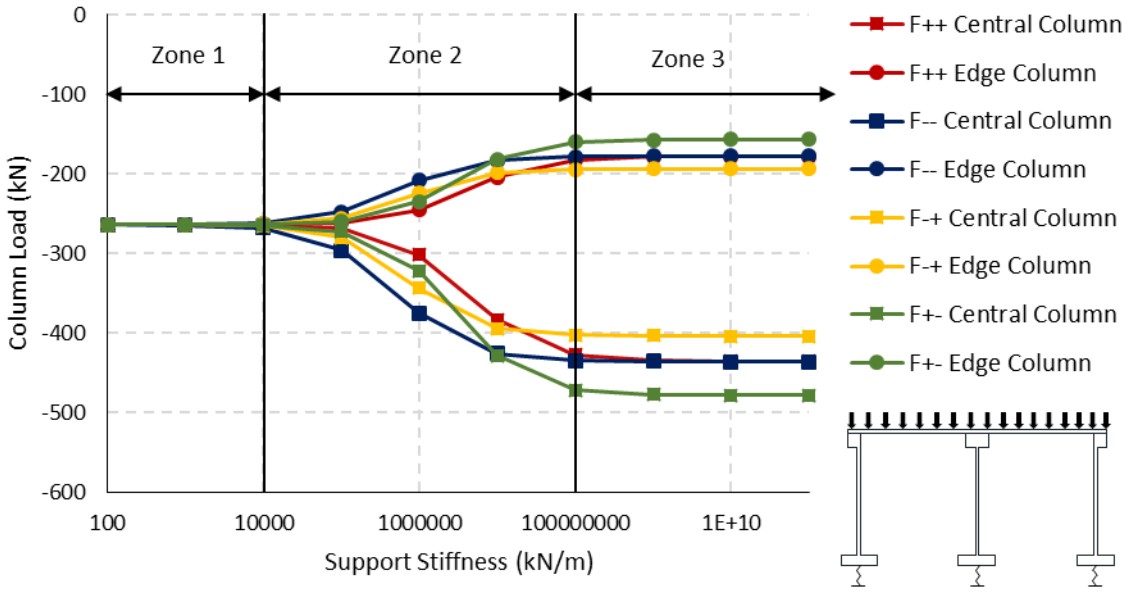

Figure 3-11: Column load distribution

The two methods complemented each other in assessing the effect of the frame stiffness and the load response of the frames. The first method showed the effect of relative frame stiffness on the expected governing mode of deformation and corroborates well with that presented by Burland and Wroth (1974). The second method showed the effect of the portal frame stiffness on the load distribution of the different frames for various support stiffness values.

3.2.3 Groundwater Simulation

The centrifuge model was designed to simulate an unconfined aquifer, with an impermeable boundary at its base. The aquifer comprised of a single homogeneous soil profile. Table 3-4 indicates the geometrical properties of the aquifer. The initial groundwater table was established at the founding level, at a depth of 50 mm below the ground surface level (see Figure 3-1). The centrifuge water supply inlet was connected to the control well which was used to control the groundwater in the model. Three solenoid valves and a pressure gauge were connected to the base of the extraction well to enable the simulation of groundwater extraction during testing (see Figure 3-22).

Table 3-4: Aquifer geometrical properties

Property	Full Scale [m]	Model Scale [mm]
Length	15.6	520
Width	12.0	400
Depth	9	300

The rectangular extraction well simulated a trench extraction well which made the plane strain assumption valid for the groundwater flow and resultant ground movement. The water table was drawn down from the extraction well while controlled from the control well, which resulted in a sloping water table throughout the modelled aquifer. Results from preliminary testing indicated that the optimum inflow rate to maintain a differential drawdown of groundwater table was 60 l//h.

3.3 INSTRUMENTATION

3.3.1 Piezometers and Pressure Gauge

The simulated groundwater response to drawdown was measured with two types of pressure transducers, namely; piezometers and a pressure meter. The pore-water pressures were measured with piezometers. The piezometers (see Figure 3-10) were made of a 100 kPa pressure transducer containing a small volume of water and a 100 kPa ceramic disk encased by ultraviolet hardening glue.

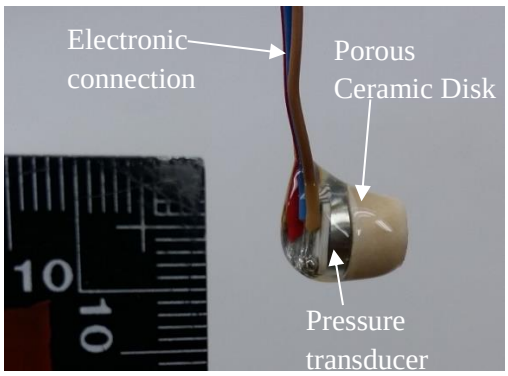

Figure 3-12: Experimental tensiometer

The reliability and measurement range of piezometers depends critically on the absence of air inside the device (Ridley and Burland, 1993; Guan and Fredlund, 1997; Toll et al., 2013). The formation of air bubbles by entry through the porous ceramic disk or by cavitation within the stone and reservoir is the only restraint to the proper functioning of the instrument. Tarantino and Mogiovi (2001), furthermore, observed that the repeated cavitation of tensiometers seemed to improve the measurement results and that the instruments worked better with repeated use. The saturation of the ceramic disk and the water reservoir is performed by applying high values of positive pressures to force any residual air present to dissolve in water. Take and Bolton (2003) and other researchers in the field of unsaturated soil mechanics have identified that it is important to remove air from the device by applying a vacuum,

before imposing a saturation pressure. The following procedure was used to saturate piezometers at the University of Pretoria:

- Oven drying stage: The tensiometers were dried in an oven for four hours at 60 °C to remove any excess moisture from the instrument,
- Vacuum stage: the tensiometers were placed in the saturation cell, as indicated in Figure 3-13, and a vacuum applied for a minimum of 10 minutes,
- Flooding under vacuum stage: while under vacuum, the de-aired water line was opened and left running through the saturation vessel for a few seconds,
- Pressurisation stage: 200 kPa pressure (double the air entry value of the piezometer ceramic disk) was applied for at least 24 h in the saturation cell. After 24 h the response was tested by varying the pressurisation pressure in 50 kPa intervals from 0 kPa to 150 kPa. If the piezometer response was sluggish, the instruments were left longer under a saturation pressure of 200 kPa.

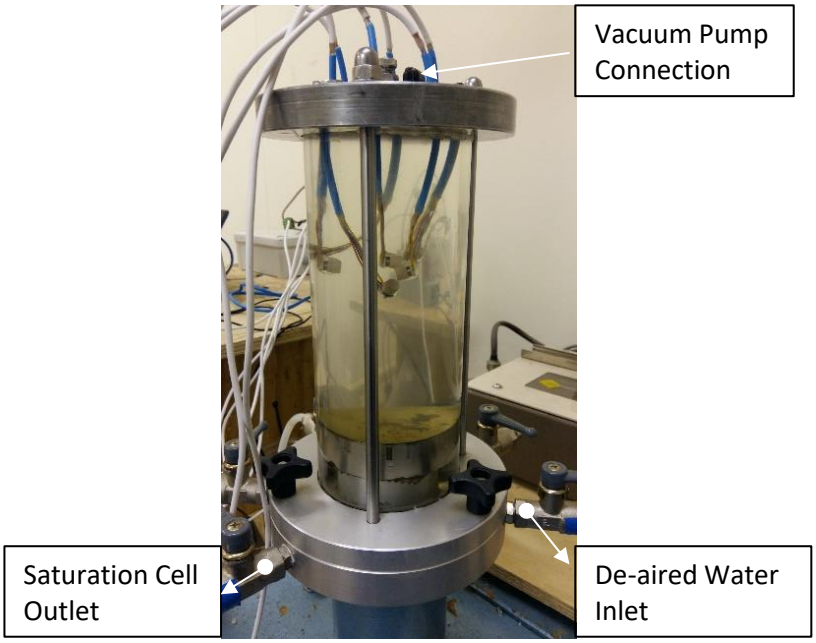

Figure 3-13: University of Pretoria tensiometer saturation cell

The pressure response file from the saturated piezometers was then used to calibrate the instrument, determining the voltage-pressure relationship. Although the piezometer was calibrated in the positive zone range in which it was predominantly used, direct extrapolation was used for the negative range. Research by Meilani et al., (2002), as well as Take and Bolton (2003), have found this to be an acceptable practice. Tarantino and Mongiovi (2003), furthermore, found that by directly calibrating the back of the tensiometer the error accrued from the direct extrapolation was 1-1.5 % which they concluded to be satisfactory. The calibration coefficient was determined as 489 kPa/Volt.

As the piezometers could measure positive and negative pressures, the installation depth was chosen as 250 mm below the initial water table (50 mm above the base of the strongbox) for the GSSI tests, and at 200 mm below the initial water level for the GSI. Five piezometers were used for the preliminary test and the first GSI settlement test (see Figure 3-14(a)). The piezometers were spaced at 100 mm, with the central piezometer in-line with the centre line of the strongbox. Six piezometers were used for the GSSI Frame (--) test (see Figure 3-14(b)). Three piezometers were installed below the frame footings (Piezo 1F to 3F), in line with the centreline of the columns on the frame investigation side and three more in line with the centreline of the footings on the soil free-field settlement side (Piezo 1S to 3S).

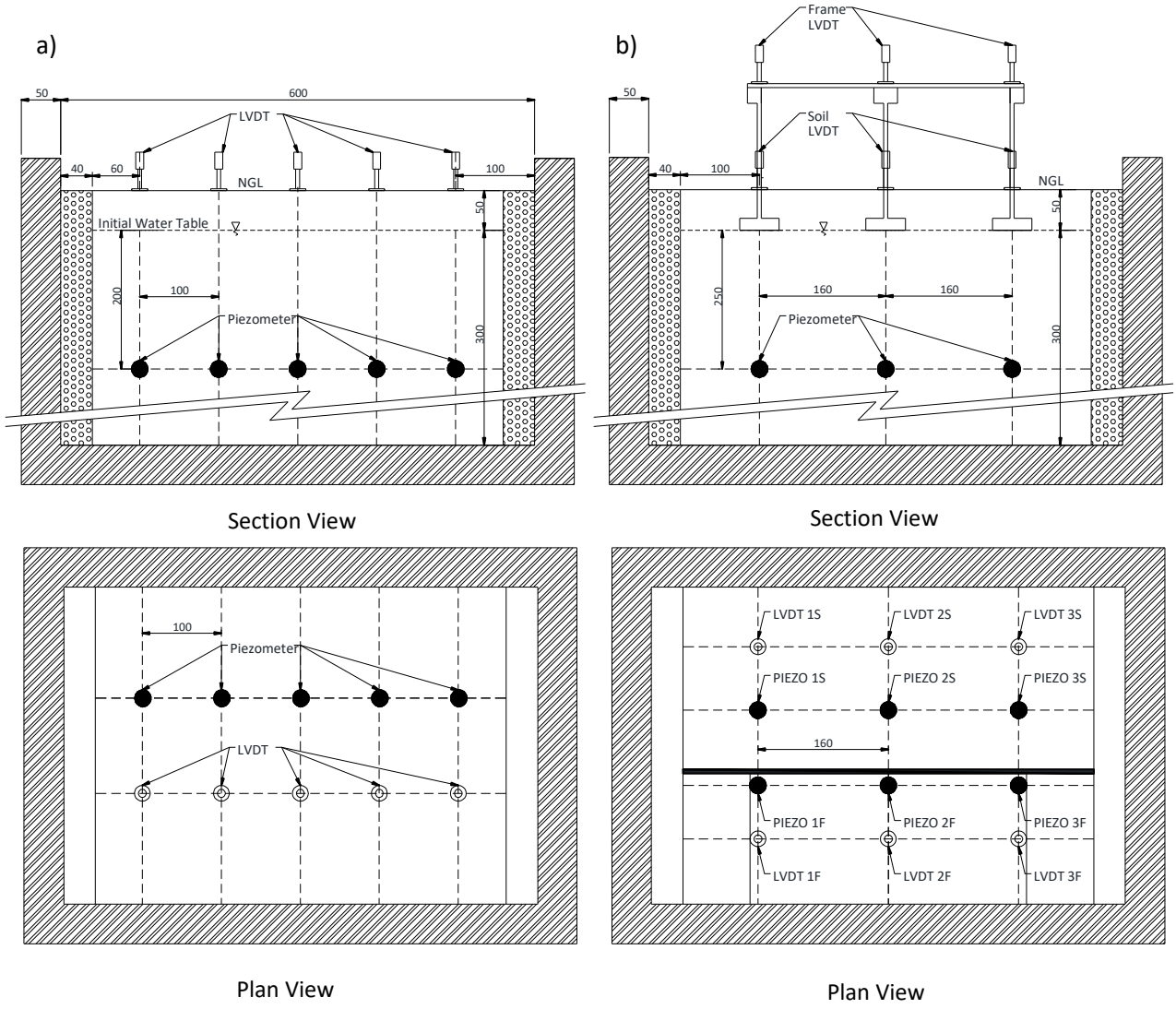

Figure 3-14: Piezometer setup

There was, however, some variation in the installation depth of the piezometer brought about by the difficulty in installing to a precise depth. Table 3-5 shows the final piezometer installation depths, in terms of elevation head with the datum at the base of the strongbox, back-calculated from the piezometer readings before testing commenced as well as the variation from the intended elevation head (value in brackets), for the GSI test and the GSSI Frame (--) test.

Table 3-5: Piezometer elevation head

GSI Test		GSSI Test 1	
Piezometer	Elevation Head [mm]	Piezometer	Elevation Head [mm]
Piezo 1	80 (-20)	Piezo 1S	56 (+6)
Piezo 2	60 (-40)	Piezo 2S	39 (-11)
Piezo 3	60 (-40)	Piezo 3S	37 (-13)
Piezo 4	75 (-25)	Piezo 1F	25 (-25)
Piezo 5	65 (-45)	Piezo 2F	16 (-34)
		Piezo 3F	14 (-36)

A commercial pressure gauge (see Figure 3-22), was used to monitor the extraction well water level. The calibration factor of the pressure gauge was -387 kPa/Volt as determined at the centrifuge facility. The pressure meter readings were used to determine when the steady state flow rate was reached as well as when the water table was re-established to the required level after the initial drawdown.

3.3.2 Displacement Transducer

Linear variable differential transducers (LVDTs) were used to measure the vertical soil and structural settlement. Five LVDTs spaced at 100 mm intervals (see Figure 3-14 (a)), and in line with the piezometers were used to measure the vertical soil settlement for the GSI tests. Six LVDTs (see Figure 3-14 (b)), were used for the GSSI tests. Three LVDTs, positioned on top of the frames (LVDT 1F to 3F) in line with the centreline of the columns were used to measure the vertical settlement of the frames. Three more LVDTs were placed on the soil settlement investigation side (LVDT 1S to 3) in line with the centreline of the frame columns to measure the free-field soil settlements. Figure 3-15 shows the GSI and GSSI centrifuge models.

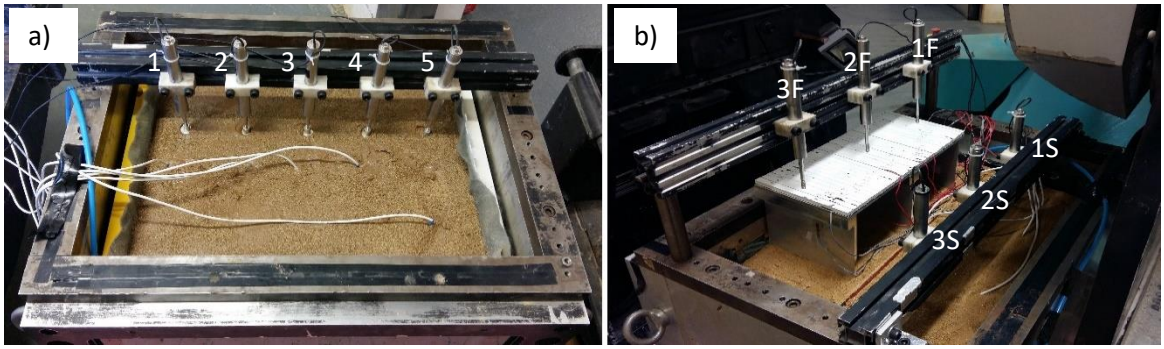

Figure 3-15: LVDT installation

3.3.3 Strain Gauges and Wheatstone Bridges

HBM 3/350 LY13 linear foil strain gauges were used for strain measurement to assess the structural frame distortion. The gauges had a nominal resistance of 350 ohms with a gauge factor of 2.06 as provided by the manufacturer. Figure 3-16 shows the HBM strain gauge configuration, with dimensions, a = 3 mm, b = 1.6 mm, c = 8.5 mm, and d = 4.5 mm (HBM, 2017).

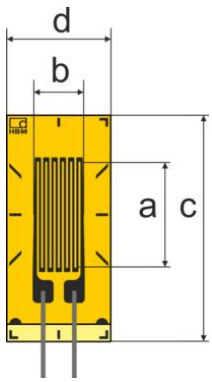

Figure 3-16: HBM strain gauge illustration (HBM, 2017)

The strain gauges were glued to the portal frames with a cyanoacrylate adhesive. The adhesive cures at room temperature under pressure which was applied through a fluoropolymer strip to allow the strain gauge to bond to the aluminium. Sanding paper (400 and 600-grade) was used to prepare the surface and to increase the adhesive bonding surface area. The 400-grade sanding paper was used for dry sanding only whereas the 600-grade sanding paper was used for dry and wet sanding. The surface was cleaned with acetone and ethanol before installation of the strain gauges. The electrical connection of the strain gauges was completed by soldering the strain gauge leads to the strain gauge electrical wires using solder terminals.

The Wheatstone bridges were configured for the quarter and half bridges. Every frame configuration had two half bridges and eight quarter bridges. Therefore, the Wheatstone bridge set-up comprised of ten Wheatstone bridges. Precision resistors with a nominal resistance of 350 ohms were used to complete the Wheatstone bridge circuits. Figure 3-17 (a) shows the half bridge configuration and the Figure 3-17 (b) shows the quarter bridge configuration. The external circuit comprised of strain gauges whereas precision resistors were used in the completion network. Equation 3-3 indicates the output voltage (Ua) to strain relationship as presented by Hoffman (1974).

$$\varepsilon = \frac{U_a \times 4}{U_e \times k \times B} \qquad \text{Equation 3-3}$$

Where:

ε = Strain

Ua = Output voltage,

Ue = Excitation voltage, 5 Volts

k = Gauge factor which is equal to 2.06,

B = Bridge factor, 2 for half bridge and 1 for quarter-bridge.

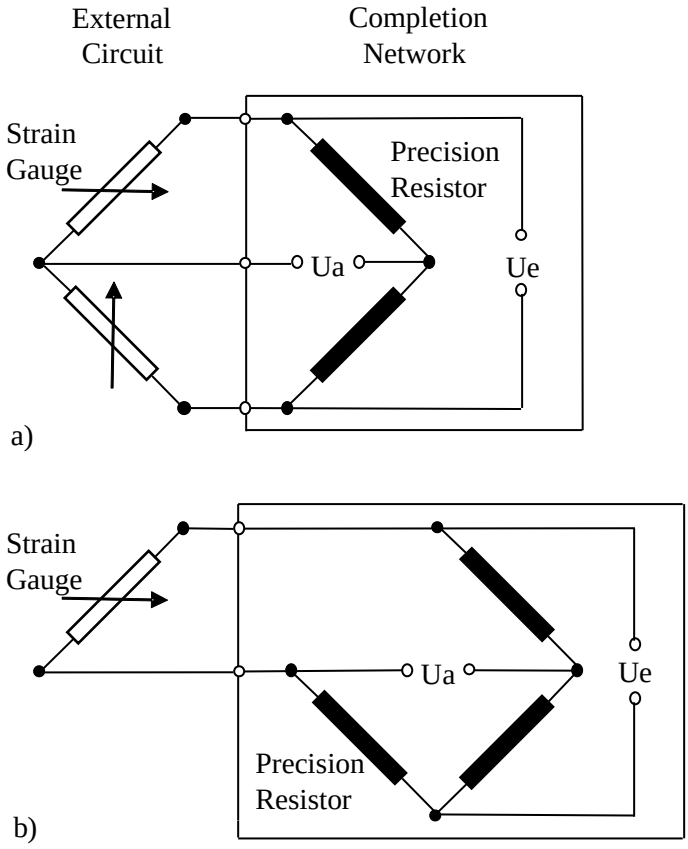

Figure 3-17: Wheatstone bridges (adapted from (Hoffman, 1974))

3.3.4 Digital Image Correlation

Digital image correlation (DIC) was used to track the ground movement for the duration of the tests. DIC is a non-intrusive process where the displacement of a selected patch is traced through consecutive images to determine the total displacement of the patch (White et al., 2013).

The availability of cameras that can capture high-resolution photographs has resulted in the wide use of DIC in geotechnical engineering. These photographs allow enough detail of the material fabric to be captured for image analysis software to be able to trace the displacement of a patch of material and the subsequent strains to be determined (Lesniewska and Wood, 2009). Lesniewska and Wood (2009) state the following two criteria need to be in place for DIC to be conducted:

- A transparent medium through which digital images can be taken,
- The material needs to have enough texture for the image analysis software to track throughout the photos.

The natural texture of granular soil eliminates the need for additional texture and colour to be added to the soil. White et al., (2003), Figure 3-18 and 3-19, illustrates the DIC process. The first digital image is subdivided into patches L x L pixels in size, patch A is used for illustration purposes. A search patch is then identified in the second image in which the displacement of patch A will be searched, which has the same central pixel coordinate as patch A but is s_{max} pixels greater than patch A. The cross-correlation between patch A and the search zone is evaluated and normalised. The resulting normalised correlation plane $R_n(s)$ indicates the degree of match between patch A and the search patch over the offset range in the domain of s, as indicated in Figure 3-19(a). The highest peak in the normalised correlation plane indicates the displacement vector of the test patch, s_{peak}, as indicated in Figure 3-19(b). To establish the displacement vector, the correlation plane is evaluated at single pixel intervals by fitting a bicubic interpolation to the region close to the integer peak, as shown in Figure 3-19(c) (White et al., 2003). The process is repeated for the remaining patches to determine a displacement field.

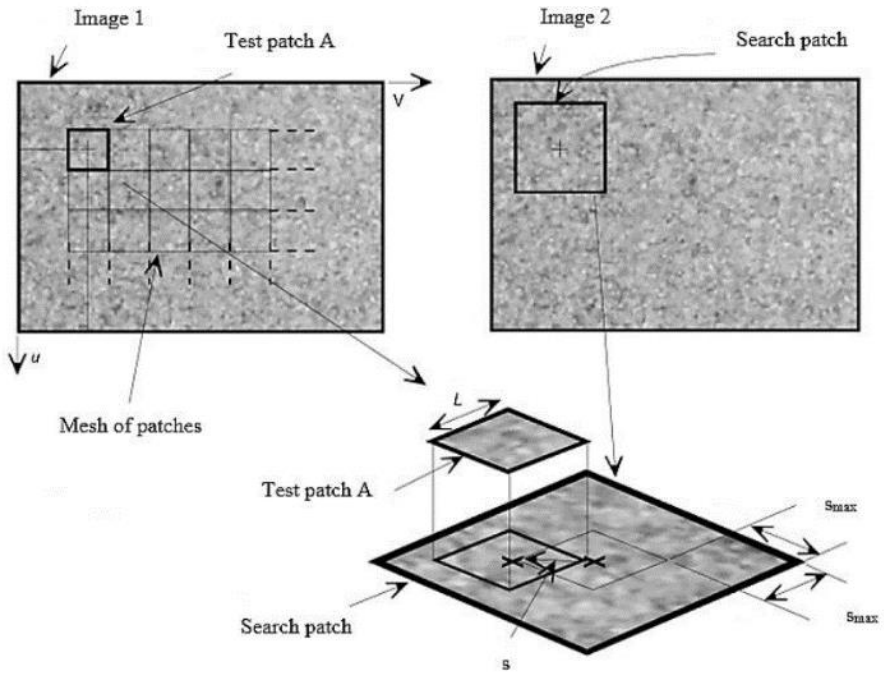

Figure 3-18: Image manipulation during DIC (White et al., 2003)

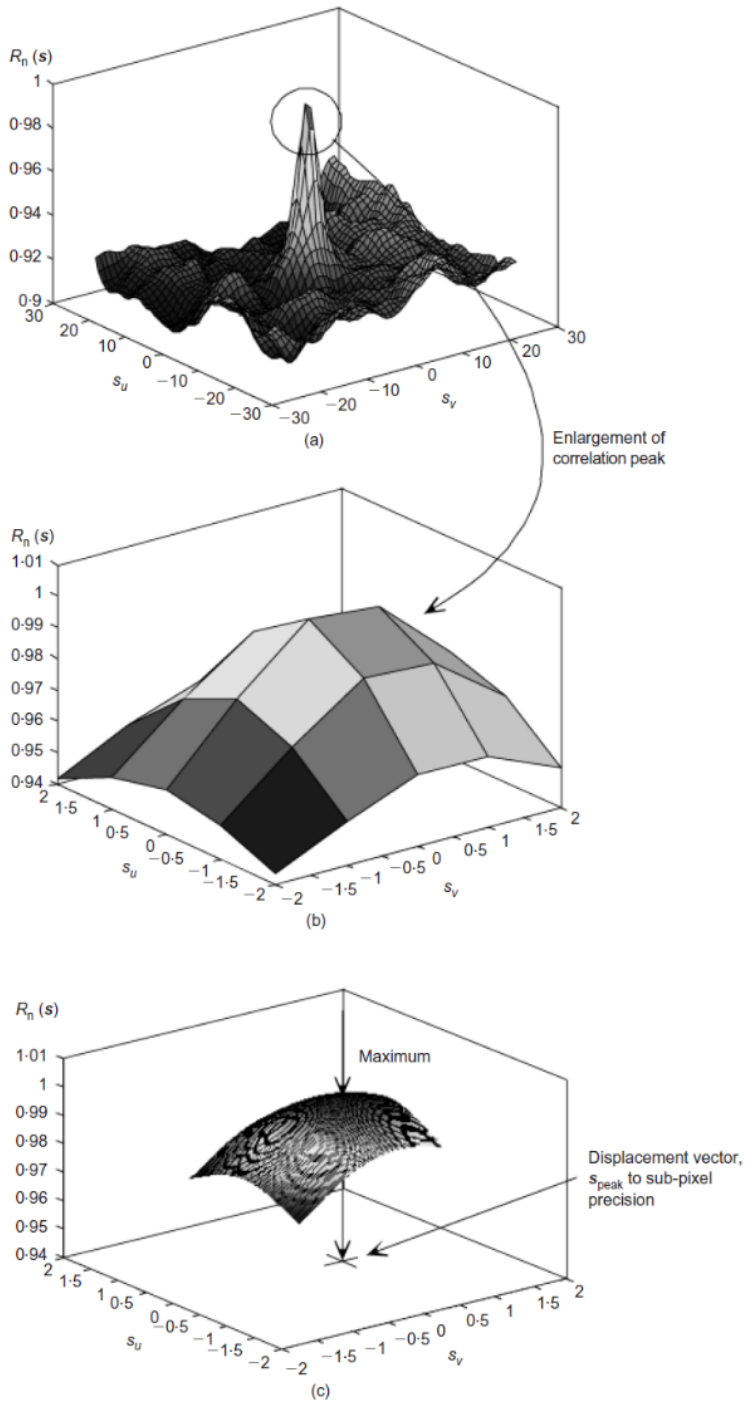

Figure 3-19: Evaluation of displacement vector from correlation plane (White et al., 2003)

A Canon EOS 100D digital camera with a Canon EF 40 mm f/2.8 STM macro lens was used for capturing the photographs used for DIC (Canon, 2017). The camera had 18 MP image sensor and the images captured were 3456 x 2305 pixels. Photographs were taken before the start of the test, at specific intervals during acceleration to 30 g and once at 30 g, time-lapse photographs were taken at 6-second intervals. Figure 3-20 shows a schematic of the camera setup on the centrifuge gondola.

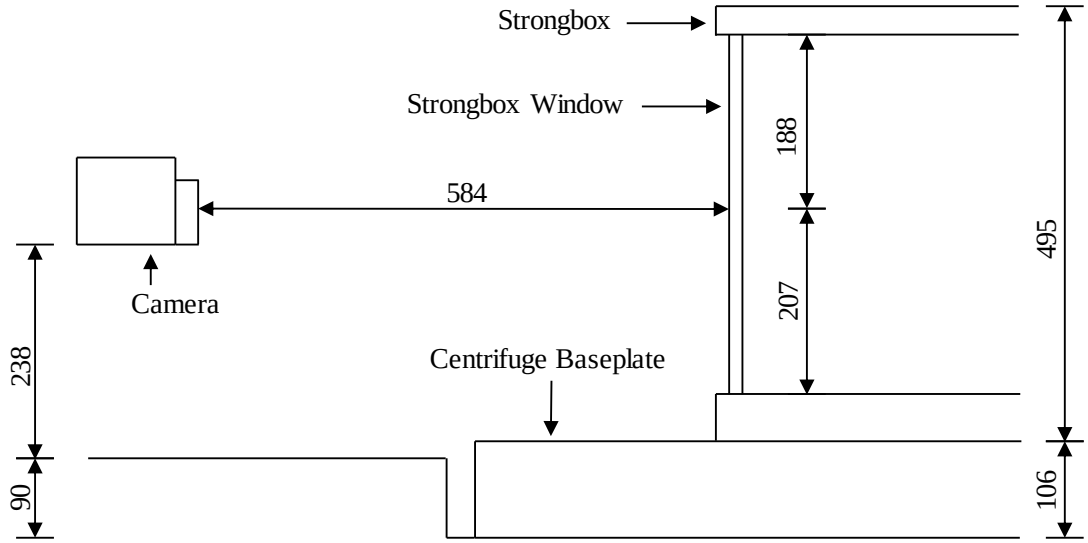

Figure 3-20: DIC camera setup (adapted from (Lemmen, 2015))

Four 10 W LED spotlights were used to ensure adequate lighting for the test duration. Two lights were fixed to the centrifuge baseplate and two fixed to the gondola. Figure 3-21 shows the positions of the spotlights in the test setup.

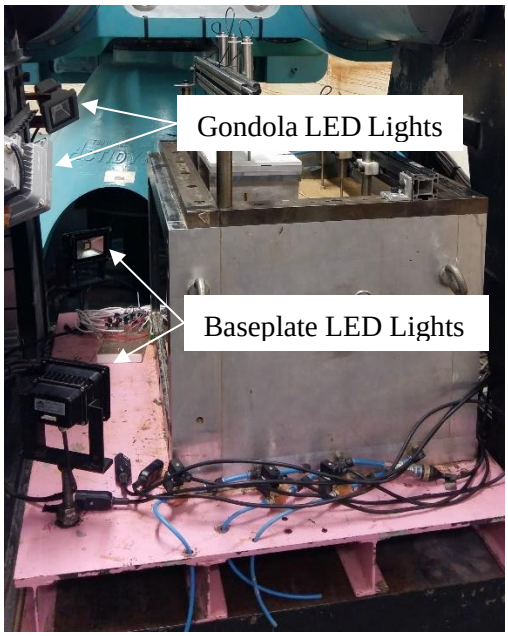

Figure 3-21: Centrifuge LED lights

3.3.5 Solenoid Valves

Three Burkert 6011 230 V plunger valve (Burkert, 2017) solenoid valves were used for groundwater extraction during testing. The stopper and plunger guide tube are welded together to enhance pressure resistance and leak-tightness of the valves. The valves had push-in fittings for plug-in house connections which allowed the valves to be used with the rest of the centrifuge piping. Figure 3-22 shows the three solenoid valves and the pressure gauge connected to the base of the extraction well.

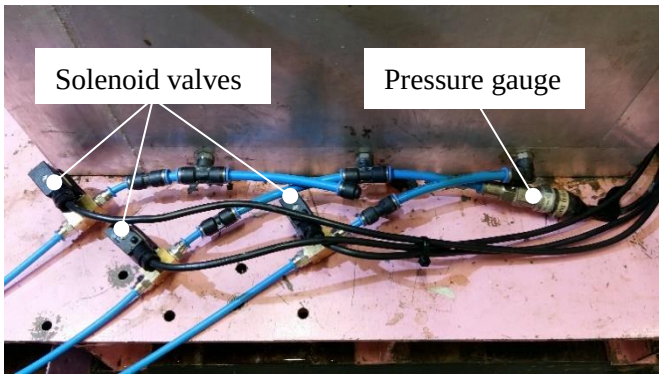

Figure 3-22: Solenoid valves and pressure gauge

3.4 DATA ACQUISITION SYSTEM

The output data file for the test comprised of soil and frame settlement readings, pore-water pressure and water level readings, structural strain readings and a series of images taken throughout the test duration. The centrifuge is equipped with three modules of the DigiDaq data acquisition system developed by the University of Western Australia which provides a total of 24 channels for operation onboard the centrifuge, capable of operating in an elevated gravitational field of up to 300 times Earth's gravity. Unlike computer-based data acquisition solutions, the system allows for the full sequence of amplification, conditioning, digitisation, and storage on a single circuit board via an independent micro-controller allocated to each pair of instrumented channels (Gaudin et al., 2009).

The DigiDaq system was used to record data from piezometers, pressure meter, LVDTs, and strain gauges simultaneously. The benefit of the single system simultaneous logging was that relationships could be determined without compensating for measuring differences brought about by using different acquisition systems. The strain gauge readings were amplified 50 times during testing. The amplification allowed for improved real-time assessment of the strain during testing.

3.5 EXPERIMENTAL PROCEDURE

The ground movements induced by groundwater extraction and the soil-portal frame interaction as well the frame response to the ground movements were investigated with two centrifuge models. The GSI centrifuge models were designed to investigate the relationships between the groundwater extraction, pore-water pressure and the resultant ground movements. The GSSI centrifuge models were designed to investigate the soil-portal frame interaction and the response of the frames to the imposed settlement. The following sections summarise the experimental procedures followed for the tests.

3.5.1 Groundwater Extraction-Induced Ground Movement Modelling

Figure 3-23 depicts a typical setup for the GSI centrifuge tests. Preliminary testing was conducted to determine the manner in which and the moisture at which the soil was to be placed during model preparation, the optimum percentage vermiculite that would yield the desired compressibility and permeability for the soil and the optimum inflow to achieve differential drawdown of the water table.

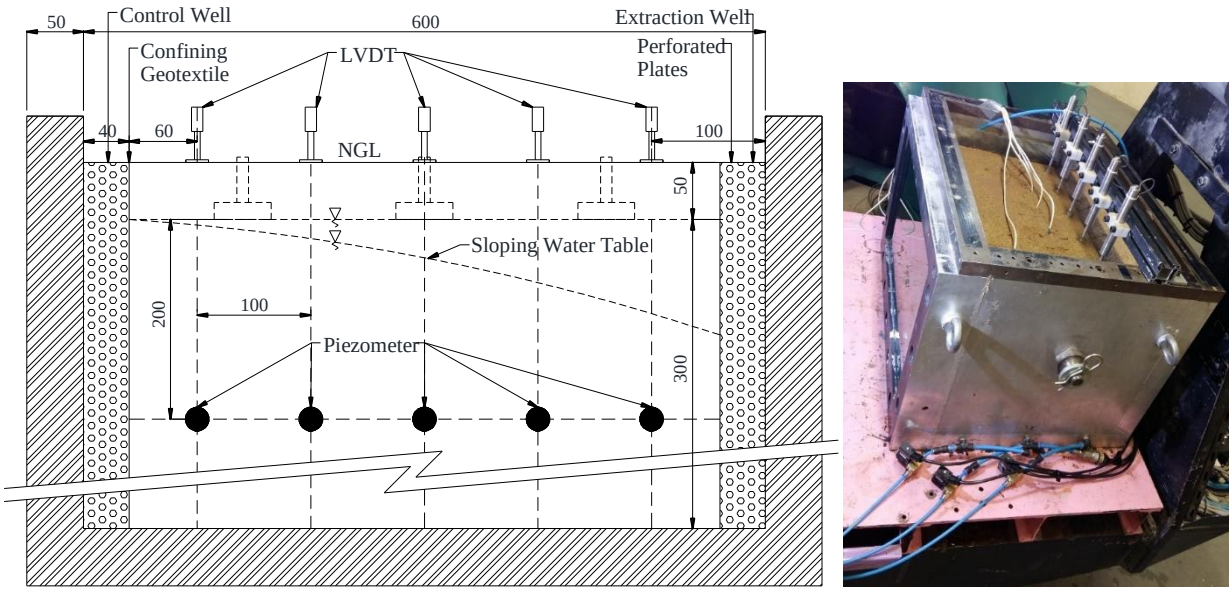

Figure 3-23: GSI Test centrifuge model

A centrifuge test was conducted for each vermiculite content (0 %, 10 %, 20 % and 30 %). The soil was placed loose and dry in layers of 25 mm, without any compaction. Compaction was not considered for two reasons, namely: it was desired to have a soil that would undergo significant settlement during groundwater extraction and the soil mass was expected to settle to a certain degree under its increased self-weight during acceleration of the model. Due to the vermiculite particles segregating from the sand when the soil was pluviated from the sand hopper, the use of the sand hopper was not considered.

The quasi-steady state water table level is the lowest level the water table can be drawn down to within the soil mass for a given inflow and extraction rate of the groundwater. The inflow rate during testing could be controlled from the centrifuge control room but the extraction rate was limited by the capacity of the solenoid valves. The soil permeability, therefore, became the determining factor as to the percentage vermiculite was to be used. Increasing the vermiculite percentage resulted in an increase in the permeability of the soil which in-turn resulted in the water table lowering more horizontally rather than differentially throughout the soil mass. The 10 % vermiculite soil mixture and an inflow rate of 60 l/h was, therefore, used for further testing as it yielded acceptable settlement and sufficient permeability to maintain differential drawdown of the water table.

The following testing procedure was followed for the GSI tests:

1. The partitions were inserted into the strongbox to create the control and extraction wells (see Figure 3-3),
2. The dry soil was placed in layers of 25 mm up to a model height of 300 mm,
3. The water level was raised to a height of 300 mm and the strongbox weighed,
4. The model was left overnight for the water table to stabilise throughout soil mass,
5. The piezometers were installed and the soil filled up to a height of 350 mm and the LVTDs installed,
6. The model was accelerated to 30 g and the instrumentation allowed to equilibrate. Photographs were taken before the start of the test, and at set time intervals during acceleration, and after the instrumentation normalised,
7. The control well inflow was opened to 60 l/h and the extraction well solenoid valves opened simultaneously. Photographs were captured at 6-second intervals,
8. Once steady state water level was reached, the water inlet was closed and the water table lowered throughout the strongbox,
9. The test was stopped when all the piezometer readings levelled out (readings do not change with time).

3.5.2 Soil-Structure Interaction Modelling

The strongbox was divided into 2 compartments along the length of the model for the GSSI tests (see Figure 3-3). The compartments were made to allow the soil settlement and the frame settlement to be investigated under the same drawdown conditions during a given test. Figure 3-24 shows the typical GSSI test setup.

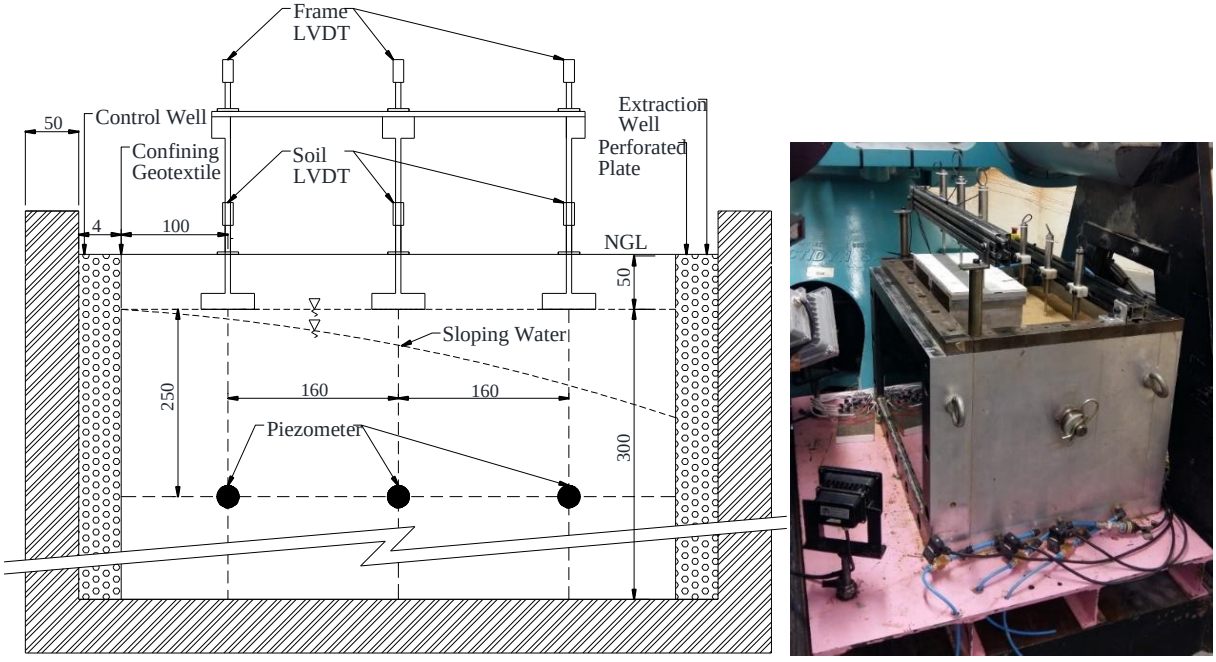

Figure 3-24: GSSI centrifuge model

Four different tests were conducted for the four different frames, starting from the founding level onwards (300 mm height):

1. The frames were placed at founding level and the soil filled up to 350 mm,
2. The LVDTs were installed and the model accelerated to 30 g. Photographs were taken before the test started, at set intervals during acceleration, and after the instrumentation equilibrated.
3. The control well inflow was then opened to 60 l/h and the extraction well solenoid valves opened simultaneously. Photographs were captured at 6-second intervals,
4. The water table was lowered differentially until the quasi-steady state water table level was reached. At this point, the water extraction well solenoid valves were closed and the water table re-established at founding level.
5. The control well flow was then closed and once the instrumentation equilibrated, the extraction well solenoid valves were opened and the water table lowered throughout the strongbox.
6. The test ended when all the instrumentation equilibrated.

The results from the centrifuge tests and the analysis of the results are discussed in the following chapter.

4 RESULT DISCUSSION AND ANALYSIS

In this chapter, the results of the five centrifuge tests are presented and discussed. The results for the groundwater extraction-soil interaction (GSI) test will be presented and discussed first. This is followed by the results of the groundwater extraction-soil-structure interaction (GSSI) tests with the four portal frames. The results for the portal frames are discussed individually followed by a comparative assessment of all four frames.

The results from the GSI tests were analysed to determine the relationships between groundwater extraction and the pore-water pressure reduction throughout the soil mass. This was followed by the assessment of the vertical soil settlement due to the reduction in pore-water pressure and changes in the state of stress within the soil mass. The discussion of the GSI concludes with the assessment of the ground movement, horizontal and vertical, as induced by the extraction of the groundwater.

The GSSI results and discussion focused on the interaction between the soil undergoing groundwater extraction-induced movement and the portal frames, examining the effects of varying global and relative stiffnesses. The discussion touches on factors such as the change in the soil movement due to the presence of the portal frames, alteration in load paths and the response of the portal frames to the vertical and horizontal ground movement.

Before the GSI and GSSI test results are discussed, the response of the soil to the acceleration of the centrifuge to the required acceleration of 30 g as well as groundwater extraction-induced settlement in terms of density throughout the test duration is presented. The water table fluctuation during testing is also discussed.

4.1.1 Soil density during testing

One of the requirements for the centrifuge tests was to use approximately the same soil density throughout all the tests. The soil was placed loosely with the same mass of soil used for all the test to fill the strongbox to the desired depth. For the GSI tests, 88 kg of soil was placed to a depth of 350 mm in layers of 25 mm thickness. For the GSSI tests with the portal frames, 75 kg of soil was placed to a depth of 300 mm, the founding level of the foundations, in layers of 25 mm. Once the portal frames were placed on the soil, the strongbox was filled to 350 mm depth. The dry density of the soil before testing commenced was therefore calculated as 1122 kg/m^3 with a relative density of 15 %. The low dry density of the soil could be attributed to the presence of vermiculite.

The self-weight of the soil increased as the models were accelerated to 30 g. The increase in self-weight caused the soil mass to settle, thereby, increasing the density of the soil mass. Figure 4-1 shows the soil

settlement as the model for GSSI Frame (++) test was accelerated to 30 g. The average soil density, calculated by averaging the measurements of the LVDTs, was calculated at three stages throughout the testing procedure, namely at 30 g acceleration prior to the commencement of the first drawdown, before the commencement of the second drawdown and at the end of the test. Table 4-1 shows the results for the soil density at the aforementioned positions.

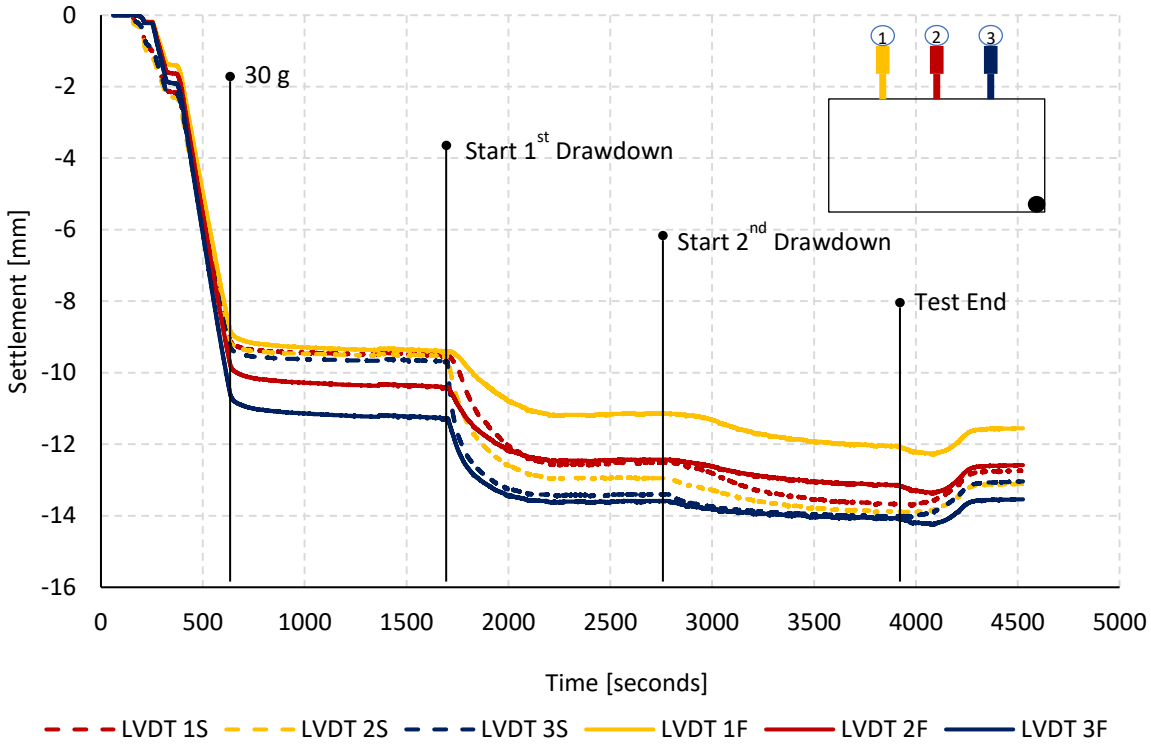

Figure 4-1: Soil settlement with acceleration of centrifuge and groundwater extraction

Table 4-1: Soil density for centrifuge tests

Test	Start 1st Drawdown [kg/m³]		Start 2nd Drawdown [kg/m³]		Test End [kg/m³]	
GSI	1159		1169		1173	
	SIS	**FIS**	**SIS**	**FIS**	**SIS**	**FIS**
GSSI Frame ++	1153	1156	1167	1165	1170	1167
GSSI Frame --	1145	1157	1155	1165	1160	1170
GSSI Frame -+	1138	1131	1149	1139	1152	1141
GSSI Frame +-	1161	1177	1179	1192	1182	1195

***SIS – Soil Investigation Side, FIS – Frame Investigation Side**

The results from Table 4-1 indicate that the soil density for the GSI test and GSSI Frame (++) soil investigation side (SIS) were similar prior to the commencement of the first drawdown. The difference in density for Frames (--), (-+) and (+-) GSSI SIS tests could be attributed to the final 50 mm soil layer which was not controlled as strictly as the soil layers up to the founding layer when placing. The increase

in density throughout testing was however comparable for all the tests. The average increase from the start of the first drawdown to the start of the second was 12 kg/m^3 and 3 kg/m^3 for the final drawdown corresponding to an average percentage increase in relative density of 6.7 % and 1.7 % respectively. The results show that soil density was comparable for all the tests.

4.2 WATER TABLE FLUCTUATION DURING TESTING

This section illustrates the changes in the water table throughout the duration of the centrifuge tests. Lowering the water level in the extraction well caused the soil mass to desaturate forming a drawdown curve. It was assumed that the drawdown curve depicted by the visible front (see Figure 4-3) was the saturation front below which the soil was saturated and unsaturated above this front. The phreatic surface would, therefore, be located below the saturation front but for purpose of this discussion, the phreatic surface is assumed to be at the saturation front level. Figure 4-2 shows the total head variation throughout the soil mass with time and Figure 4-3 is a photographic depiction of the corresponding saturation front for the GSSI Frame (--) test. The saturation front positions depicted in Figure 4-3 correspond to the points illustrated in Figure 4-2.

The piezometric total head readings together with the saturation front can be used to illustrate the distance of influence and the cone of depression. The distance of influence is the distance from the extraction well to the point where the drawdown curve re-joins the original phreatic surface or reaches the end of the aquifer and is indicative of the cone of depression and the distance to which significant settlements will extend (Cashman and Preene, 2013). The extent of the cone of depression is indicated by the distance of influence yet the magnitude of depression/settlement is a function of the reduction in the total head.

Figure 4-2 and 4-3 shows that lowering the extraction well water level caused the water table to drop differentially throughout the soil mass. Lowering the water level in the extraction further, caused the distance of influence to propagate further away from the extraction well while the water table continued to lower differentially, stage 1 (see Figure. 4-3). This continued until the distance of influence reached the edge of the simulated aquifer, stage 2. Stage 2 coincided with the point at which the differential drawdown of the water table was at its maximum. The differential settlement of the soil mass would, therefore, also be a maximum at stage 2. Lowering the extraction well water level beyond this point caused the water table to drop throughout the soil mass but the differential drawdown ceased. The water table continued to drop until the quasi-steady state water level was reached, stage 3, which was the lowest level of the water table for the given replenishing/inflow rate and the extraction rate from the simulated aquifer. During stages 4 to 6, the extraction well valves were closed and the water table re-established to the original position. The water table rose in a manner that could be viewed as a reversal

of the propagation of the distance of influence. During stages 7 to 9, the control well inflow was closed and the water table lowered throughout the strongbox. The differential shape of the water table as it was lowered throughout the strongbox is evident during this period. The response of the water table during testing corresponds well with that described by Budhu and Adiyaman (2010) who analytically modelled groundwater extraction and Cashman and Preene (2013) who investigated field aquifers during groundwater extraction.

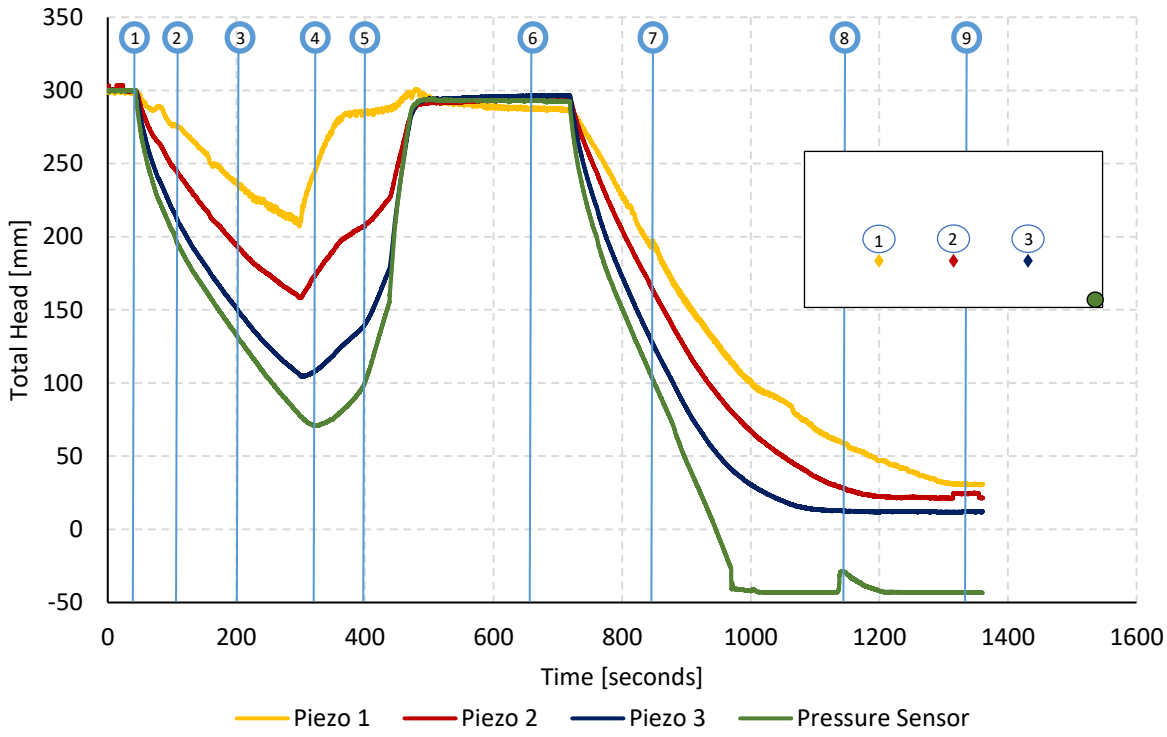

Figure 4-2: Pore Water Pressure and extraction well total head variation throughout testing

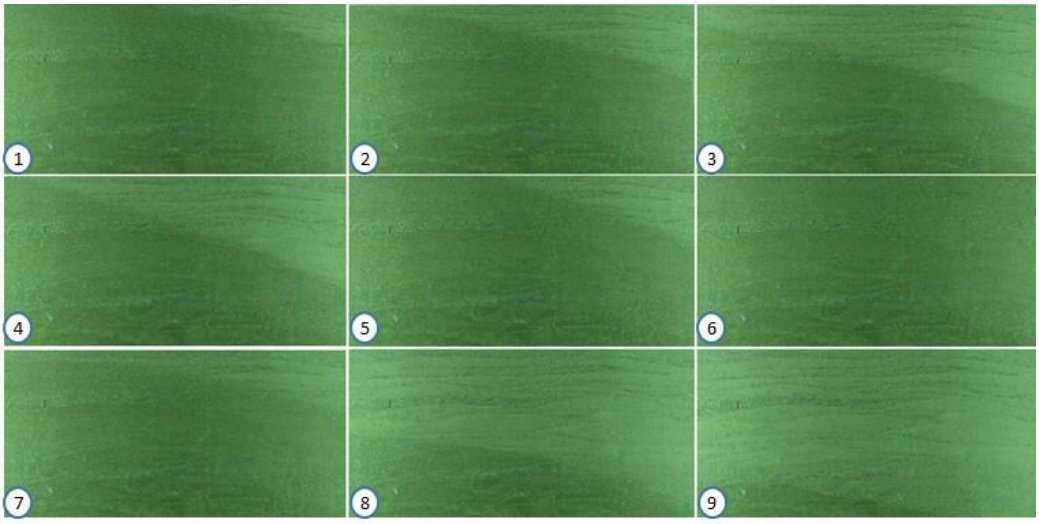

Figure 4-3: Zone of influence propagation and water table

4.3 GROUND MOVEMENT INDUCED BY GROUNDWATER EXTRACTION

4.3.1 Pore Water Pressure and Soil Surface Settlement

In this section, the relationship between the pore-water pressure and the vertical soil settlement, as observed in the GSI test, is discussed. Figure 4-4 shows the pore pressure variation, converted to total head, measured by the 5 piezometers, Piezo 1 to 5, throughout the soil mass for the GSI test. Figure 4-5 shows the total head variation along the length of the strongbox for the relevant test stages indicated in Figure 4-4. The elevation head (see Figure 4-5) indicates the position of the piezometers in the soil mass with the datum taken at the base of the strongbox.

The area of the simulated aquifer affected by the pore-water pressure reduction caused by the lowering of the water table is indicated by the propagation of the zone of influence. However, the of the magnitude reduction in pore-water pressure within the aquifer is dependent on the level to which the water table is lowered. The total head results from Figure 4-4 show that a reduction in the extraction well water level caused a reduction in the total head within the soil mass. As the extraction well water level was lowered a hydraulic gradient was established which facilitated groundwater flow towards the extraction well. The distance of influence propagated away from the extraction well resulting in a differential drawdown of the water table. The pore-water pressure reduced non-uniformly throughout the soil mass as the water table was lowered differentially. This is indicated by the difference in total head reduction depicted by Figures 4-4 and 4-5. As expected the reduction in the total head was greater for the piezometers closer to the extraction well than it was for the piezometers further from the extraction well.

The GSI test also investigated the effects of a fluctuating water table. Therefore, two drawdown cycles were carried out before the water table was lowered to the quasi-steady state level. The first cycle ended at the point labelled ‘end 1st drawdown’ while the second ended at the point ‘end 2nd drawdown’ (see Figure 4-5). Sloping the saturation front was achieved by slightly lowering the extraction well water level (by opening the solenoid valves) and increasing the inflow rate. Increasing the inflow rate resulted in the water table rising in the soil closer to the control well (see Figure 4-4, piezo 1). This was repeated by lowering the extraction well water level more and the inflow rate increased for the second cycle. A similar response in the saturation front can be seen in Figure 4-4. However, it took longer for the saturation front to respond closer to the extraction well, the more the extraction well water level was lowered. A similar response was recorded with the water table when the extraction well outflow was closed for the GSSI test thereby reducing the outflow instead of increasing the inflow.

The water table was then lowered to the quasi-steady state level at which point the control well inflow was closed and the water table lowered throughout the strongbox. Figure 4-5 shows that water table dropped evenly throughout the soil mass while maintaining the differential shape when the maximum

distance of influence was reached resulting in an even reduction in pore-water pressure throughout the soil mass. The total head level at the 'test end' point (see Figure 4-5) fell below the elevations of the piezometers, reflecting the negative pore pressures in the soil after desaturation associated with the drop in the saturation front. The piezometer readings levelled out at this point and reached a steady suction value which for sand is close to the air entry point for the soil.

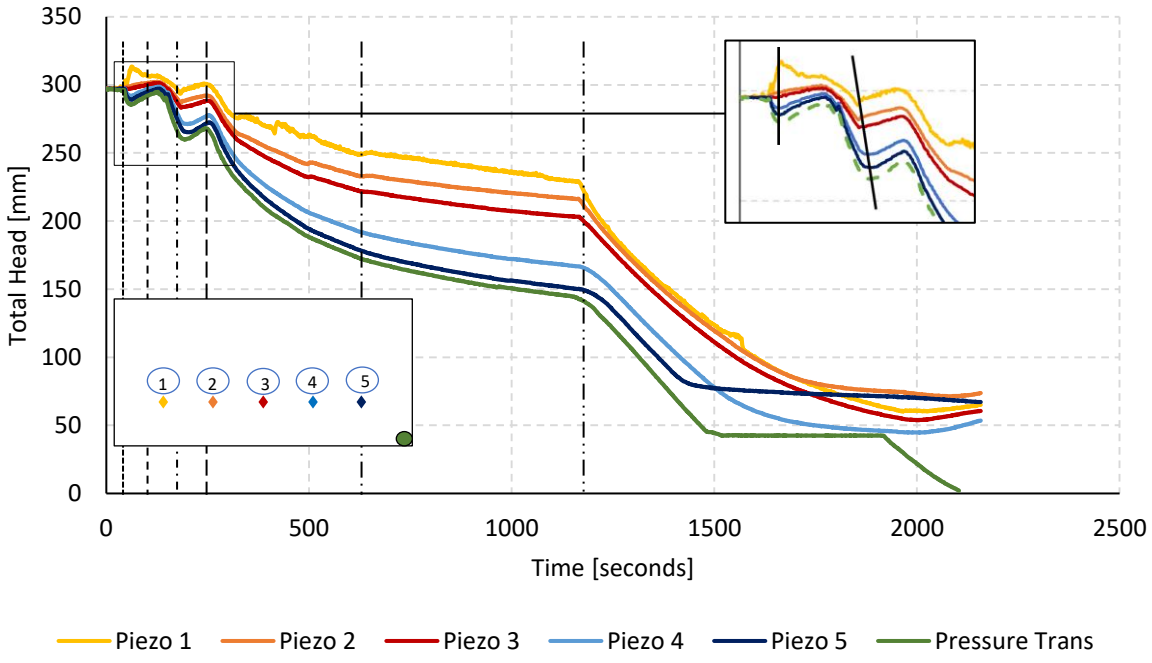

Figure 4-4: Total head with time

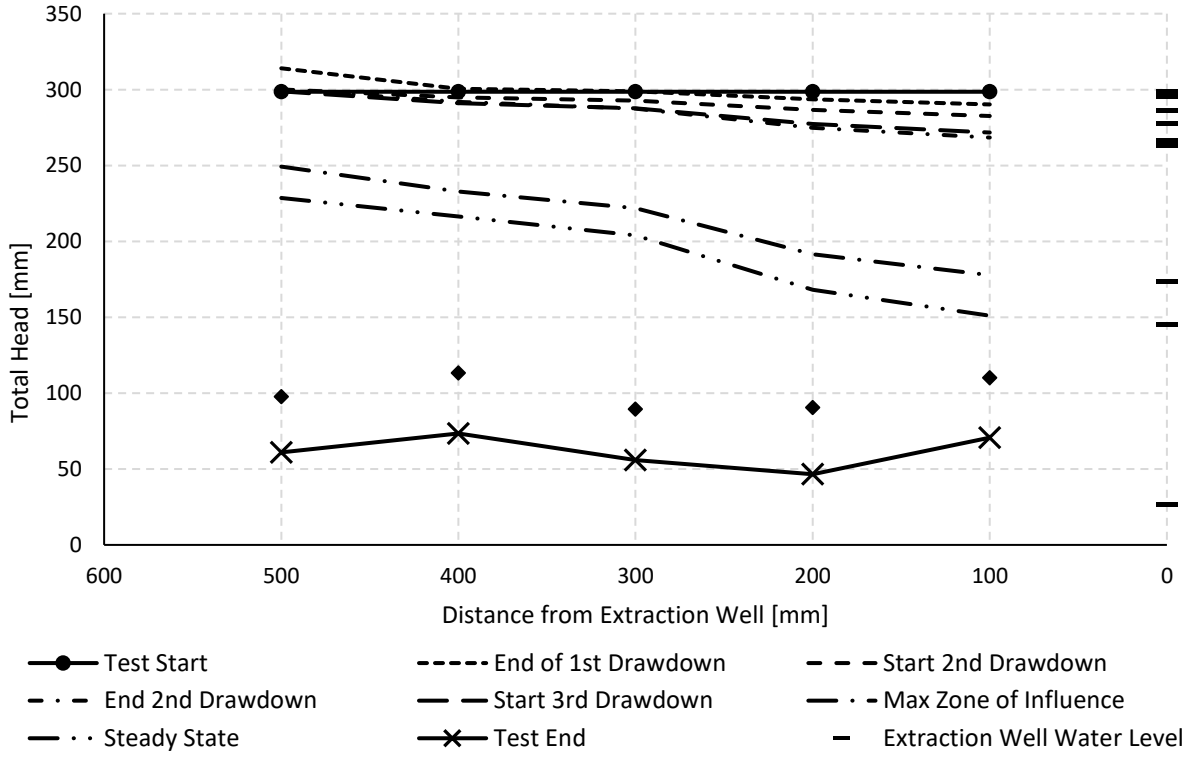

Figure 4-5: Total head along length of strongbox

Terzaghi's principle of effective stresses (Terzaghi, 1943) stipulates that a decrease in pore-water pressure should result in an increase in the effective soil stresses. Therefore, the decrease in pore-water pressure was accompanied by an increase in the effective soil stresses. The effective stress increase followed a similar pattern to that of the pore-water pressure reduction propagating away from the extraction well with the distance of influence and increasing in magnitude as the water table was lowered. Thus, the increase in effective soil stresses due to the reduction in pore-water pressure caused the soil to settle.

Figure 4-6 shows the settlement of the soil mass due to the increase in effective stresses. Figure 4-7 shows the soil settlement along the length of the strongbox at the stages indicated in Figure 4-6. Comparing these results with the results from Figure 4-5 show that the soil settlement followed the same trend as the reduction in pore-water pressure, increasing as the pore-water pressure reduced. The fluctuating water table simulated during the 1st and 2nd drawdown cycles resulted in progressive differential settlement of the soil mass. During the slight drawdown of the water table, the settlement was mainly confined to the soil closer to the extraction well. With an increase in the differential drawdown of the water table, the differential settlement increased with a clear distinction in the magnitude of settlement closer to the extraction well (between LVDTs 4 and 5) compared to the LVDTs further from the extraction well.

The drawdown of the water table towards the quasi-steady state level resulted in further settlement of the soil. Beyond the 'max zone of influence' (see Figure 4-5), the reduction in pore pressure was constant throughout the soil mass which should have resulted in an even settlement throughout the soil mass maintaining the differential settlement profile at 'max zone of influence'. However, due to the confining geotextile dislodging from the top of the control well-partitioning plate at the start of the 3rd drawdown cycle the settlement closer to the control well increased substantially. This is evident from the increased slopes for LVDTs 1, 2 and 3 at the start of the 3rd drawdown and resulted in the curves of these LVDTs dropping by approximately one millimetre.

The soil behaviour can, however, still be studied from the data. At the steady state water level, the water table was still sloping towards the extraction well within the soil mass (see Figure 4-5) and the settlement profile would have been reflected by this if it was not for the geotextile dislodging. Lowering the water table beyond this point resulted in an even rate of decrease in the pore-water pressure and subsequently an even rate of increase in settlement. However, due to the water table being lower closer to the extraction well, the total decrease in pore-water pressure was less for this soil. This resulted in the soil further from the extraction well settling more due to the larger total decrease in pore-water pressure and subsequent increase in effective soil stresses. This was indicated by the larger increase in settlement for the LVDTs further from the extraction well beyond the quasi-steady state water table level.

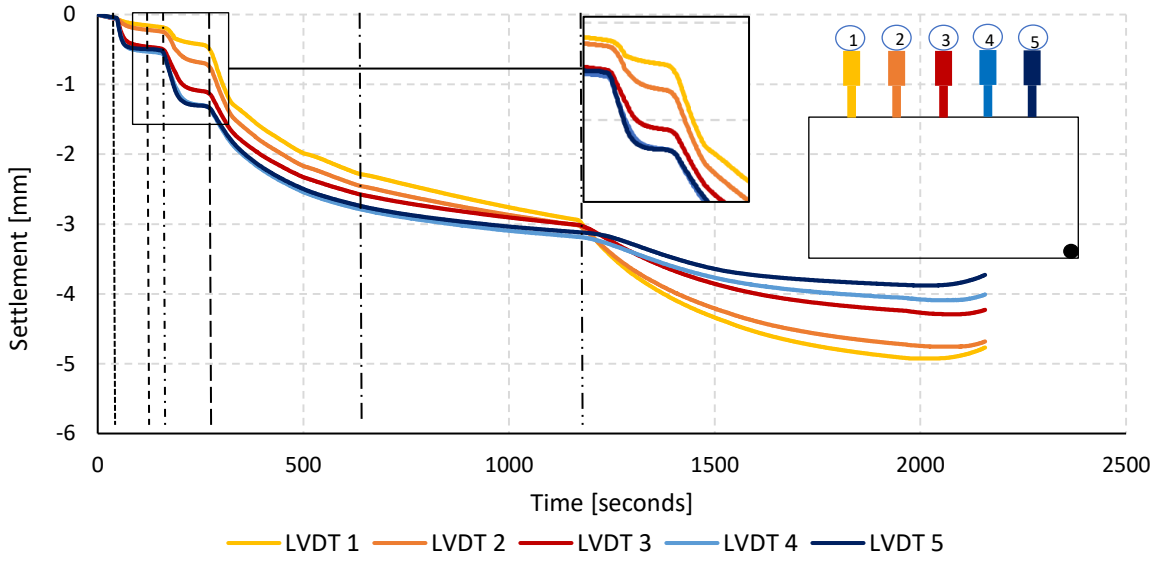

Figure 4-6: Soil surface settlement with time for GSI Test

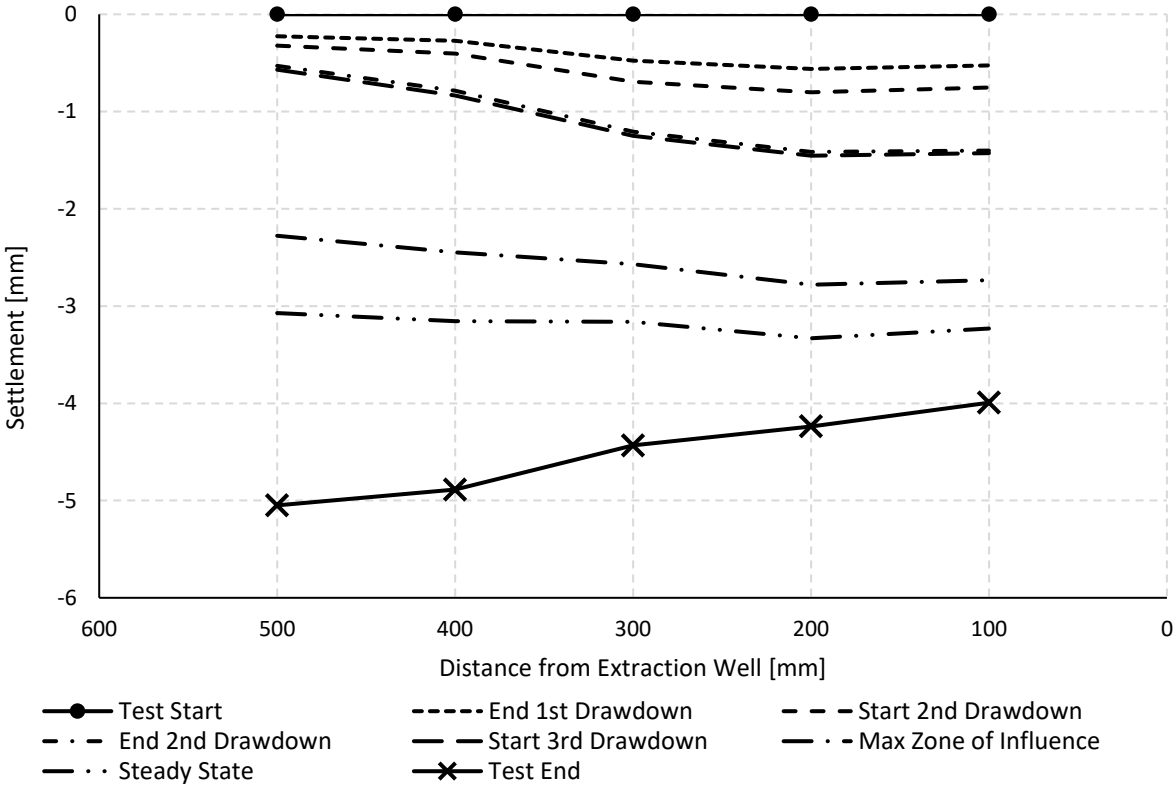

Figure 4-7: Surface LVDT settlement along length of strongbox for GSI Test

The soil settlement results show that the cone of depression induced by groundwater extraction is a function of the zone of influence and the degree to which the water table was lowered in the soil. The pore-water pressure reduction and soil settlement results correlate well with the results obtained by Budhu and Adiyaman (2010) and Yang et al. (2015) (see section 2.3.2).

4.3.2 State of Stress within Soil Mass

Soil settlement is a function of the increase in effective soil stresses but also the stress history of the soil. Fahmi et al., (2015) showed the nonlinear behaviour of soil under cyclic loading created by a fluctuation in the water table. This showed that the degree to which soil would settle for a given increase in effective stresses is dependent on the over-consolidation ratio of the soil, which indicates whether the soil was normally consolidated or over-consolidated. This research together with other researchers such as Budhu and Adiyaman (2010) who found similar results, were however based on FE models. In order to investigate this phenomenon for groundwater extraction-induced soil settlement in a centrifuge setting, pore-water pressure and settlement results for the Frame (--) GSSI tests were examined. In this test, the water table was lowered to the quasi-steady state at which point the solenoid valves were closed and the water table replenished to its original position. A second drawdown phase was initiated where the control well inlet valve was closed and the extraction well solenoid valves opened. Figure 4.8 shows the pore-water pressure variation over time throughout the test.

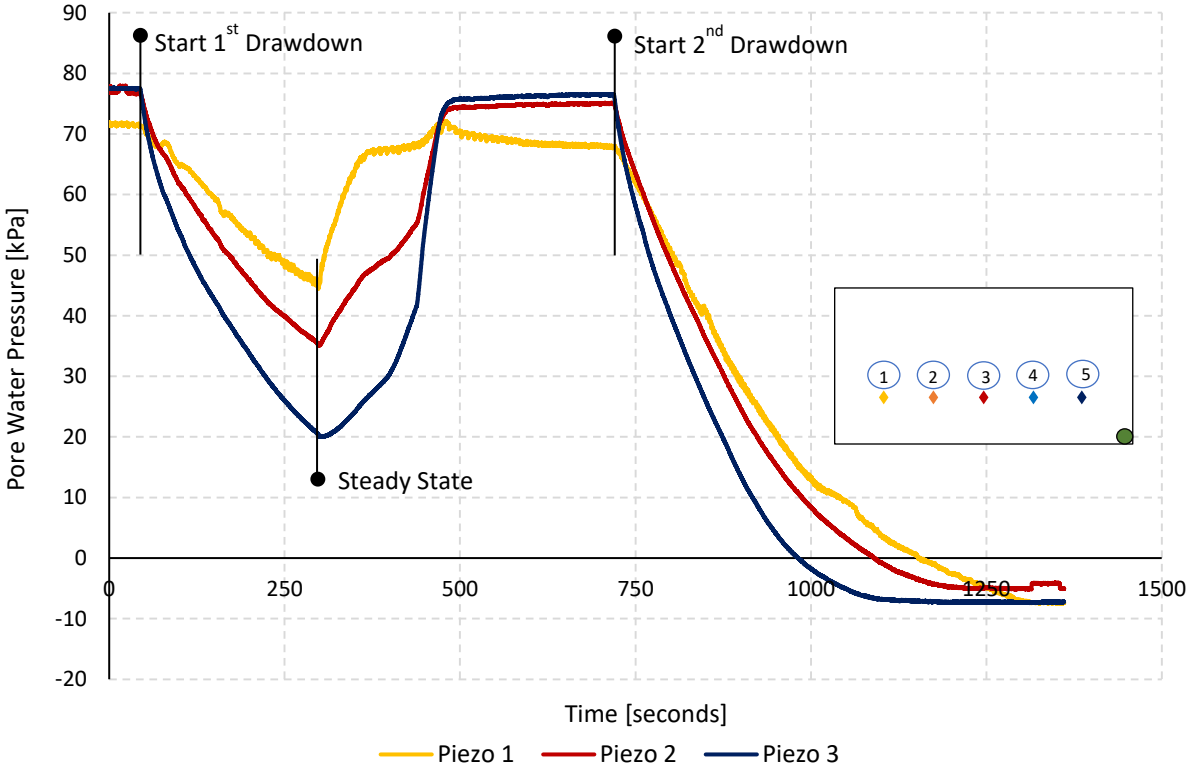

Figure 4-8: Pore water pressure with time for GSSI Frame (--) Test

Figure 4.9 shows the soil settlement as a result of the reduction in pore-water pressure. During the first drawdown, the soil closest to the extraction well, depicted by LVDT 3S, settled the most with the soil settlement decreasing progressively away from the extraction well. During the replenishing stage, the soil settlement ceased remaining constant with time. From the start of the second drawdown, the soil furthest from the point of extraction settled more.

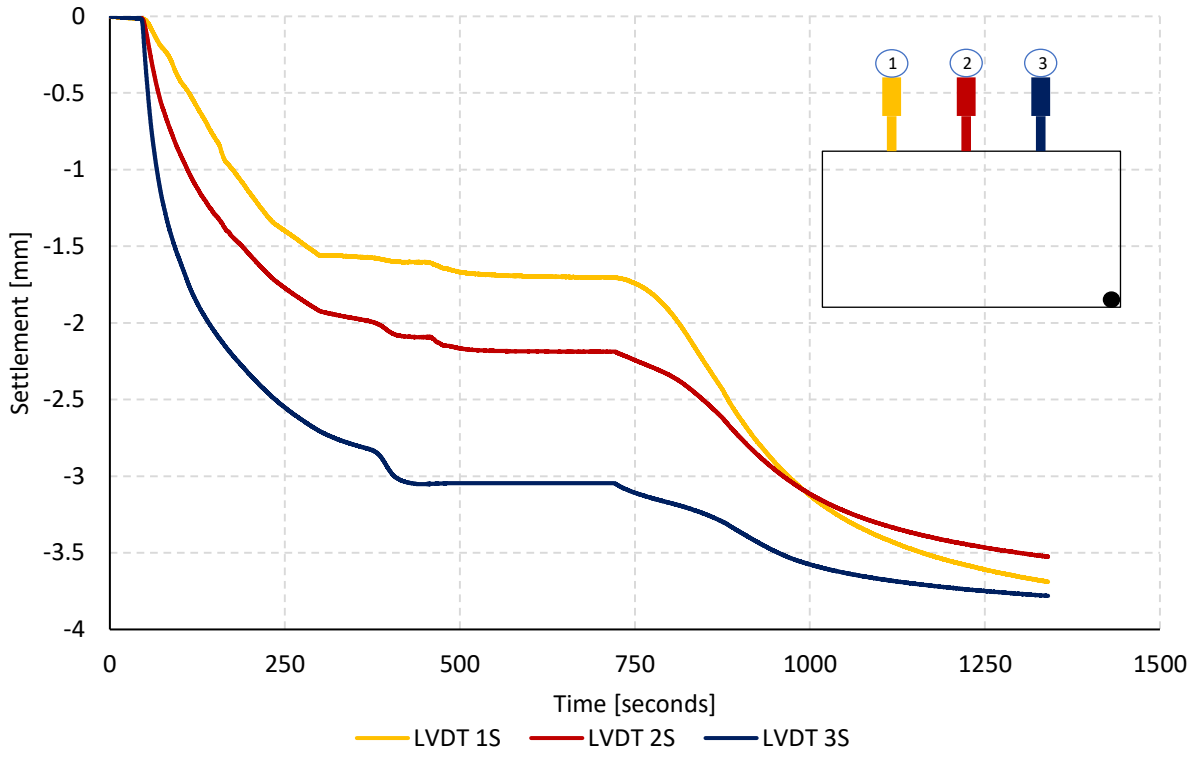

Figure 4-9: Soil surface settlement with time for GSSI Frame (--) Test

In order to further investigate this phenomenon, the logarithm of the change in pore-water pressure, indicative of the logarithm of change in effective soil stress, was plotted against the resultant increase in soil surface settlement (see Figure 4-10). Figure 4-10 presents the relationship between the change in effective soil stress and the increase in soil surface settlement. The soil columns represent the piezometer and LVDT readings at that point i.e. Soil Colum 1 represents piezometer 1 and LVDT 1 (see Figure 4-10).

When the water table was drawn down for the first time, the entire soil mass settled along the virgin compression line, indicating normally consolidated behaviour of the soil. The soil closest to the point of extraction, soil column 3, travelled further down the virgin compression line as the increase in effective stresses and resultant settlement were larger for that column. At the quasi-steady state water level, the water table was replenished to the original level, and the graphs traversed along the over-consolidated part of the consolidation curve. When the water table was lowered for the second drawdown sequence, the soil furthest from the extraction well, re-joined the virgin compression line earlier than the rest of the soil. Therefore, the soil represented by soil column 1 settled more during the second drawdown phase. Soil column 1 had settled more than 1 mm by the time soil column 3 re-joined the virgin compression line.

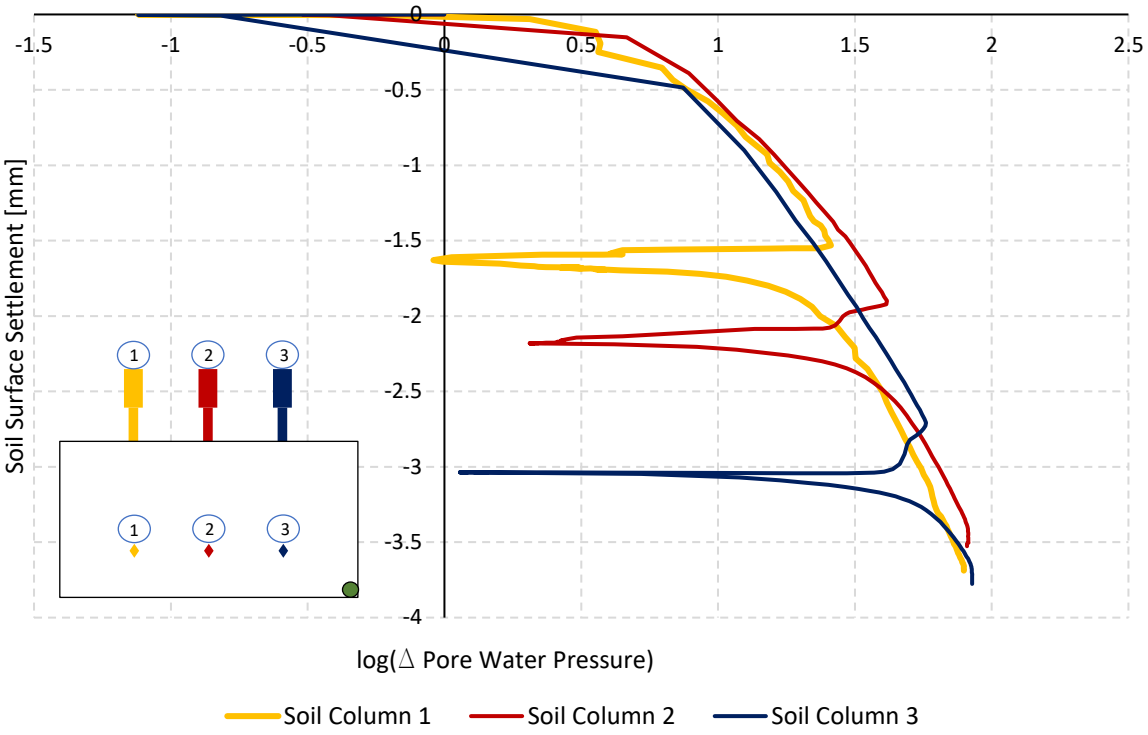

Figure 4-10: Effective stress vs soil surface settlement for GSSI Frame (--) Test

These results illustrate how the soil settlement caused by groundwater extraction is dependent on historical water table levels and the degree of differential drawdown of the water table. The results also show that the centrifuge modelled groundwater extraction-induced soil effective stress response corresponds well with the numerically modelled soil effective stress responses presented by Budhu and Adiyaman (2010), Fahmi et al. (2015) and Yang et al. (2015).

4.3.3 Vertical and Horizontal Ground Movement

The discussion thus far has focussed only on the relationship between pore-water pressure reduction and the vertical soil settlement. However, research conducted by researchers such as Yang et al. (2015) has shown that there is a component of horizontal ground movement present in groundwater extraction-induced ground movement. Research conducted in the fields of tunnelling and deep excavation-induced (Mair et al., 1996) and mining induced (Deck and Harlalka, 2010) ground movement, furthermore, indicated that horizontal ground movement has detrimental effects on structures founded within the distance of influence. The component of horizontal ground movement can induce horizontal strain within structures that can add to structural damage and ultimately contribute to structural failure.

To fully investigate the groundwater extraction-induced ground movement, DIC was used to track the movement of the soil mass throughout the test duration for the GSI test. DIC patches were tracked through subsequent photographs captured during testing. Figure 4.11 shows the patches that were tracked which measured 32 pixels by 32 pixels in size spaced at 32-pixel intervals. The vertical and

horizontal ground movements were extracted from the movement of representative patches that were in line with the LVDT centrelines (see Figure 4-11).

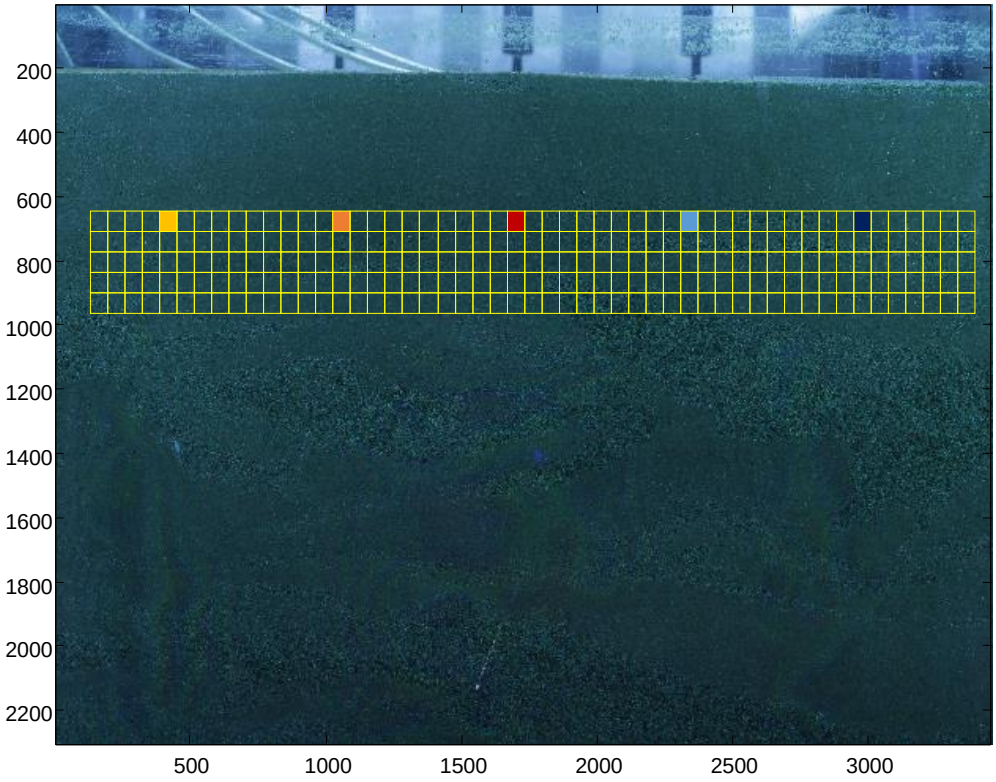

Figure 4-11: DIC patch configuration for GSI Test

Figure 4-12 shows the vertical (V) and horizontal (H) ground movement for the patches colour coded in Figure 4-11. L1 to L5, coincide with the LVDTs 1 to 5 from the GSI test (see Section 4.3.1), with L5 closest to the extraction well. The vertical settlement of the patches was similar to the surface settlement recorded by the LVDTs (see Figure 4-6). DIC tracking, however, failed to capture the settlement due to the first drawdown (the intervals at which pictures were taken to long). The settlement induced by the geotextile dislodging also had a lesser effect deeper in the soil mass effecting mainly only the L1 patch.

There was, however, also a component of horizontal ground movement present which would be disregarded if only vertical surface settlement was measured as in the case of Figure 4-6. The horizontal ground movement increases with the vertical ground movement as the groundwater is extracted. The ground movement follows a similar trend as the vertical soil movement, with the ground movement greater closer to the extraction well in the direction of the groundwater flow where the seepage forces acting on the soil skeleton is the greatest. The soil closer to the extraction well reached the maximum horizontal movement at the quasi-steady state water table level. However, lowering the water table beyond this point, caused the soil further from the extraction well, L1 H and L2 H, to move in the direction opposing the flow of the groundwater. This phenomenon is discussed further with the aid of the quiver plot results below.

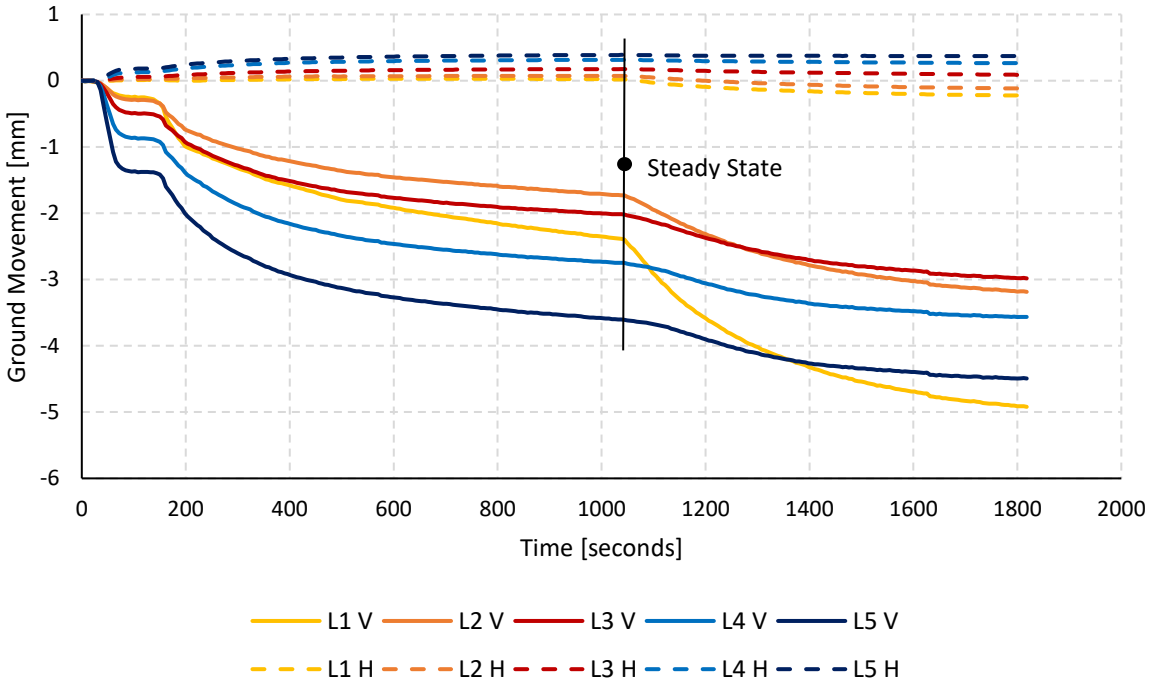

Figure 4-12: Groundwater extraction induced soil movement for GSI Test

Figure 4-13 a) shows the quiver plot depicting the ground movement for the drawdown sequences up to the quasi-steady state water table level. The movement of the ground further away from the extraction well was predominantly vertical whereas the horizontal ground movement increased closer to the extraction well. This could be due to seepage forces acting on the soil skeleton. During groundwater extraction, seepage velocities in the soil are greater than would usually be in the soil. This increased seepage velocity, therefore, exerts greater forces on the soil skeleton resulting in horizontal ground movement. The seepage velocity was also greater closer to the point of extraction, therefore the horizontal movement was greater at this point.

Figure 4-13 b) shows the quiver plot depicting the ground movement from the quasi-steady state water level to the impermeable boundary at the base. During this period the soil closest to the point of extraction well settled mostly vertically. The soil that settled vertically during the initial drawdown had an element of horizontal ground movement, in the direction opposing the seepage direction. To understand the movement of the soil in this area, it is important to assess the state of the soil closest to the point of extraction. The soil closest to the point of extraction was compacted in the vertical direction, due to a reduction in pore-water pressures and in the horizontal direction due to the seepage forces. As the seepage flow rate did not increase any further, the soil can only settle vertically with further pore-water pressure reduction. The soil further away from the point of extraction could settle vertically but the compressed soil closer to the extraction well forced the soil to move in the direction opposing the groundwater flow. Figure 4-13 c) shows the resultant ground movement from the start to the end of the test.

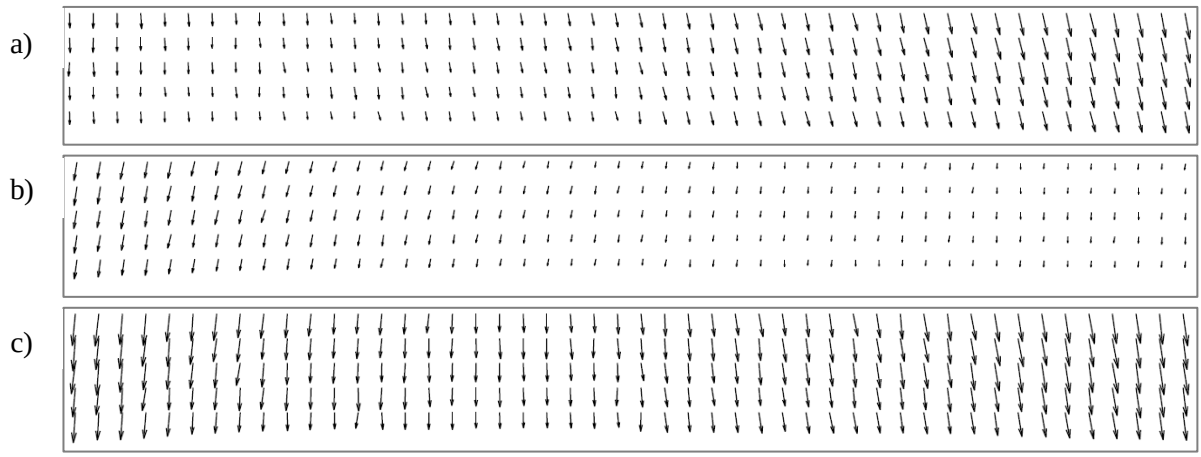

Figure 4-13: Quiver plots of ground movement

The results from this section show that not only vertical soil settlement should be assessed when investigating groundwater extraction-induced ground movement and that the horizontal component of the ground movement should be also considered. The results further correspond well with the groundwater extraction-induced ground movement presented by Yang et al. (2015). Furthermore, the agreement of the results from the discussion on groundwater extraction-induced ground movement with results from the literature shows that groundwater extraction and groundwater extraction-induced ground movement can be successfully simulated in a geotechnical centrifuge. The following section focuses on the interaction between the soil and the portal frames and response of portal frames founded within the distance of influence with varying global and local stiffness to the induced ground movement.

The response of the frames to the induced settlement was assessed throughout the test duration as well as at selected stages during testing. Figure 4-14 depicts the selected stages at which the frame's response was assessed. Stage 1 coincides with the original water table level prior to commencement of the GSSI tests. The replenished water table level prior to commencement of the second drawdown coincided with the original water table level as well. Stage 2 was the stage at which the distance of influence reached the edge of the simulated aquifer and at which the differential settlement throughout the soil mass was a maximum. At stage 3, the water table had reached the lowest level within the soil mass for the given inflow and outflow rates and stage 4 the water table level at the end of the test. The ground movements coinciding with these stages were discussed in the previous sections on groundwater extraction-induced ground movements.

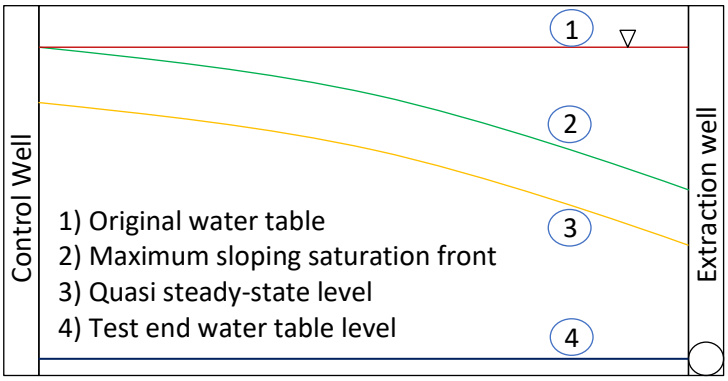

Figure 4-14: Water table position at interaction assessment stages

4.4 SOIL-PORTAL FRAME INTERACTION DUE TO GROUNDWATER EXTRACTION INDUCED GROUND MOVEMENT

The presence of surface structures is known to alter soil settlement profiles associated with ground movement induced by various stimuli (Boscardin and Cording, 1989; Ritter et al. (b), 2017). There is, however, a lack of data quantifying the groundwater extraction-induced soil movements in the presence of surface structures. The change in soil response was investigated by assessing the variation in vertical soil settlement. The free-field soil settlement and the portal frame settlement was compared to assess the degree to which the presence the frames altered the vertical soil settlement. This was done for the four GSSI tests that consisted of a soil investigation side, where the free-field soil settlement was measured and a frame investigation side, where the frame settlement was measured during the same centrifuge test. The free-field soil settlement and frame settlement results for the various GSSI tests are discussed first in this section, followed by the soil structure interaction investigation using the proposed foundation movement parameters.

4.4.1 Free-Field Soil Settlement versus Portal Frame Settlement

Two drawdown sequences were carried out for the GSSI tests. For the first sequence, the water table was drawn down to quasi-steady state level. Thereafter it was replenished and the second drawdown sequence was initiated for which the water table was lowered throughout the strongbox. These sequences correspond with those described in Section 4.2.

4.4.1.1 GSSI test 1: Frame (++)

Figure 4-15 shows the free-field soil settlement, Frame (++) settlement and the extraction-well water level throughout the duration of the test. The presence of the frame resulted in a reduction in the induced vertical settlement compared to that of the free-field soil settlement. The overall average difference in vertical settlement between the free-field LVDTs and the frame LVDTs was 1.2 mm.

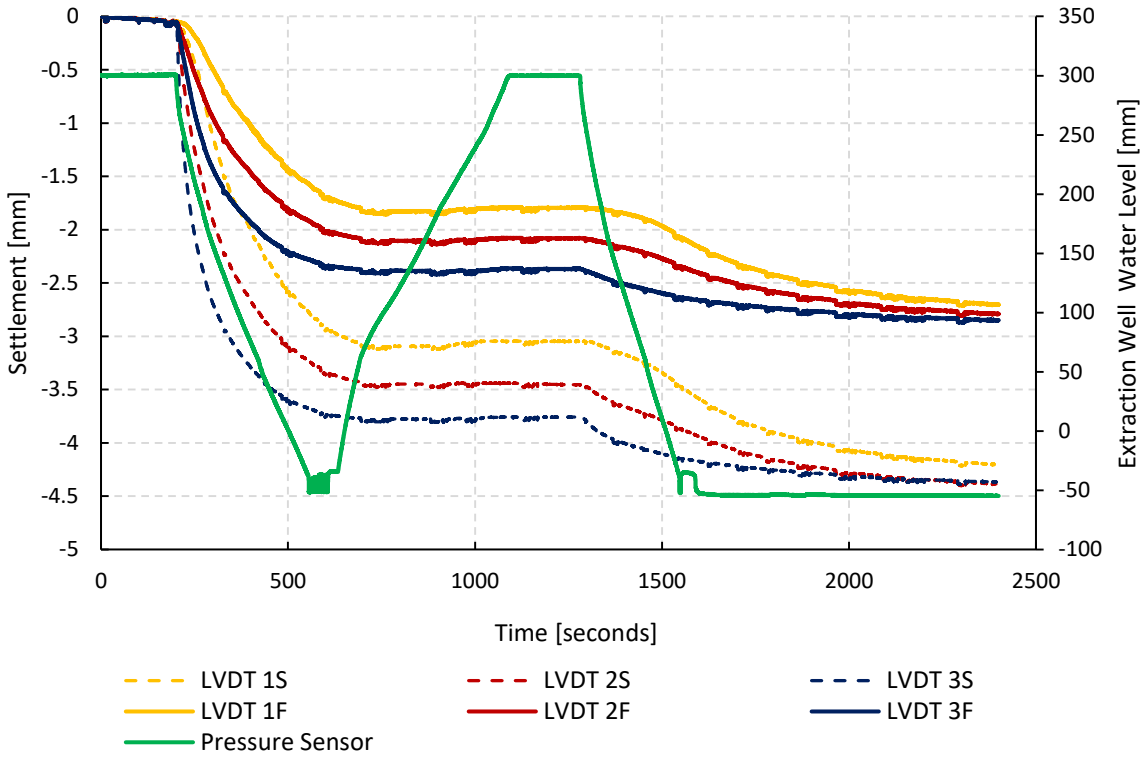

Figure 4-15: Free-field and Frame (++) settlement with time

Figure 4-16 presents the free-field and frame settlement versus the change in extraction well water level. The difference in response to the frame settlement versus that of the free-field soil is clearly evident. The data showed that LVDT 3S started to settle first as the extraction well water level was lowered. This was followed by LVDT 2S which was positioned in the middle of the strongbox in line with the middle column of the frame. LVDT 1F started to settle simultaneously with LVDT 2S albeit that the soil gauge settled faster as depicted by the steeper slope and, therefore, a larger increase in settlement occurred. This shows that the part of the frame closest to the extraction well only started settling at the same time the second soil LVDT started to settle. The frame investigation side (FIS) settlement, therefore, lagged behind the soil investigation side settlement (SIS) settlement by 160 mm along the length of the model. The SIS settlement also took place at a greater rate compared to that of the FIS settlement.

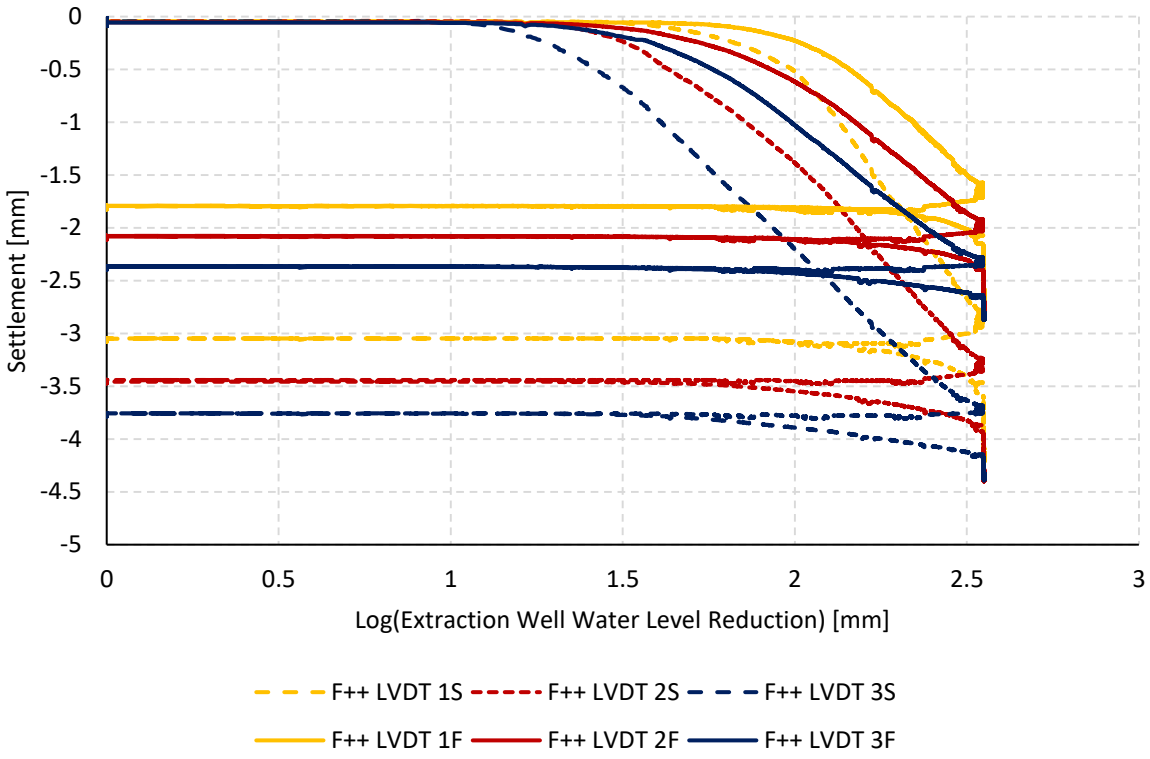

Figure 4-16: Free-field and Frame (++) settlement vs extraction well water level change

4.4.1.2 GSSI test 2: Frame (--)

Figure 4-17 shows the LVDT settlement results throughout the test duration for Frame (--). The data showed that the vertical settlement changed to a lesser degree compared to that of Frame (++). The average difference in settlement between the LVDTs throughout the test duration reduced to 0.4 mm, on average a third of that for Frame (++).

Figure 4-18 shows the free-field and Frame (--) settlement results versus the extraction well water level change. For this frame, LVDT 3S and 3F started to settle at the same time yet the frame settlement slightly lagged behind the soil settlement. It is also evident from Figure 4-18 that the rate of settlement was similar for the SIS and FIS LVDTs although the free-field soil settled more than the frame. This continued for the other settlement measurements with a reduction in the extraction well water level. The frame settlement was much closer to the free-field soil settlement than that of Frame (++).

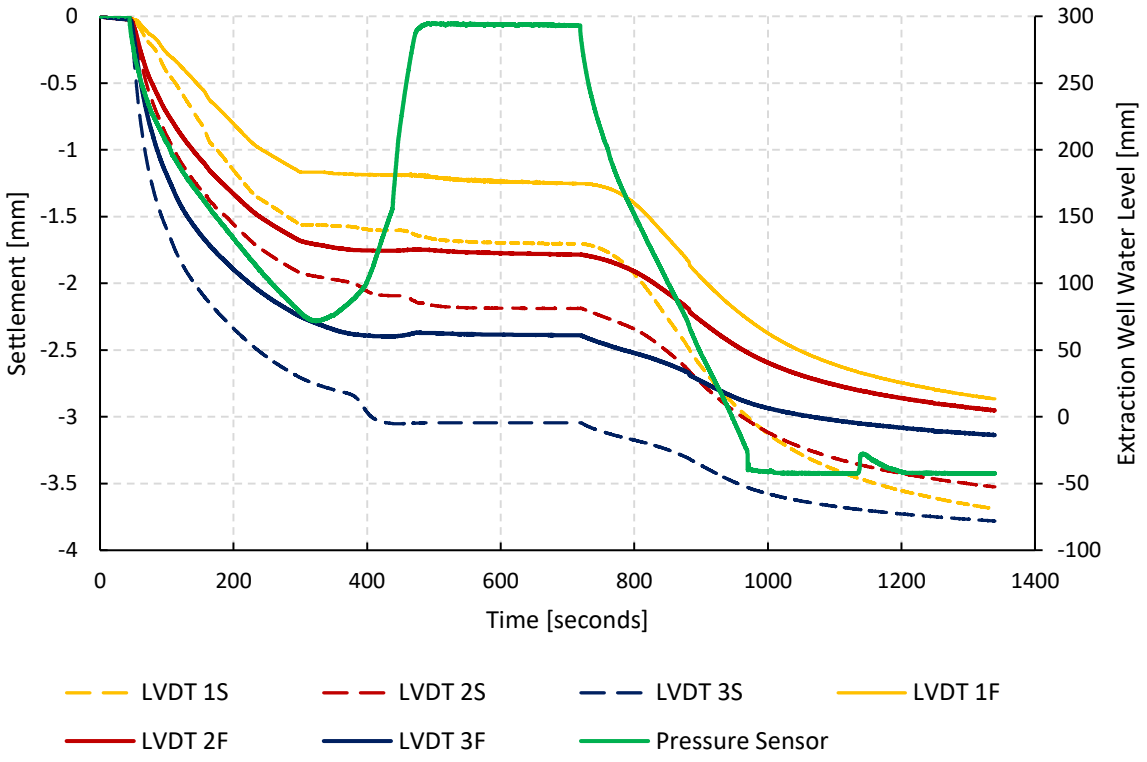

Figure 4-17: Free-field and Frame (--) settlement with time

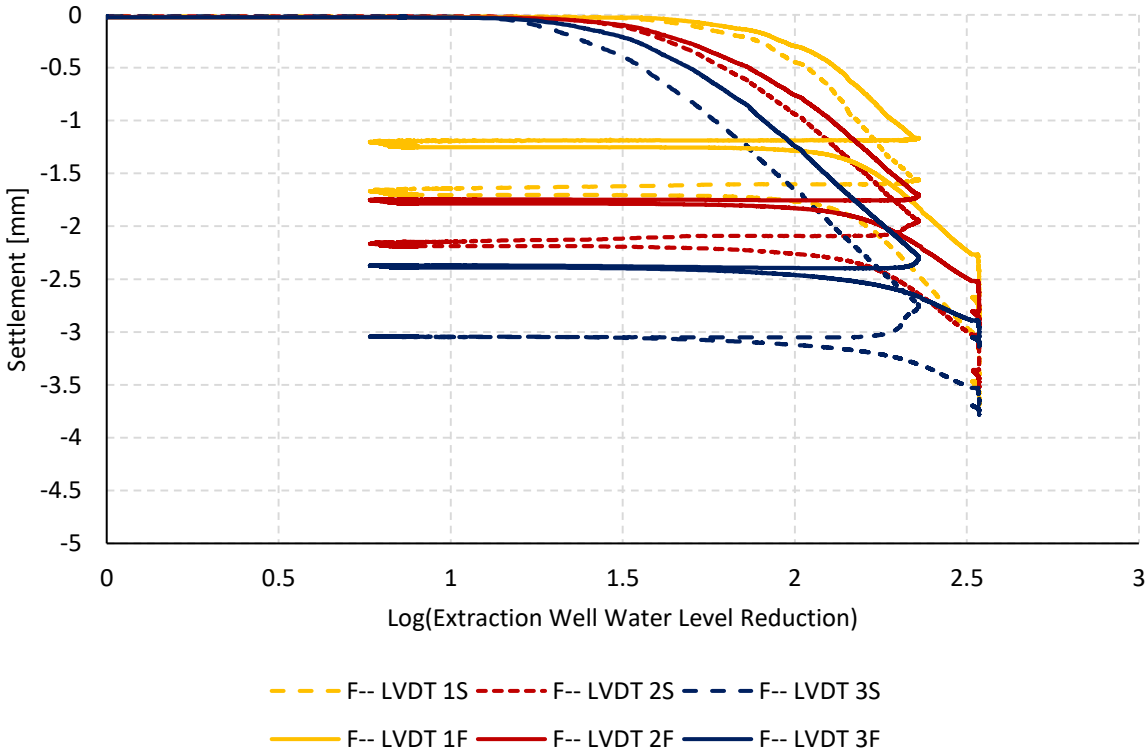

Figure 4-18: Free-field and Frame (--) settlement vs extraction well water level change

4.4.1.3 GSSI test 3: Frame (-+)

Figure 4-19 shows the vertical settlement for Frame (-+). The change in vertical settlement due to the presence of Frame (-+) was between the settlement change for Frames (++) and (--). The vertical settlement was affected to a lesser degree compared to that of Frame (++) but to a greater degree compared to that Frame (--). The average difference in settlement between the free-field and frame LVDTs was 0.73 mm. Data for LVDT 2S could not be retrieved due to the malfunctioning of the LVDT during testing.

Figure 4-20 shows the free-field soil settlement and Frame (-+) settlement versus the extraction well water level change. For this test, the response of the SIS and FIS gauges were similar to that of the Frame (--) test. The FIS LVDTs slightly lagged the SIS LVDTs but the slope, and therefore the increase in settlement was different. The SIS LVDTs settled at a faster rate compared to that of the FIS LVDTs which indicated that the free-field soil settled faster and more than the soil beneath the frame.

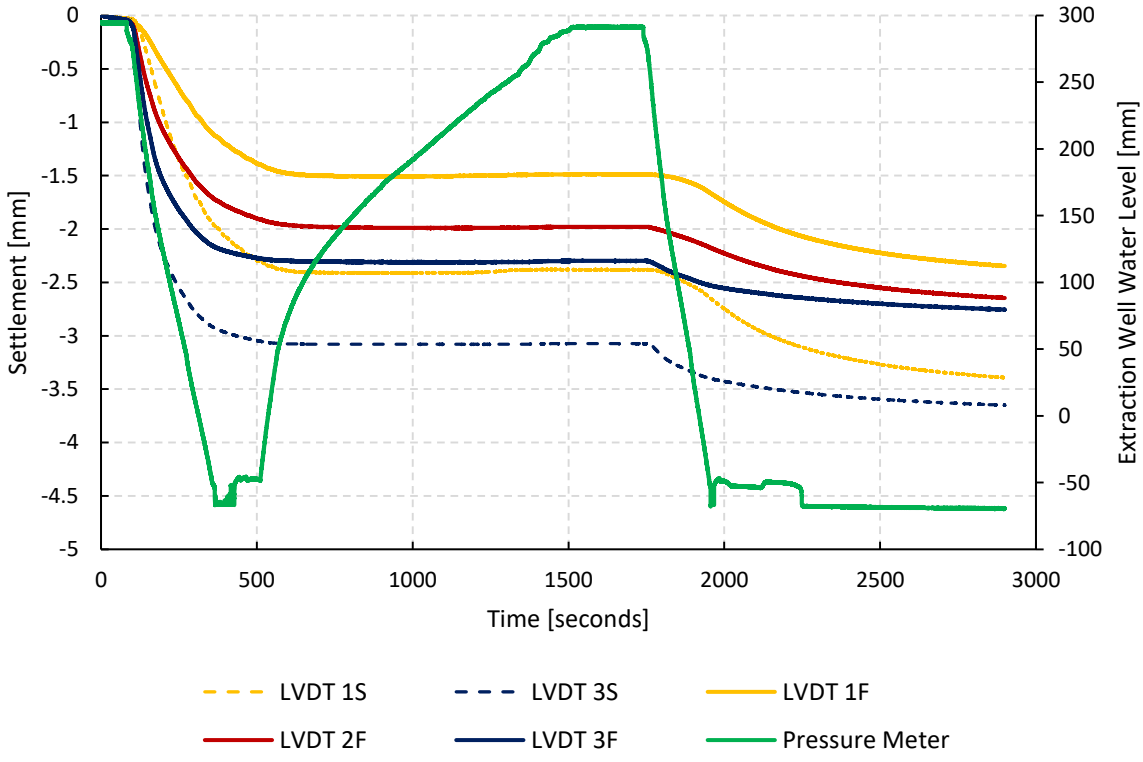

Figure 4-19: Free-field and Frame (-+) settlement with time

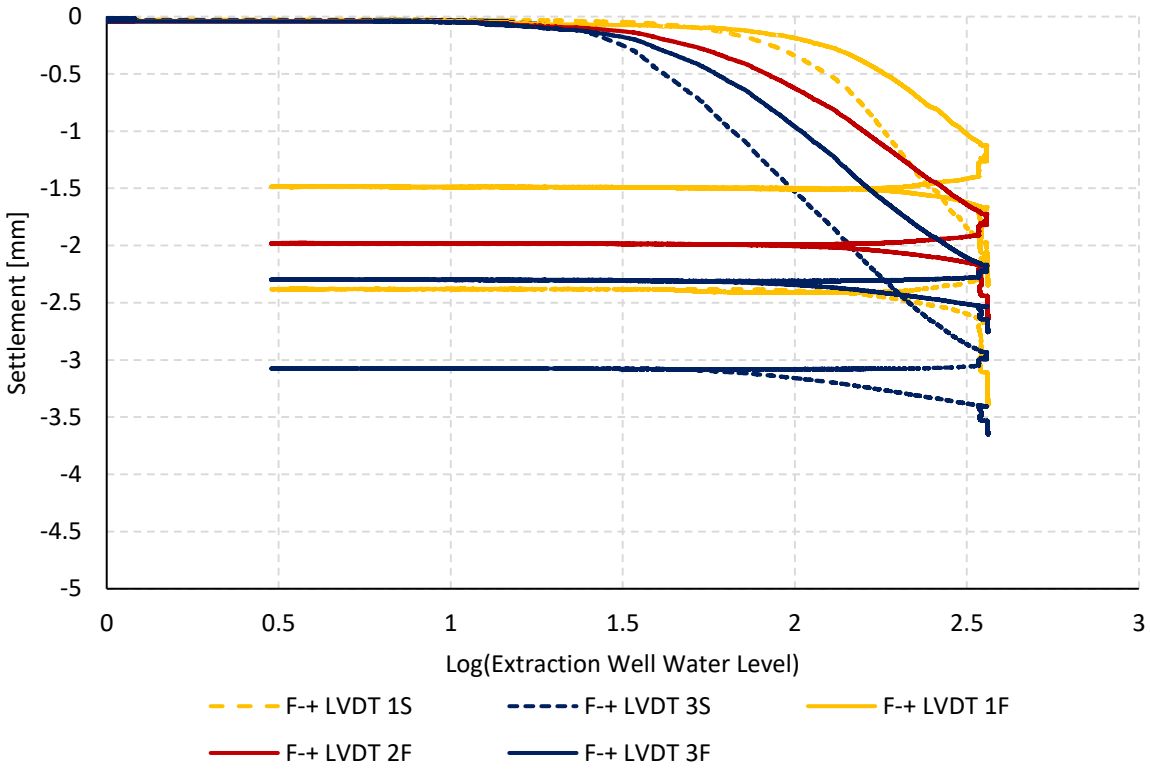

Figure 4-20: Free-field and Frame (-+) settlement vs extraction well water level change

4.4.1.4 GSSI test 4: Frame (+-)

Figure 4-21 presents the vertical soil settlement for Frame (+-). Minimal differential settlement occurred during this test due to the reduction in the rate at which the extraction-well water level was lowered caused by malfunctioning solenoid valves. The differential drawdown of the water table could, therefore, only be achieved to a lesser degree than for the previous test, resulting in reduced differential soil settlement.

Similar to the results for Frame (-+), the degree to which soil settlement was changed by the presence of the frame was between that of Frames (++) and (--). The average difference in settlement between the free-field and frame LVDTs was 0.78 mm which was similar to that of Frame (-+).

Figure 4-22 shows the free-field soil settlement and Frame (+-) settlement versus the extraction well water level change. The settlement response for Frame (+-) was similar to that of Frame (-+) albeit with less differential settlement. The FIS settlement slightly lagged the SIS settlement and the rate of settlement and total settlement for the SIS LVDTs were greater than that of the FIS LVDTs.

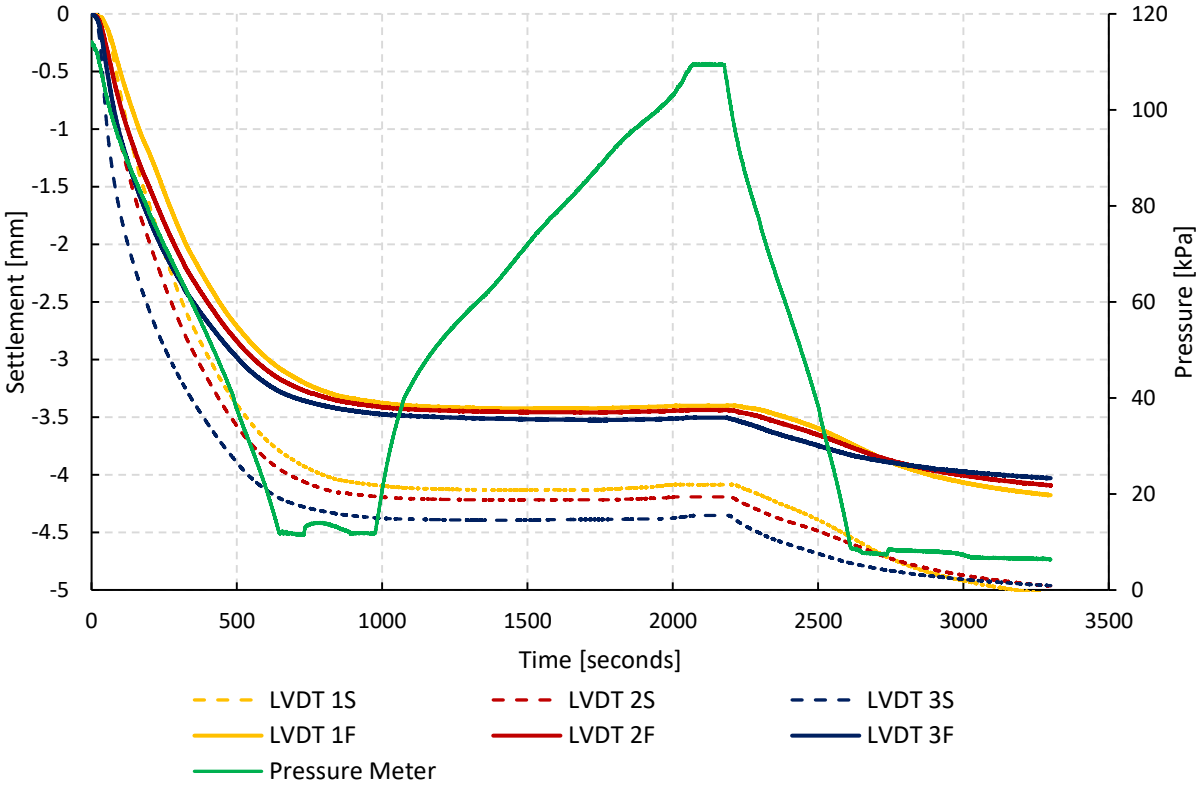

Figure 4-21: Free-field and Frame (+-) settlement with time

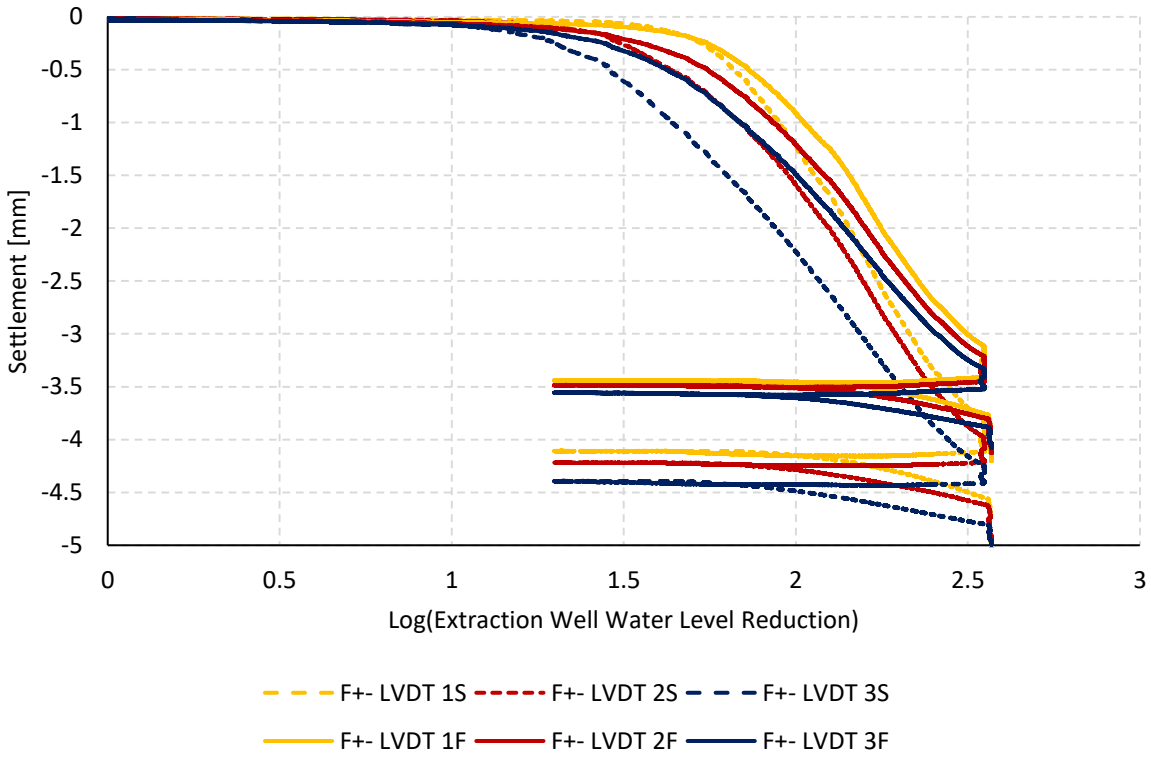

Figure 4-22: Free-field and Frame (+-) settlement vs extraction well water level change

4.4.1.5 Discussion of settlement vs frame stiffness and mass properties

The change in vertical soil settlement could be attributed to two factors, namely; stiffness and mass of the frames. The stiffness of the frames influenced the manner in which the frames settled. The Frames (++) and (+-) which had stiffer slabs and therefore, had a greater vertical shear and bending stiffness, resisted the vertical differential settlement more than Frames (--) and (-+) with the flexible slabs. This was shown by LVDT 1F lagging behind LVDT 2F to a greater degree for Frames (--) and (-+) compared to that of Frames (++) and (+-). This is also an indication of rigid body rotation tilt of the slabs or entire frames for Frames (++) and (+-) and a vertical shear type deformation for Frames (--) and (-+) as can be seen from the free-field and frame settlement vs extraction well water level change graphs. The mass of the frames, furthermore, compacted the soil beneath the footings causing it to be at a higher stress state than the free-field soil. The heavier the frame the greater this effect was. The consequence of this is that the settlement of the FIS soil would lag behind the SIS soil as the soil beneath the frames would have a higher over-consolidation ratio.

Figure 4-23 to Figure 4-25 presents the difference in settlement between the free-field soil LVDTs and the frame LVDTs for the four portal frames plotted against the extraction well water level reduction. The data substantiates the differences in settlement between the different tests discussed in the preceding sections. The difference in settlement between the SIS and FIS LVDTs at the end of the drawdown sequences was greatest for Frame (++) which is the heaviest and the least for Frame (--) which was the lightest frame. The difference for Frames (-+) and (+-) were between that of Frames (++) and (--). This trend is present for all three LVDTs considered. This shows that the heavier frames do indeed compact the soil more resulting in a greater over-consolidation ratio thus the founding soil settling less compared to the lighter frames (see Table 3-3 for the mass of the frames).

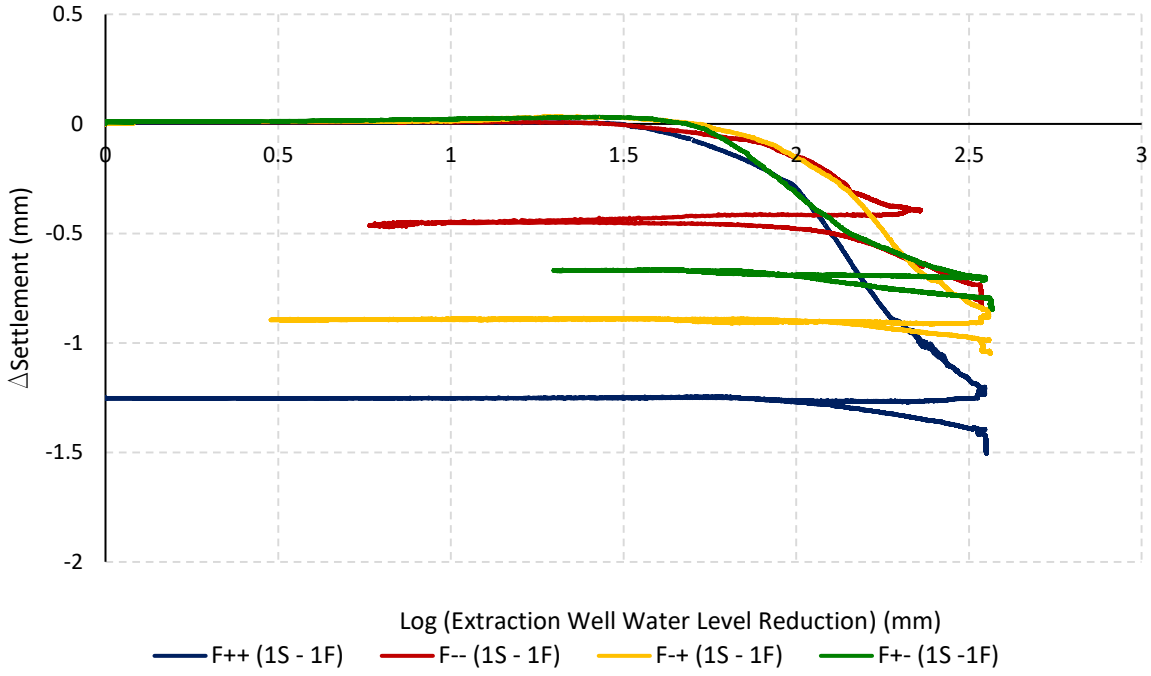

Figure 4-23: LVTD (1S -1F) vs extraction well water level reduction

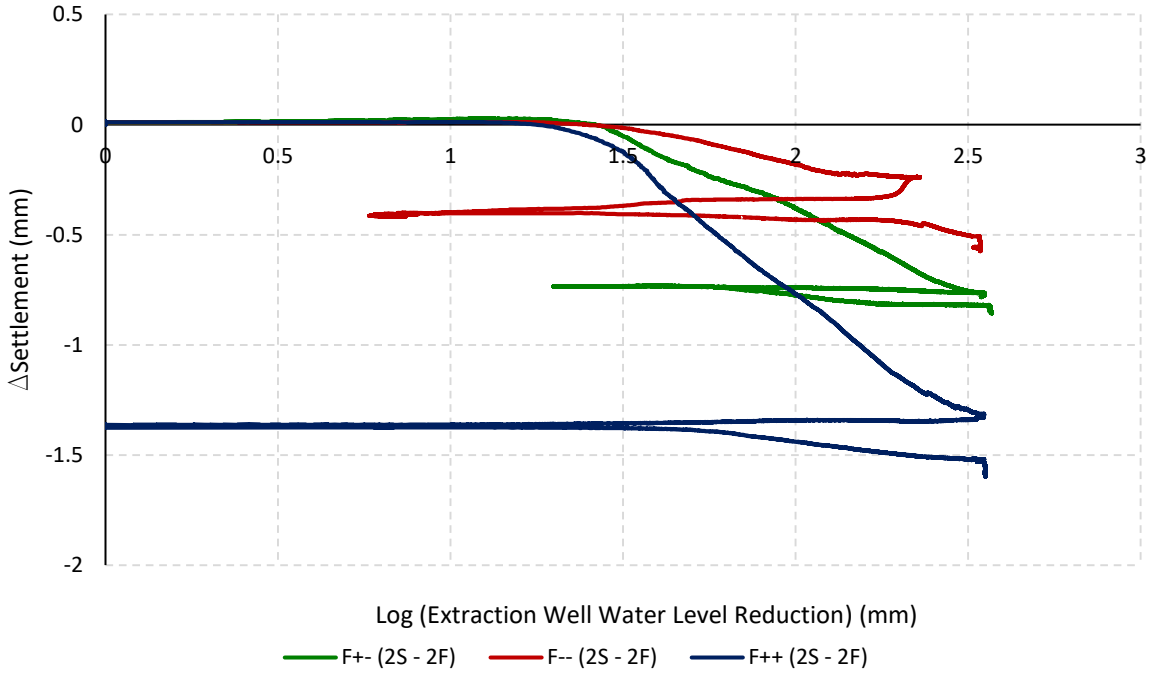

Figure 4-24: LVDT (2S - 2F) vs extraction well water level reduction

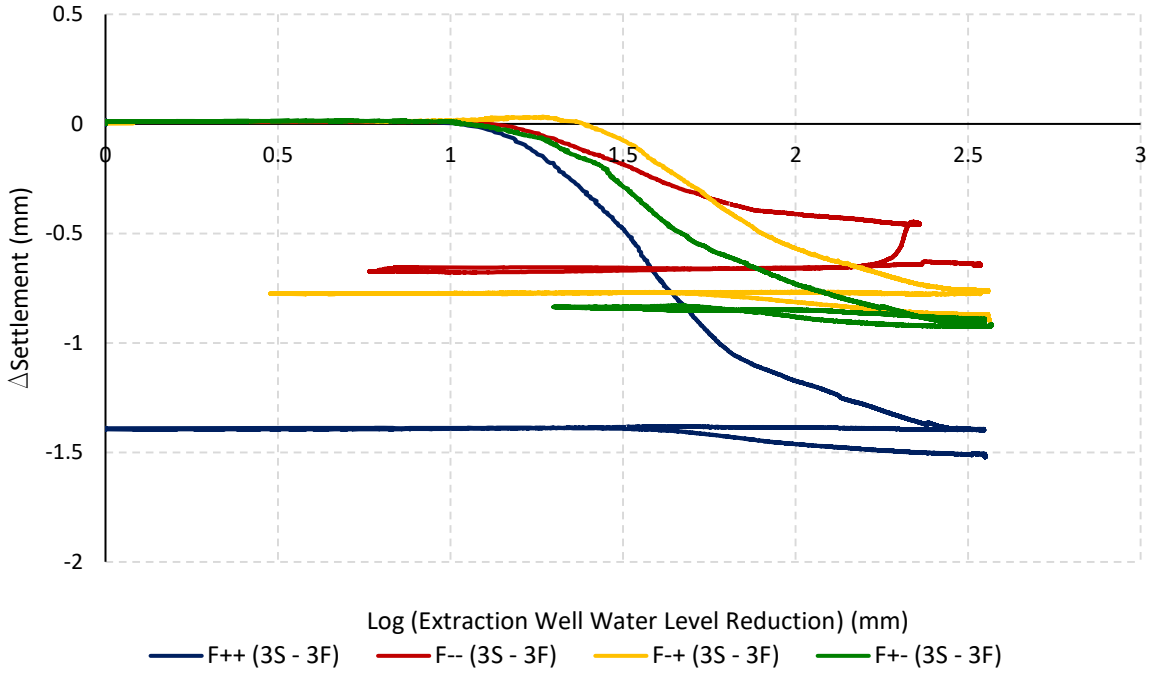

Figure 4-25: LVDT (3S - 3F) vs extraction well water level reduction

The change in the vertical soil settlement gave a good indication of the soil-structure interaction and the degree to which the presence of the structural frames altered the soil response to groundwater extraction-induced ground movement. This however only focused on the soil deformation and alteration and failed to capture how the structural stiffness influenced the way in which the frames deformed due to the imposed ground movements. For example, if only the lag between free-field and frame LVDTs were considered it would be concluded that Frame (++) and (+-) and Frames (--) and (-+) responded in a similar manner. Furthermore, Frames (-+) and (+-) seemed to behave in a similar manner, if only the vertical soil movement was considered as the 0.72 mm difference for Frame (-+) was close to the 0.78 mm difference for Frame (+-). Therefore, widely used foundation movement parameters, namely; angular distortion and average slope were used in the next section to further investigate the influence of structural stiffness on the way the frames deformed.

4.4.2 Comparing Free-Field Soil versus Frame Settlement in terms of Foundation Movement Parameters

Widely used methods to estimate possible building damage caused by ground movements make use of foundation movement parameters (Burland and Wroth, 1974; Burland et al., 1978; Boscardin and Cording, 1989). Normalised angular distortion and normalised average slope were used to determine conformance factors to assess the soil-structure interaction problem (see Section 2.4.1). Figure 4.26 presents a schematic of the GSSI setup depicting the LVDTs and relevant parameters used to determine the normalised angular distortion and normalised average slope. The two parameters were determined using Equation 4-1 and 4-2 as follows:

$$\beta_N = \frac{\Delta_{f(n+1)} - \Delta_{fn}}{\Delta_{s(n+1)} - \Delta_{sn}}$$ Equation 4-1

Where:

β_N = Normalised Angular Distortion between adjacent columns

f = Frame LVDT

s = Soil LVDT

$\Delta_{f/s}$ = Frame or Soil Settlement in line with relevant column

n = Portal Frame Bay

$$s_N = \frac{\Delta_{f3} - \Delta_{f1}}{\Delta_{s3} - \Delta_{s1}}$$ Equation 4-2

Where:

s_N = Normalised average slope for entire structure

$\Delta_{f/s}$ = Frame and Soil Settlement in line with column 1 and 3

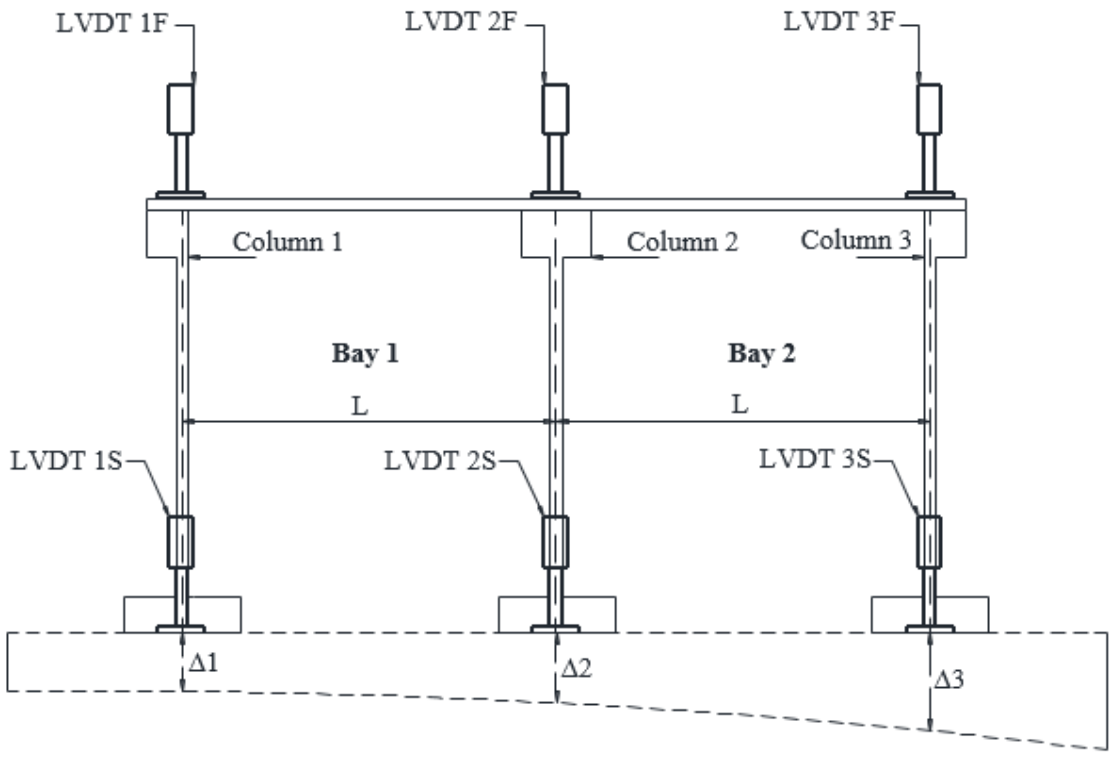

Figure 4-26: GSSI schematic for soil-portal frame interaction

The foundation movement parameters were used to investigate the structural frame deformation due to imposed ground movements and to evaluate how the stiffness of the frames affected the vertical settlement of the frames. The normalised angular distortion (see Equation 4-1) gave an indication of how the individual structural bays deformed. Relative column settlement for a given bay is deemed more critical for structural damage estimation than the overall relative settlement for the portal frame structures (Halim and Wong, 2012)). The normalised structural slope (see Equation 4-2) gave an indication of how the entire structure deformed relative to the soil deformation. The normalised values (hereafter referred to as conformance factors), closer to 1 indicated that the differential structural deformation closely followed that of the soil, whereas, values less than and greater than 1 indicated that the differential structural deformation differed from that of the soil. A negative value indicated a change in slope from positive to negative for either the frame or soil. The angular distortion and slope were determined at four stages during testing (see Figure 4-14), namely; at maximum differential settlement, end of the first drawdown, prior to the start of the second drawdown and at the end of the test (see section 4.2).

Figure 4-27 presents the settlement profiles for the GSSI Frame (++) test at the aforementioned stages (see Figure 4-14) throughout the duration of the test. At stage ‘maximum differential settlement’, the portal frames were exposed to the maximum differential settlement, with the differential settlement for bay 2 greater than for bay 1. Between stages ‘maximum differential settlement’ and the ‘end of the first drawdown’, the differential settlement of the free-field soil decreased slightly at the positions corresponding to bay 1 while remaining relatively unchanged for positions corresponding to bay 2. The slope of the free-field soil decreased as a result while the frame deformations remained relatively unchanged during this stage. The stiffness of the soil, furthermore, increased as the water table was drawn down which resulted in the frames being constrained to the imposed soil deformations at the end of the first drawdown. As the water table was raised from the ‘end of the first drawdown’ to the ‘start of the second drawdown’ stage, the pore-water pressure increased once more resulting in a decrease in the stiffness of the soil. This enabled the structures to relax somewhat, thus, redistributing excess stresses and deforming accordingly while no additional ground movement was imposed onto the structures. During the second drawdown, the slope of the soil decreased to the point where it was close to horizontal, and the differential settlement was minimal for the soil.

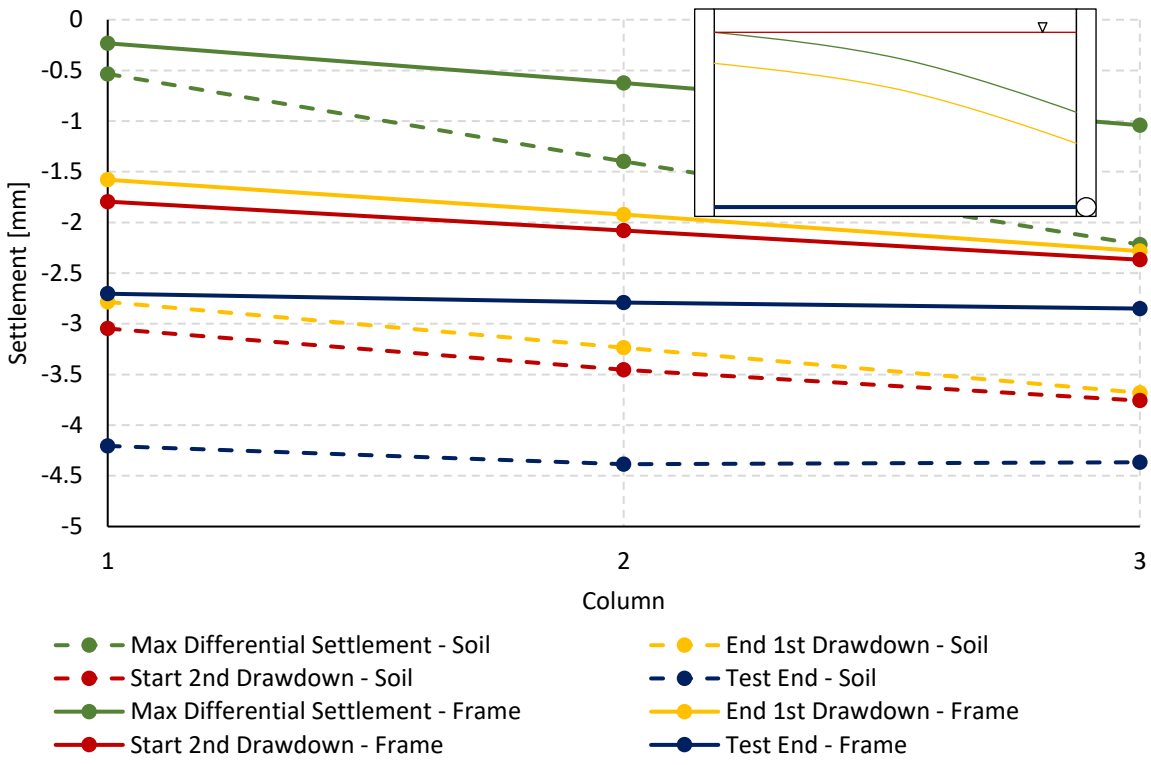

Figure 4-27: Frame (++) settlement profiles

4.4.2.1 Conformance factors at 'Max Differential Settlement'

Figure 4-28 presents the conformance factors when the frames were exposed to the maximum differential settlement. The results showed that Frame (--) had the closest conformance to the imposed settlement for the angular distortion of bay 1, bay 2 and the slope. Frame (++) had the lowest conformance factors for the imposed settlement for bay 1 and the slope and on average the lowest overall factor. These were the frames with the flexible slab-flexible column (Frame --) and rigid slab-rigid column (Frame ++) configurations. This showed that the global stiffness had the greatest effect on frame conformation to the imposed settlement when the frames were exposed to the maximum differential settlement. The rigid frame resisted the imposed deformation while the flexible frame conformed to the imposed deformation. Frame (+-) showed greater conformance for bay 1 where the differential settlement was less than it did for bay 2 where the differential settlement was greater. This showed that as the differential settlement increased the resistance of the frame to the imposed settlement became more evident resulting in a lower conformance factor. The frame also had a low conformance factor for the slope which indicated a similar response to Frame (++) with the rigid slab. The slope conformance factor for Frame (-+) was closer to that of Frame (--) which was relatively high compared to Frames (++) and (+-) which furthermore indicated that overall conformance of the frame was closer to that of the free-field soil. The angular distortion for Frame (-+) could not be determined as the test data for LVDT 2F could not be retrieved.

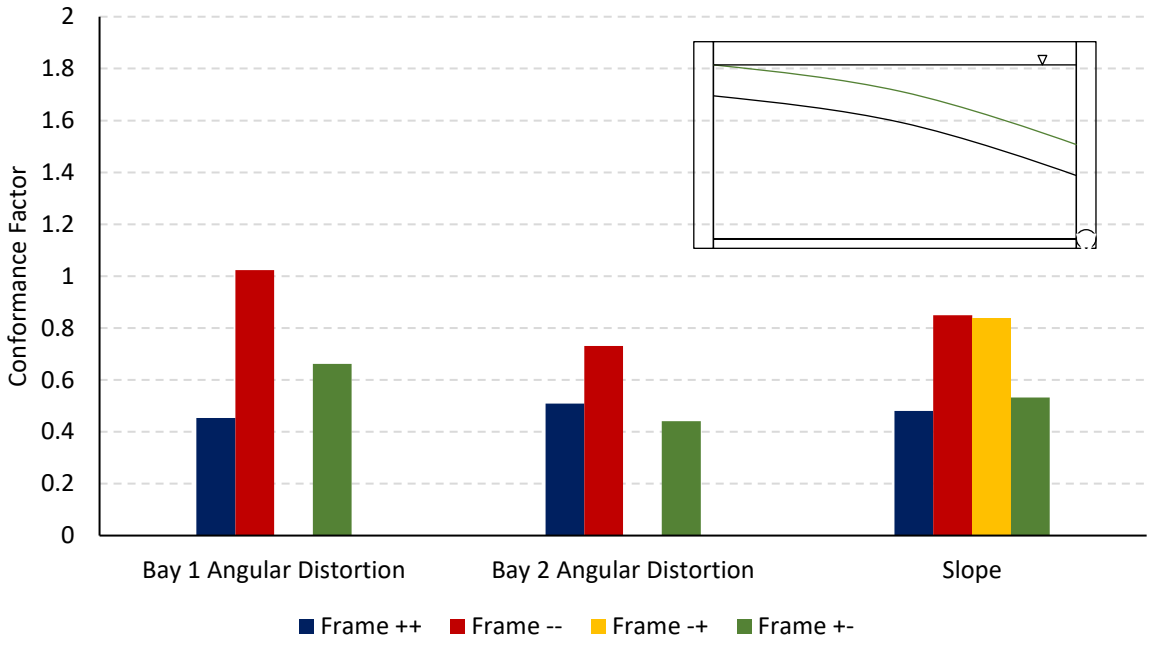

Figure 4-28: Deformation parameters at Max Differential Settlement

4.4.2.2 Conformance factors at 'End First Drawdown'

Figure 4-29 presents the conformance factors for the frames at the end of the first drawdown. At this stage, the differential settlement for bay 1 reduced slightly while remaining relatively unchanged for the points corresponding to bay 2 for the frame and the free-field soil LVDTs from that discussed previously. As a result, the conformance factors for Frame (++) increased from an average of about 0.5 to an average of about 0.8. The angular distortion for bay 1 and the slope for Frame (--) also increased during this stage. The slope conformance factor for Frame (-+) also increased during this stage. The only change in the conformance factors for Frame (+-) was a reduction in the angular distortion of bay 1 and the slope.

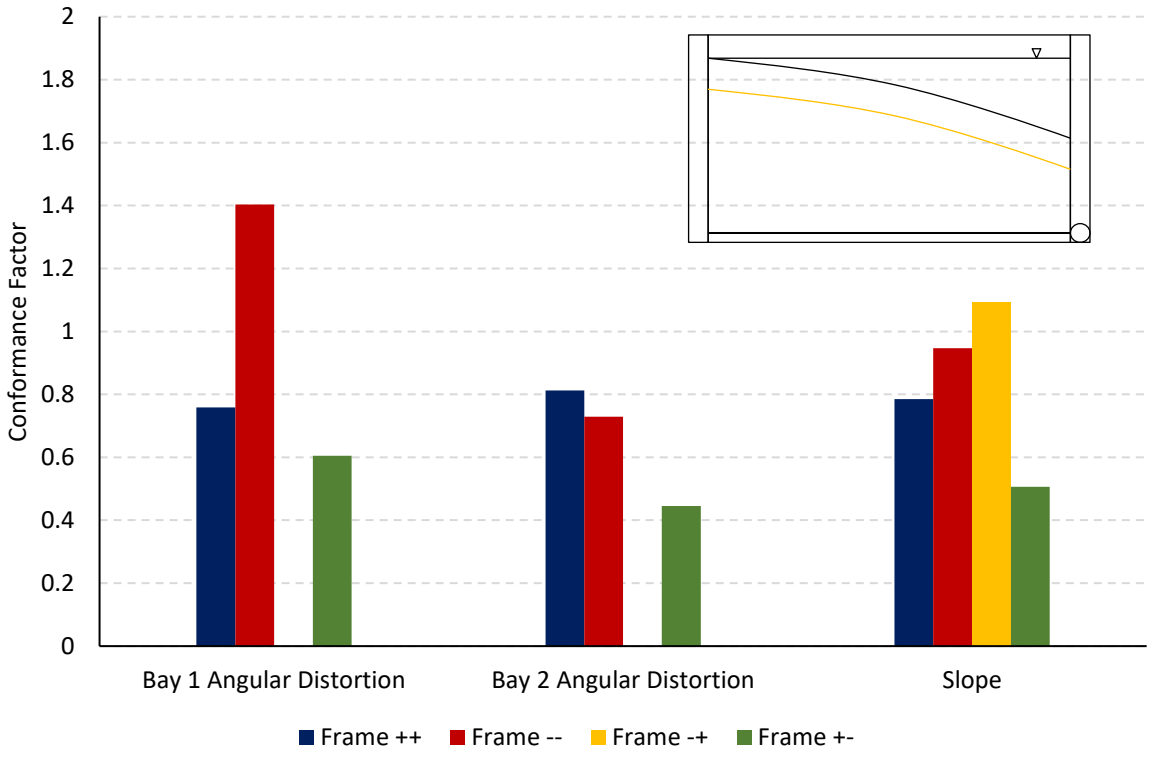

Figure 4-29: Deformation parameters at End of First Drawdown

4.4.2.3 Conformance factors at 'Start Second Drawdown'

Figure 4-30 presents the conformance factors for the frames at the start of the second drawdown. At this stage the soil stiffness decreased as a result of the increase in pore-water pressures and no settlement was imposed onto the frames. It is evident that the largest average change in the conformance factors from those at the end of the first drawdown was for Frame (++) and (+-), which were the frames with the rigid slabs and, therefore, greater bending stiffness. The slope changed slightly for Frames (--) and (-+) while the angular distortion of bay 1 decreased for Frame (--), which were the frames with the lower slab bending stiffness.

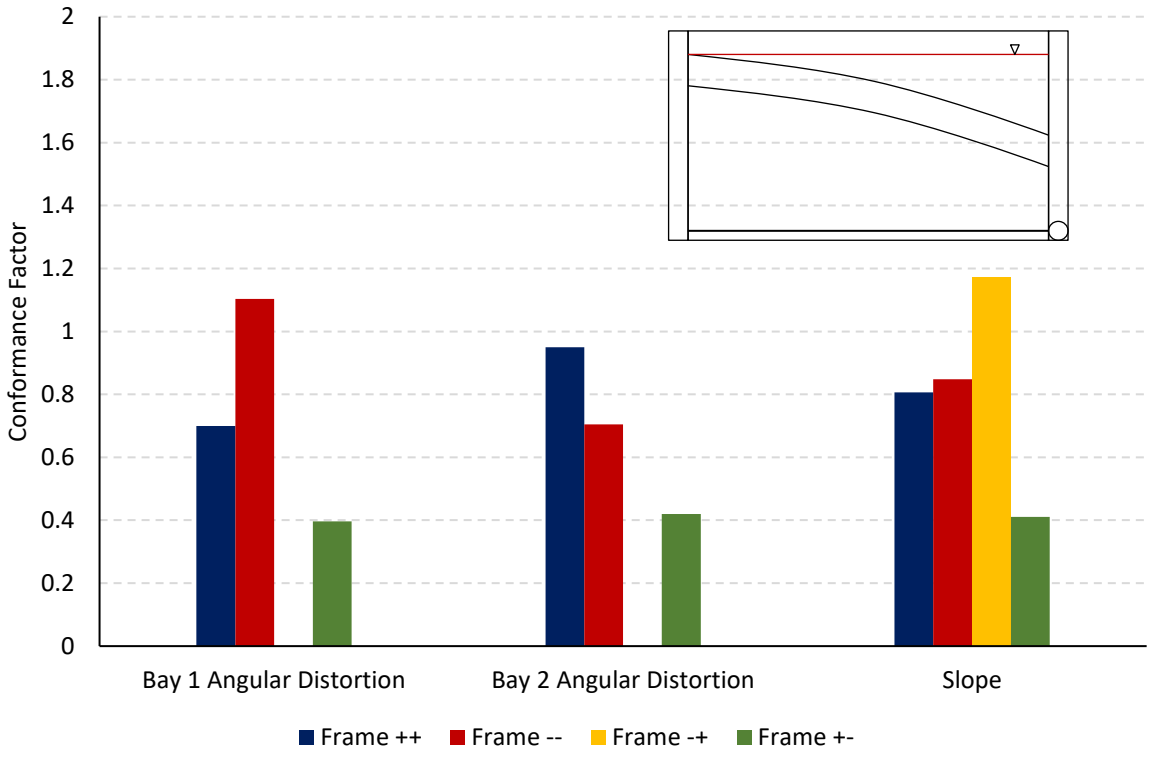

Figure 4-30: Deformation parameters at Start of Second Drawdown

4.4.2.4 Conformance factors at 'End of Test'

Figure 4-31 presents the conformance factors at the end of the tests for the four frames. At this stage, the slope of the free field soil was close to zero and the differential settlement minimal while the frames still maintained a slight slope and differential settlement. This resulted in large slope conformation factors for Frames (--) and (+-). The slope conformation factor remained relatively unchanged for the Frame (-+) throughout the test. The angular distortion for bay 2 of Frame (--) also remained relatively unchanged throughout the test while the distortion factors for Frames (++) and (+-) were negative. This was due to the frames angular distortion becoming negative while remaining positive for the free-field soil. The opposite occurred for Frame (--) angular distortion for bay 1 which was negative. The angular distortion for bay 1 increased slightly for Frame (++) while increasing close to 60 % for Frame (+-) from the start of the second drawdown to the end of the test.

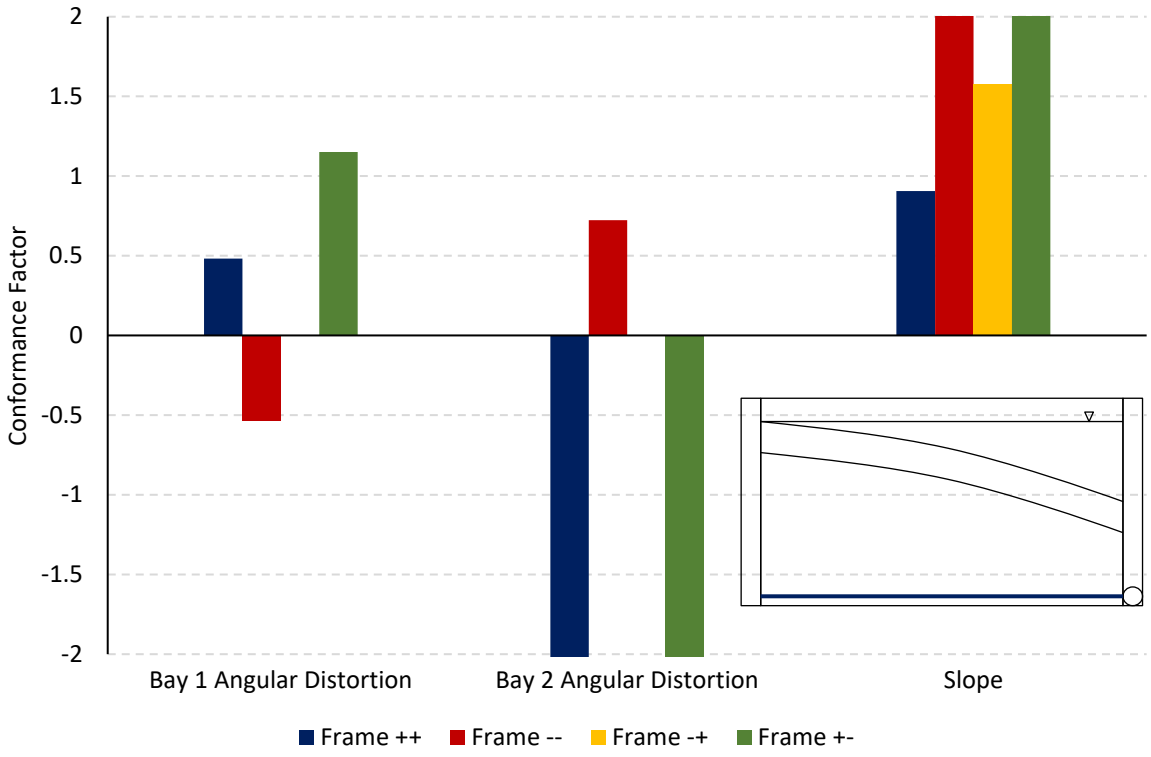

Figure 4-31: Deformation parameters at End of the Test

4.4.2.5 Summary of the conformance factors results

The conformance factors gave a good indication of how the frames responded during different periods of groundwater extraction and the resulting imposed settlements. The slope conformance factor for Frame (-+) remained relatively close to perfect conformance throughout testing with less than an average of 20 % deviation from perfect conformance. This, together, with the large variations in the slope conformance factors for the rest of the frames, indicated that Frame (-+) conformed closely to the imposed differential settlement albeit for the slope only. This could be as a result of the low vertical shear resistance due to the flexible slab and the high relative column/slab stiffness of the frame. This caused the frame to deform in a shear-type deformation conforming closely to the imposed vertical differential settlement.

The continuously low conformation factors indicated that Frame (+-) had a high resistance to the imposed vertical differential settlement. The decrease in the conformance factors during the water replenishing phase also indicated that frame exhibited signs of relaxation, redistribution of excess stresses. This was attributed to the high vertical shear resistance and bending stiffness of the slab which resisted shear deformation indicating a combination of bending type deformation and rigid body rotation of the slab. The deformed slab would, therefore, relax when the soil stiffness decreased as a result of the high bending stiffness which is evident from the conformance factors at the start of the second drawdown (see Figure 4-30).

The results for Frames (++) and (--) showed that the frames deformed in contrasting ways. Frame (++) resisted the imposed deformation while Frame (--) conformed more to the deformation as indicated by the conformance factors for the first two stages. Results for Frame (++) also showed that the frame deformed by rigid body rotation (tilt) rather than vertical differential settlement of its columns. Frame (++), furthermore, showed greater relaxation during the replenishing phase than Frame (--) (changes in the conformation factors for Frame (--) during this stage was primarily due to changes in the free-field soil than the frame). Frame (--) exhibited greater conformance to the imposed deformation and a greater shear type deformation than Frames (++) and (+-) which could be attributed to the flexible slab.

Focus thus far has mainly been in the groundwater extraction induced ground movement and the interaction between the soil and the portal frames. The next section, therefore, focusses on the response of the portal frames to the imposed ground movements.

4.5 PORTAL FRAME RESPONSE TO IMPOSED GROUND MOVEMENTS

Ground movements imposed onto portal frames cause the frames to deform which results in a redistribution of the frame loading and change of internal stresses. These factors cause an change in the forces and bending moments within structural elements of the portal frames. The forces and bending moments are redistributed until equilibrium is reached within the frames and between the frames and the founding soil or when failure is ultimately reached (Weigel et al., 1989; Son and Cording, 2005; Lin et al., 2015). The degree to which these factors change during groundwater extraction was used to investigate the response of the portal frames to the imposed ground movements.

The response of the portal frames to groundwater extraction-induced ground movements was investigated by assessing the measured strain response of the portal frames. Column axial loads and, column and slab bending moments determined from the measured strain were used to assess the response of the frames.

4.5.1 Portal Frame Strain results

Figure 4-32 presents the strain results for the four frames throughout the groundwater extraction tests for the relevant strain gauges (see Figure 3-8). The overall strain trend was the same for all the frames with the strain increasing with the initiation of groundwater extraction for all the gauges. This was followed by a decrease in strain as the water table was re-established to the original level after which it increased again as the water table was lowered for the second and final drawdown. The strain plots, therefore, indicate that the frames deformed in response to the groundwater extraction-induced ground movements.

The overall strain development was similar for Frames (++) (Figure 4-32a) and (--) (Figure 4-32d) with differences in the magnitude of strain. The strain response for Frame (--) with the flexible members was greater than that for Frame (++) for the same gauges. The strain increased almost instantly for gauges 7 and 8 while it increased gradually for gauges 1 and 2 with the latter gauges having a greater strain at the end of the tests. The general trend exhibited by gauges 3 and 4 as well as 5 and 6 were also similar for the two frames. Strain results for gauges 9 and 10 for Frame (++) could not be retrieved due to problems encountered during testing.

The difference in strain response was, however, evident for Frames (-+) (Figure 4-32b) and (+-) (Figure 4-32c). The change in strain for gauges 3 and 4 for Frame (-+) was much greater than the same gauges on Frame (+-), whereas the opposite is true for the wall gauges, 1, 2, 7 and 8. This showed that most of the deformation of these frames took place in the flexible structural members which was the slab for Frame (-+) and the columns for Frame (+-). The strain results at the column-slab connections, (see gauges 3 and 4, Figure 4-32) showed that when the relative column-slab stiffness was changed that the strain was greater in the more flexible member, the slab for Frame (-+) compared to the same gauge reading for Frame (+-).

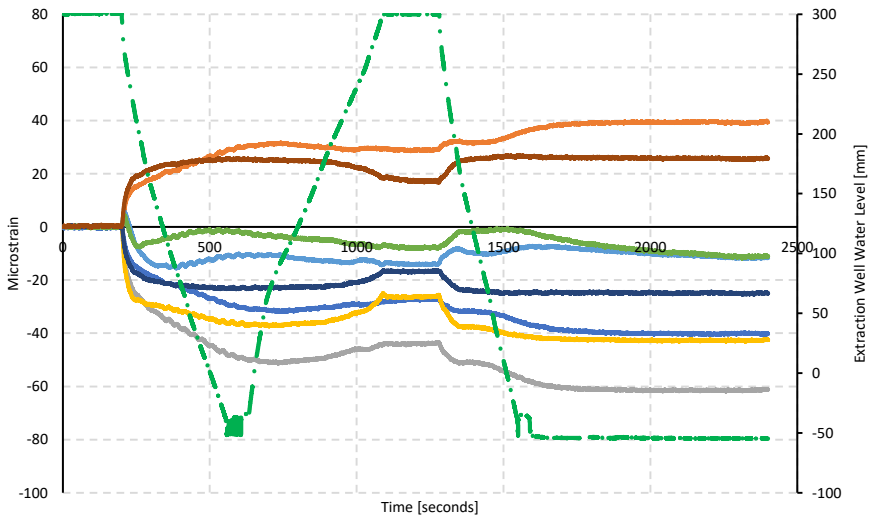

a) Frame (++)

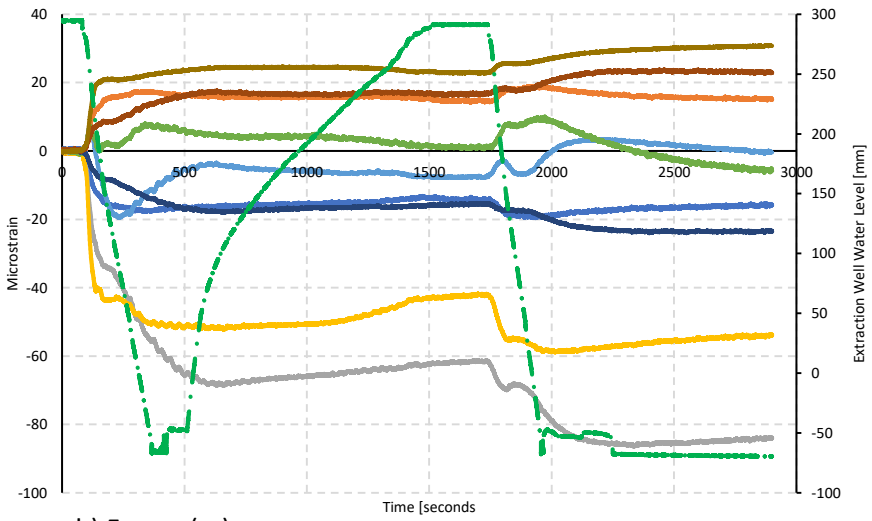

b) Frame (-+)

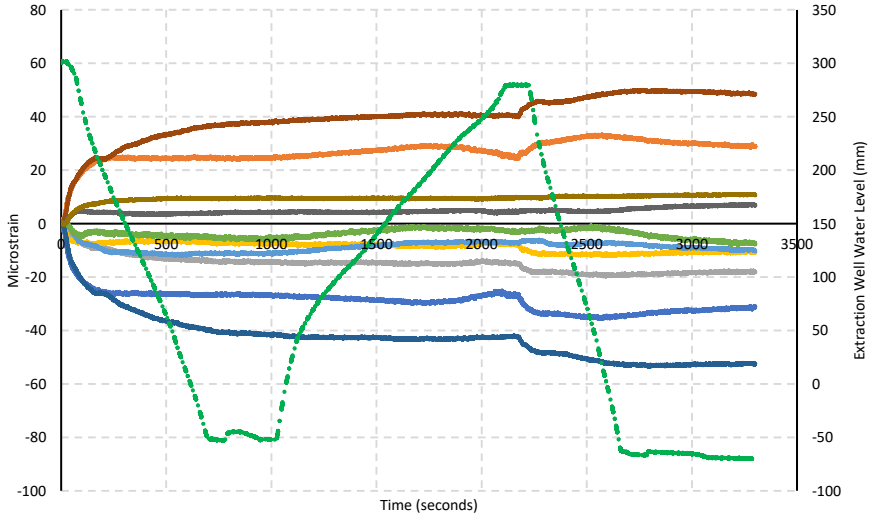

c) Frame (+-)

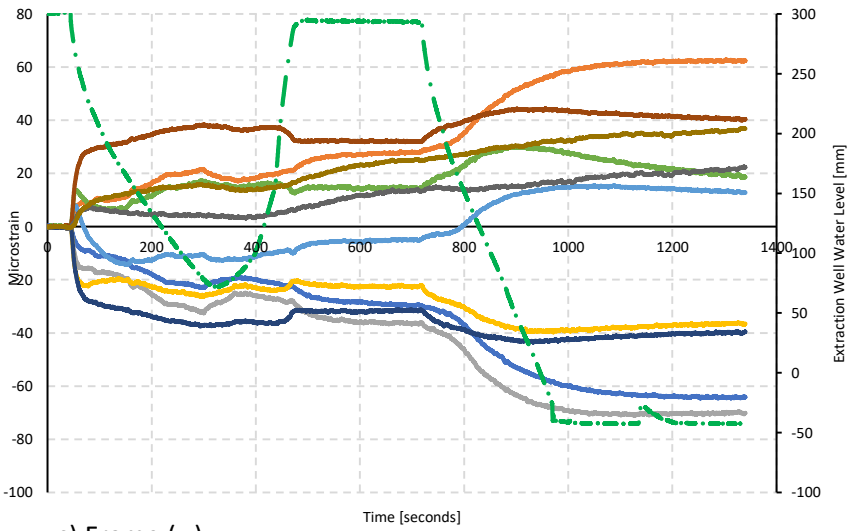

c) Frame (--)

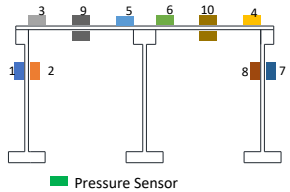

Figure 4-32: Strain results

4.5.2 Portal Frame Column Axial Force Response

The most widely used parameter for assessing structural behaviour is the column and footing load variation (Jardine et al., 1986; Weigel et al, 1989; Houy et al., 2005; Lin et al., 2015). The column loads give an indication of structural load paths and load distribution of a structure. Therefore, any variation in the column loads would give an indication of alteration in load paths and redistribution of the structural loading. The sign convention used for this section was that a positive change in column load indicated an increase in the compressive force for the column. The change in the column force for column 2 was determined from the change in load for columns 1 and 3 as load equilibrium had to be maintained for the frames. Due to excessive noise in the original column force strain results a central average of 200 points (see Figure 4-33, C1) was used to smooth out the calculated force results.

4.5.2.1 Column axial force response: Frame (++)

Figure 4-33 presents the change in compressive force for the three columns of Frame (++). As the water table was lowered for the first drawdown, there was an immediate decrease in the compressive force for columns 1 and 3 and an increase for column 2. As groundwater extraction was initiated, the settlement was localised to the soil closest to the extraction well resulting in the settlement of column 3. The induced settlement was resisted by the rigid slab causing an increase in the compressive force for column 2 which resulted in a pivoting effect about this column and therefore pulling on column 1. This pivoting effecting resulted in a decrease in the load for column 1. As the extraction well water level continued to drop, the compressive force in column 3 continued to reduce but as column 2 started to settle as well, the pivoting effect started to decrease and the compressive force for column 1 started to increase as more load was transferred to the column.

As the water table was raised for the second drawdown, the compressive force for column 1 started to decrease while increasing for column 3. This continued until the change in force for column 3 was zero and the decrease in compressive force for column 1 was equal to that of column 3 at the end of the first drawdown. This was due to excess stresses within the structural members being redistributed throughout the frame as the soil softened. A similar trend as for the first drawdown was repeated where the column loads increased and decreased for columns 1 and 3 respectively during the final drawdown. As the water table continued to lower throughout the strongbox, the differential settlement reduced, the force in columns 1 and 3 started increasing as the load was redistributed throughout the frame while decreasing for column 2.

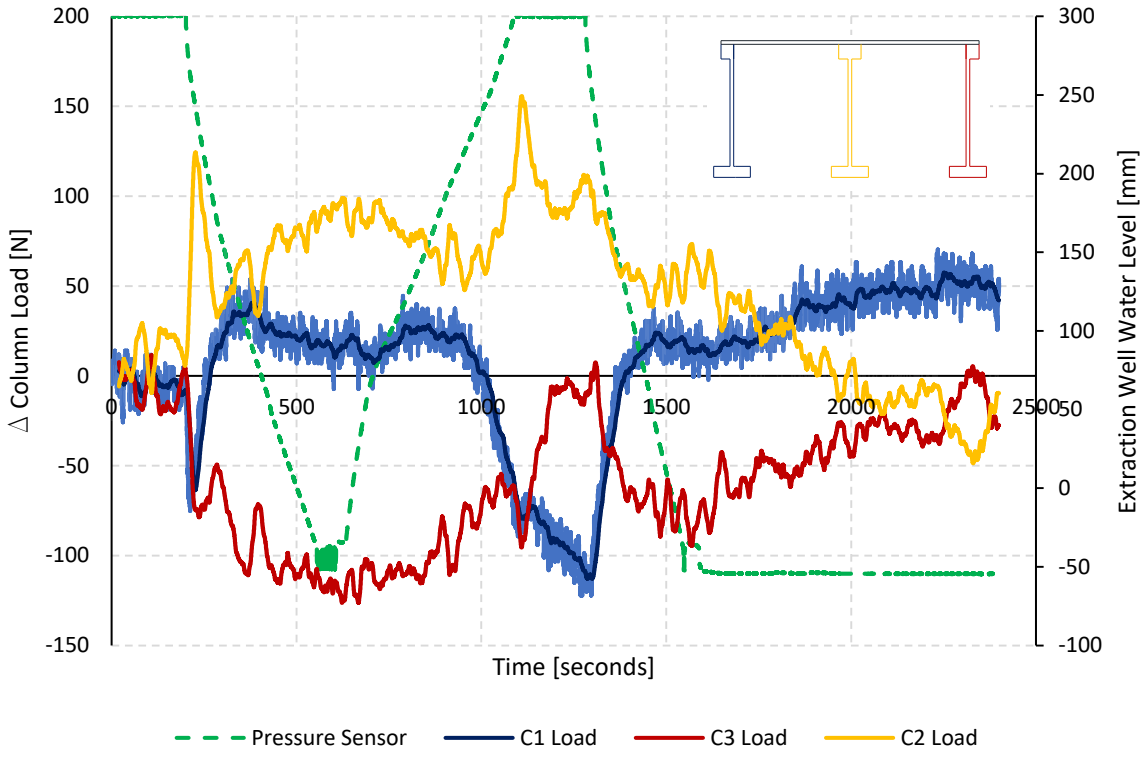

Figure 4-33: Frame (++) column load change

4.5.2.2 Column axial force response: Frame (--)

Figure 4-34 presents the change in compressive force for the columns of Frame (--). The initial response for columns of Frame (--) was similar to that of Frame (++) with an immediate decrease in the compressive forces for columns 1 and 3 with the initiation of groundwater extraction due to the pivoting effect about column 2. This was followed by an increase in the compressive force for column 1 and a decrease in the compressive force for column 2 with a slight decrease for column 3. The column compressive forces remained relatively unchanged throughout the test with slight variations during replenishing and the second drawdown. This showed that most of the load throughout the test duration was transferred from the settling columns, 2 and 3, to column 1. The flexibility of the frame also meant that minimal excess stress built up in the frame elements resulting in minimal redistribution when the soil softened during replenishing. The low global stiffness of the frame meant that redistribution of the frame loading was also not possible.

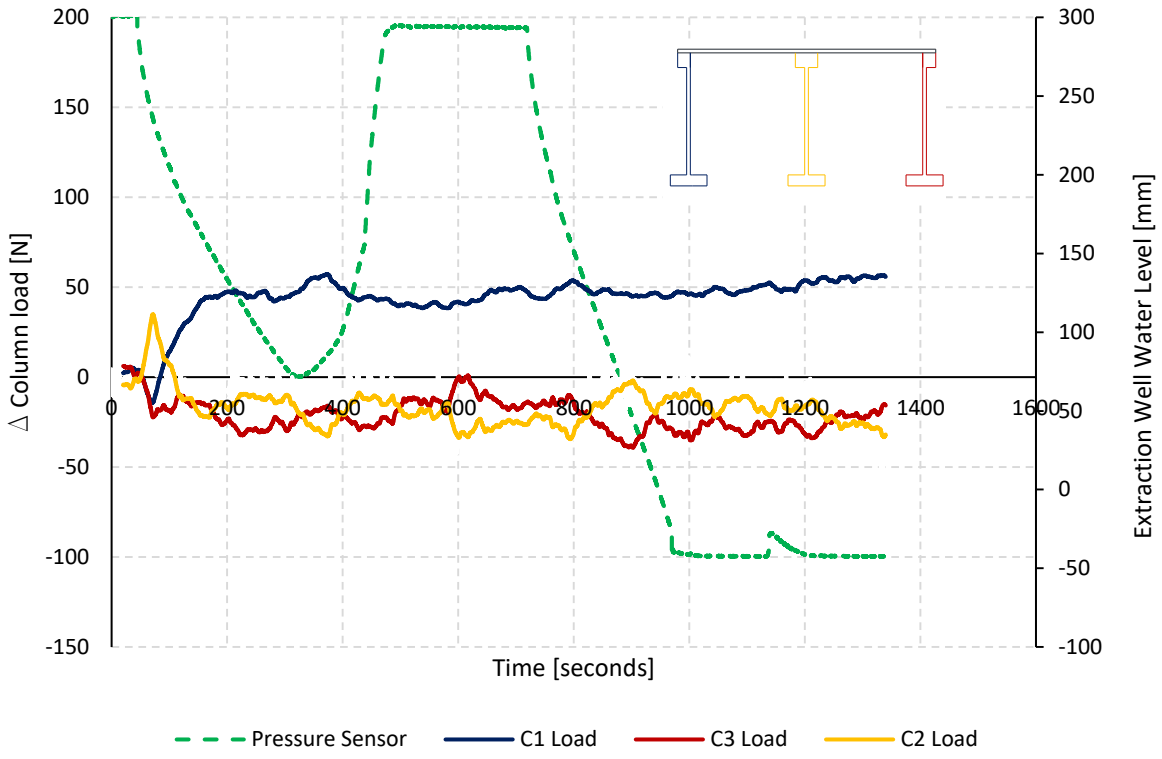

Figure 4-34: Frame (--) column load change

4.5.2.3 Column axial force response: Frame (-+)

Figure 4-35 presents the change in compressive force for the columns of Frame (-+). During this test, the compressive forces reduced for columns 1 and 3 while increasing for column 2. This was a similar response as previously seen for Frames (++) and (--) due to the pivoting effect. The compressive force in column 2 continued to increase as the first drawdown sequence continued while decreasing for column 1 and column 2. During the replenishing phase, the compressive force in columns 1 and 3 increased while decreasing for the central column. Due to the flexibility of the slab the column force change during this stage was more a result of the redistribution in frame loading as the soil softened than it was due to redistribution of excess stresses in the frame slab. When the water level reached the founding level, prior to commencement of the second drawdown, the force in column 3 reduced while increasing for column 2. With the initiation of the second drawdown, the pivoting effect happened once more followed by an increase in the compressive force for column 2 and a reduction for columns 1 and 3.

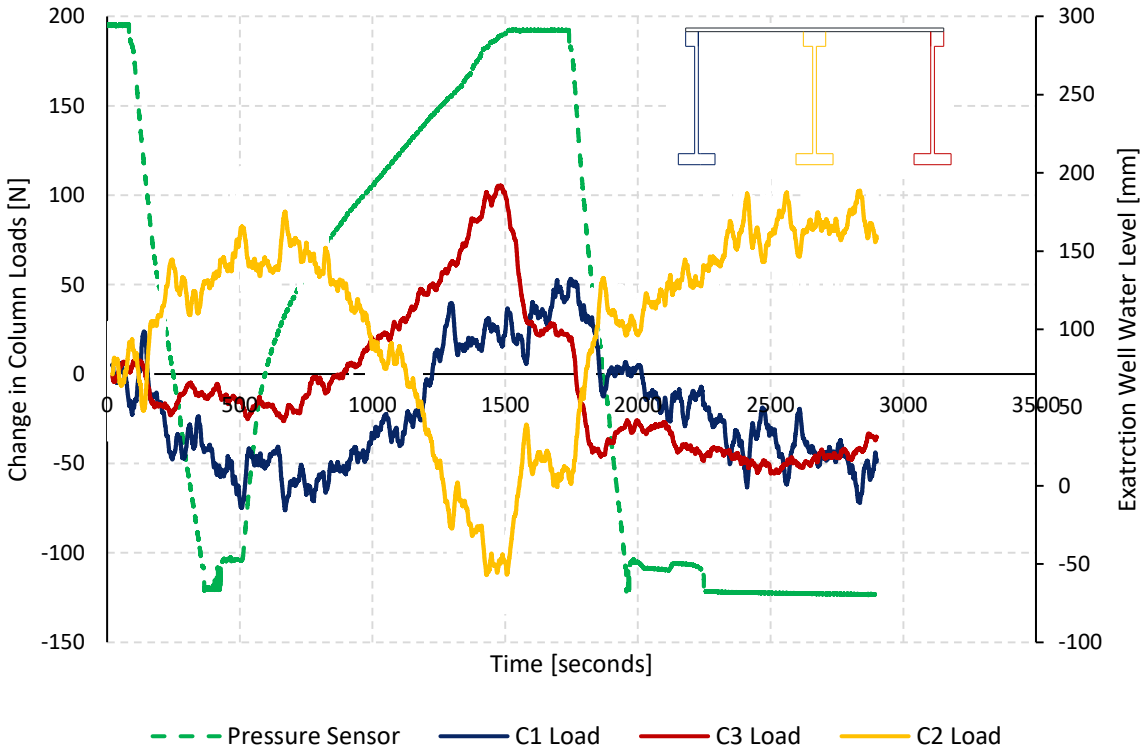

Figure 4-35: Frame (-+) column load change

4.5.2.4 Column axial force response: Frame (+-)

Figure 4-36 presents the compressive forces for the columns of Frame (+-). The column forces exhibited a similar pivoting effect about column 2 as the previous frames while the response throughout the test duration was similar to that of Frame (-+). However, the compressive force did not increase above and reduce below its starting value for column 1 and column 2 respectively as was the case for Frame (-+). The increase in the compressive force for column 3 after the initial decrease at the initiation of drawdown was also greater for Frame (+-). This response of the frame to the imposed settlement was mainly dictated by the slab, similar to Frame (++). The frame exhibited the largest increase in the load for column 2. The settling of column 3 caused the frame to tilt towards the settling columns (see Section 4.4.2.5) as the rigid slab resisted the settlement resulting in a greater pivoting effect and hence the largest increase in load for column 2 and reduction for column 1. The abrupt change of column forces during the replenishing phase and when the water table reached founding level, shows that the change in column forces were as a result of the redistribution of excess bending stresses in the rigid slab and to a lesser degree due to the redistribution in frame loading. The column forces showed a similar response for the second drawdown as for the first drawdown sequence.

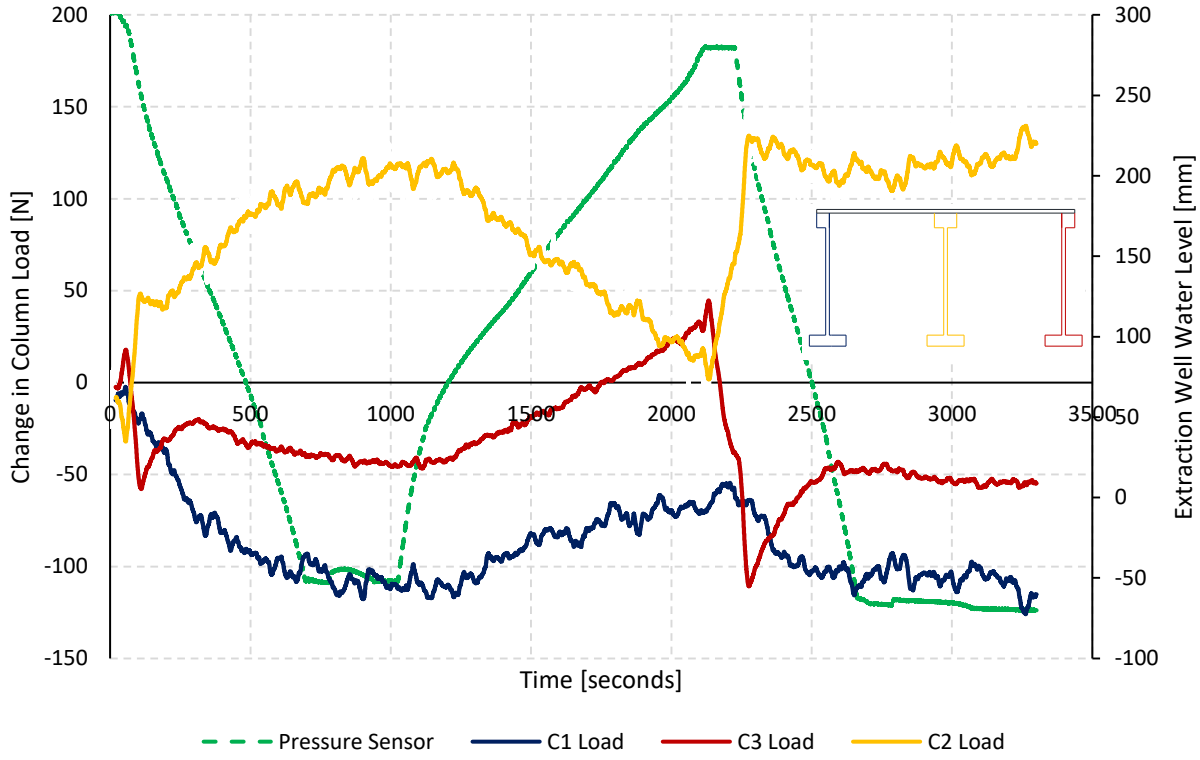

Figure 4-36: Frame (+-) column load change

4.5.2.5 Summary of column axial force response

The frames exhibited a similar response during the initiation of groundwater extraction. The compressive force reduced for columns 1 and 3 while increasing for column 2 as the slabs pivoted about this column. This effect was greatest for Frame (++) while becoming more pronounced for Frame (+-) throughout the duration of the test. The response of Frame (--), furthermore, showed that the due to the flexibility of the frame elements, that the forces in the settling columns, 2 and 3, were transferred to column 1 and remained relatively unchanged throughout the test as the frame showed greater conformance to the imposed ground movements. This also showed that there was not much build-up of excess stresses in the flexible members of the frame. Results for Frame (++) on the other hand showed that the frame deformed more as rigid body due to the rigidity of the slabs and columns which is shown by the increase and decrease in of the force in column 2 during the two drawdown cycles respectively.

Frame (-+) and (+-) exhibit the same response throughout the duration of the tests albeit that the change in forces were greater for Frame (+-). This was attributed to the rigid slab of Frame (+-) which caused greater pivoting effect and due to greater increase in excess stresses compared to the flexible slab of Frame (-+). The latter meant that the change in column forces during replenish was driven more by the redistribution of excess stresses than frame loading with the opposite true for Frame (-+).

4.5.3 Frame Response to Horizontal Ground Movements – Column Bending

Groundwater extraction-induced ground movement has a component of horizontal ground movement which needs to be considered in assessing the response of the portal frames to the imposed deformation. Boscardin and Cording (1989) found that the horizontal ground movement increased the horizontal strain which contributed to the critical strain at failure in deforming structures and, therefore, needed to be considered in structural behaviour and damage assessment.

For the single storey two-bay portal frames, the horizontal ground movement was transferred throughout the frames through bending of the frame columns in response to the imposed horizontal deformation. The measured column bending moments were, therefore, used to investigate the response of the structural frames to the horizontal ground movement. Figure 4-37 presents the sign convention used for the column moments.

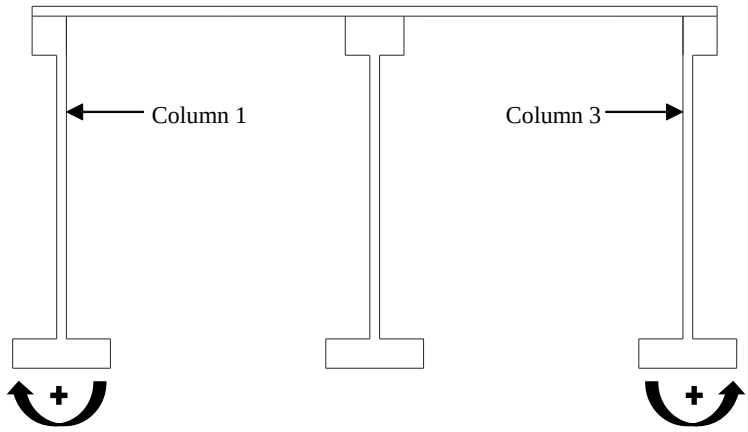

Figure 4-37: Column bending moment sign convention

The horizontal ground movement was induced with the initiation of groundwater extraction. As shown in section 4.2.3, the largest component of horizontal ground movement was closer to the point of extraction and in the direction of groundwater flow during the first drawdown. This resulted in column 3 bending more than column 1 under the imposed movement. During the second drawdown sequence, the soil mass moved away from the extraction well, with increasing movement away from the extraction well, therefore, resulting in column 1 bending more.

4.5.3.1 Column bending moment response: Frame (++)

The response of the columns to the imposed ground movement for Frame (++) is depicted in Figure 4-38. The bending moment increased for both columns during the first drawdown cycle with column 3 initially bending more than column 1. The bending moment for column 1, however, continued to increase as the bending moment for column 3 started to plateau at about 4.8 N.m. The continued increase in bending moment of column 1 could be attributed to the high global stiffness and relative column-slab

stiffness as well as the rigid body rotation of the frame. The combination of these factors resulted in continued load transfer to column 1, and subsequent increase in bending moment of the column, even though the imposed deformation had reached a maximum for the drawdown cycle.

As the water table was raised the bending moments in the columns started to decrease. The bending moment for column 1 at the start of the second drawdown sequence was 89 % of that at the end of the first cycle and a mere 71 % for column 3. The relaxation due redistribution of the excess stress in the frame caused by the decrease in soil stiffness resulted in a decrease of 11 % and 29 % in bending moment for columns 1 and 3 respectively. During the second drawdown sequence, the magnitude increase in bending moment was similar for both columns, 30 % for column 1 and 32 % for column 3.

The bending moment in column 3 was predominantly governed by the seepage induced horizontal ground movement, which was similar to the deformation caused by increased effective soil stresses and is dependent on the maximum applied stress. Therefore, as the groundwater seepage was the same as for the first drawdown cycle the seepage forces acting on the soil skeleton remained the same during the second cycle. The horizontal ground movement after the second drawdown, therefore, remained the same as after the first cycle resulting in a mere 4 % increase in bending moment from the maximum after the first cycle. The larger bending moment for column 1 at the end of the test could be due to a combination of the imposed bending during the first drawdown cycle, the transferred load and imposed bending during the second drawdown cycle caused by the horizontal movement of the founding soil.

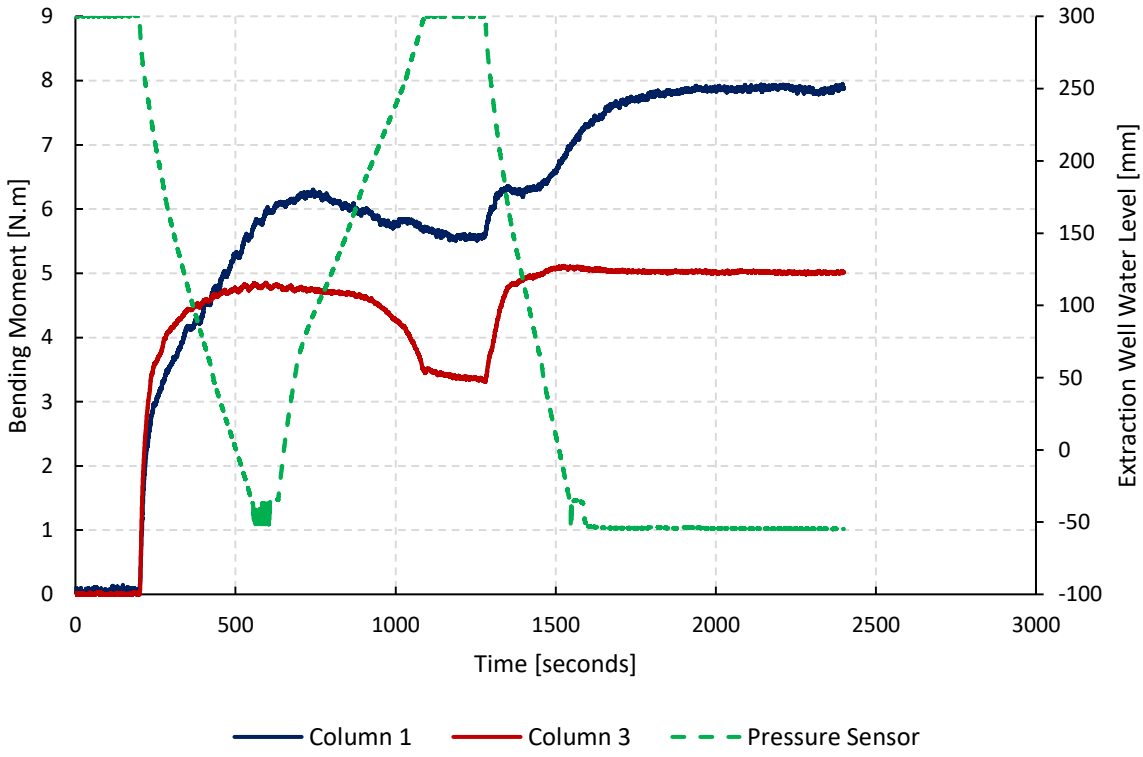

Figure 4-38: Frame (++) column response

4.5.3.2 Column bending moment response: Frame (--)

Figure 4-39 depicts the response of column 1 and 3 for Frame (--) to the imposed bending moments. The change in column bending moments for Frame (--) were significantly less than Frame (++) discussed previously. This could be attributed to the flexibility of the frame compared to Frame (++). The response of column 3 was similar to that of column 3 for Frame (++). The bending moment increased as the water table was drawn down, reaching a maximum at the end of the first drawdown cycle. The lower member stiffness, however, resulted in less bending moment being transferred to column 1 during the first cycle. The reduction in bending moment was also less for Frame (--) due to the lower stiffness of the frame with a mere 10 % reduction in column 3 bending moment due to relaxation of the frame, compared to 29 % for Frame (++).

The increase in bending moment during the second drawdown cycle differed significantly for the two columns. The increase in bending moment for column 1 was 55 % compared to a mere 19 % for column 3. The difference in maximum bending moments for column 3 between the first and second cycles remained minimal at 9.5 %. The bending moment for column 1, however, increased due to the imposed bending during the second drawdown cycle. The bending moment response together with the angular distortion factors indicated that the frame experienced localised deformation which could be due to the low bending stiffness which resulted in less transfer of moments throughout the frame.

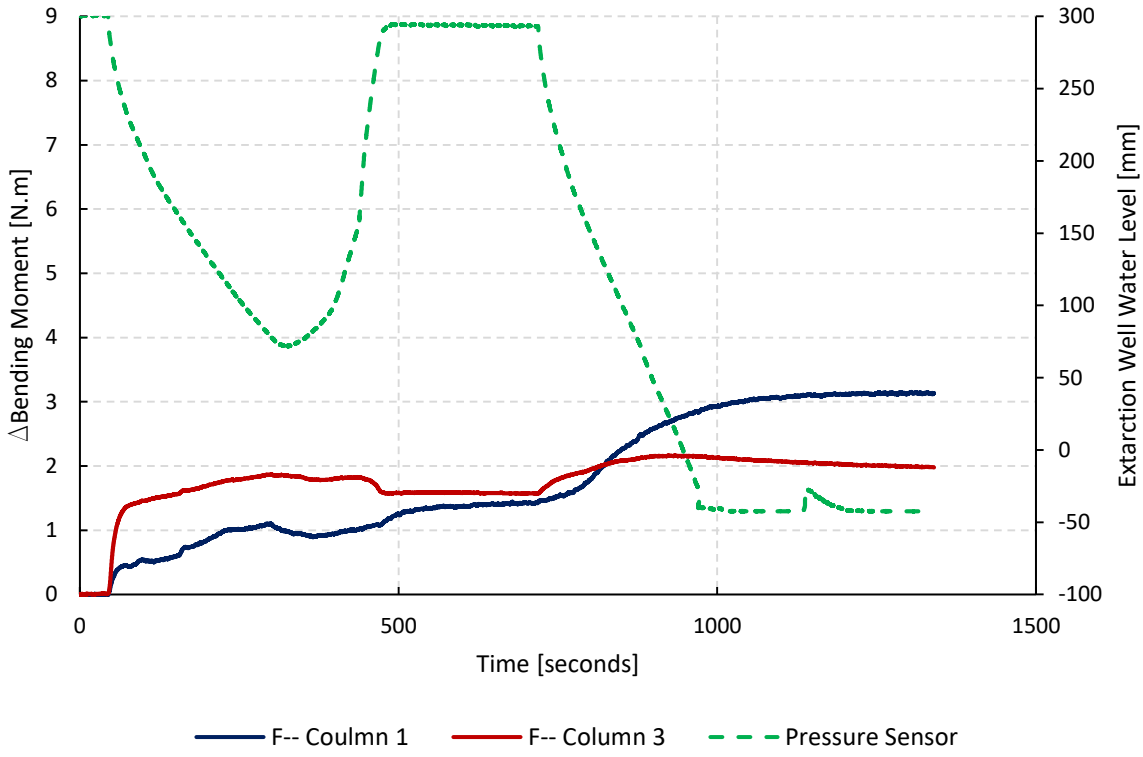

Figure 4-39: Frame (--) column response

4.5.3.3 Column bending moment response: Frame (-+)

Figure 4-40 presents the column response to the imposed ground movements for Frame (-+). The magnitude of the bending moments was greater than that for Frame (--) but less than Frame (++). The bending moments showed that there was a greater transfer of bending moment present for Frame (-+) compared to Frame (--). The response of the columns was similar to that of Frame (++), where the bending moment for column 3 increased to a maximum and the bending moment for column 1 increased gradually after an initial increase to reach a maximum. The maximum change in column bending moments after the first drawdown of 3.4 N.m was the same for the two column.

The reduction in bending moment due to relaxation of the frame was, however, minimal for Frame (-+). A mere 15 % for column 3 and 6 % for column 1. This could be as a result of the relative bending stiffness of the frame. The deformation of the frame was imposed to the stiff columns which in-turn was transferred to the flexible slab. The frame remained in the deformed position until the soil was soft enough for the frame to relax, but the flexible slab failed to bend the stiff columns in order to redistribute excess bending moments resulting in only slight relaxation of the frame.

The response of the columns was similar to that of the flexible frame during the second drawdown cycle. The increase in bending moment for column 1 was greater than that of column 3, although the difference was less for Frame (-+) (30 % increase for column 1 compared to 24 % for column 3).

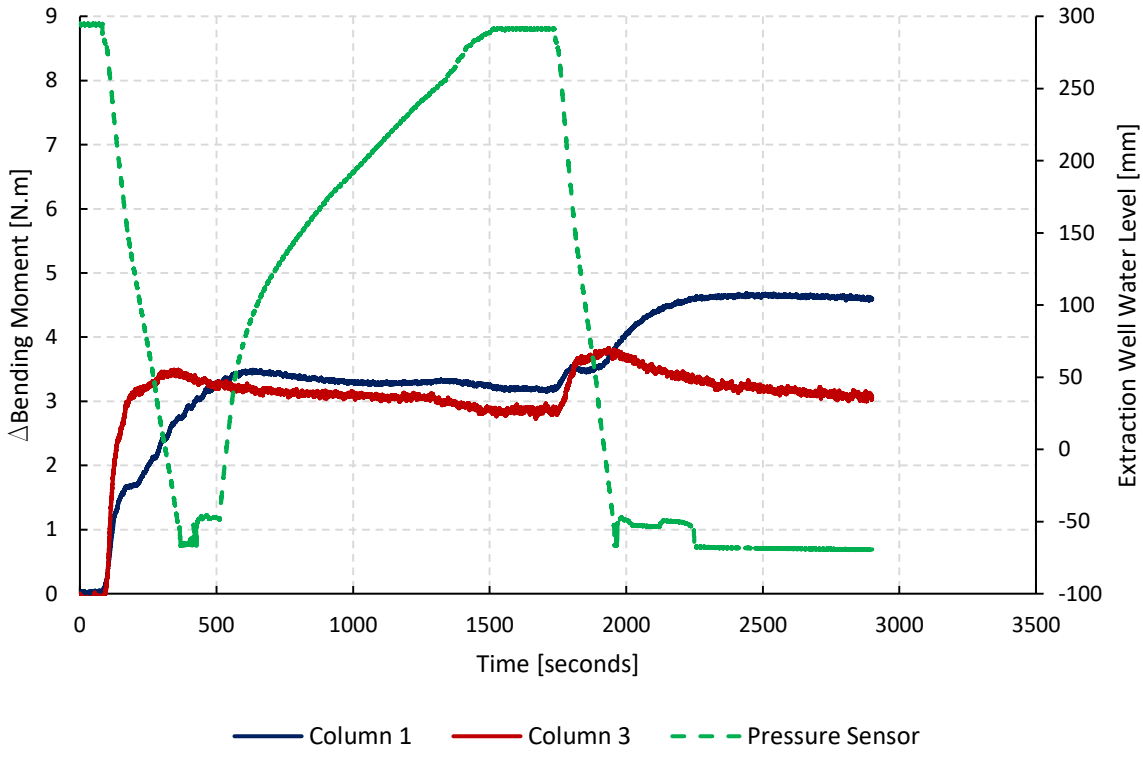

Figure 4-40: Frame (-+) column response

4.5.3.4 Column bending moment response: Frame (+-)

Figure 4-41 presents the column bending response to the imposed loading for Frame (+-). The low column stiffness resulted in lower bending moments for the columns. The column bending moments increased simultaneously and similar to Frame (++), column 3 reached a plateau before column 1 and the moment for column 1 increased gradually before reaching its plateau. The large increase in column 1 bending moment could be due to the manner in which the stiff slab deformed. The rigid body rotation of the slab resulted in more of the load being transferred to column 1, which translated into bending of the column.

The reduction in bending moments due to relaxation of the frame was also minimal. The reduction in bending moment for column 3 was a mere 7 % and practically zero for column 1. There was a slight difference in the increase in bending moment for the columns, an increase of 19 % for column 1 and 23 % for column 3 from the start of the second drawdown to the end of the test. This was similar to the response of Frame (++) which, furthermore, suggested that the thick slab resulted in greater transfer of the column bending moments and in turn the horizontal ground movements throughout the frame.

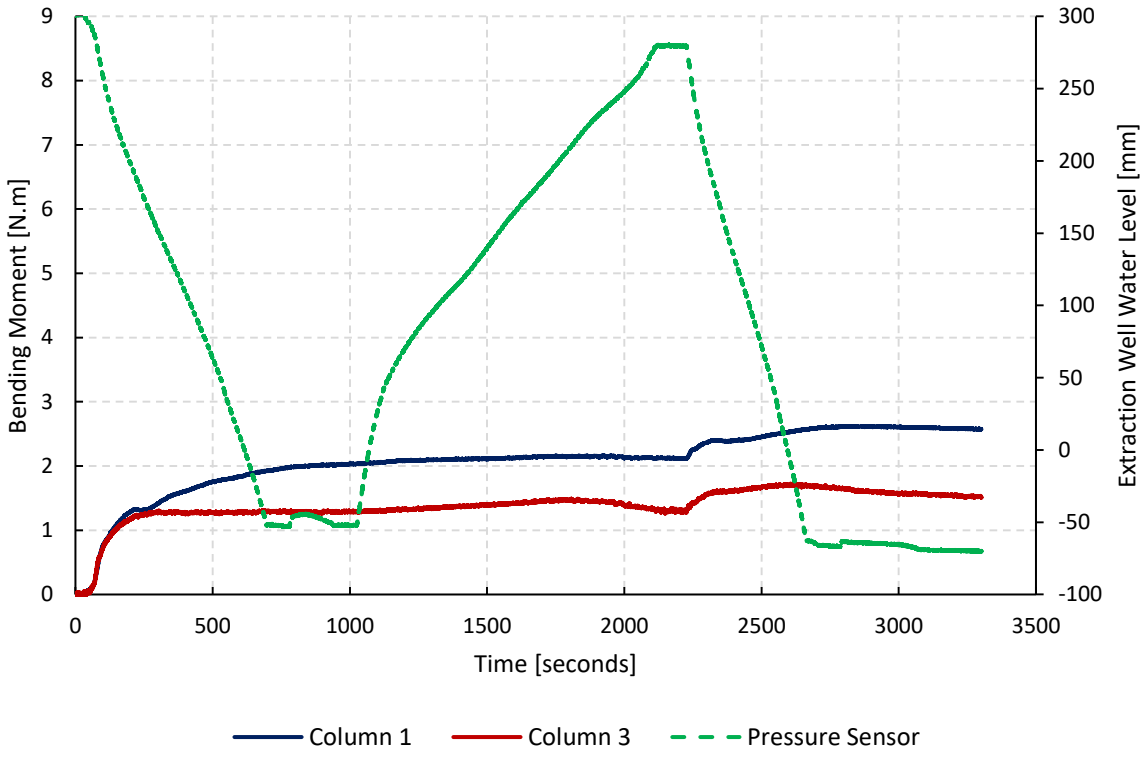

Figure 4-41: Frame (+-) column response

4.5.3.5 Summary of column bending moment response

The column bending moment response showed that there was a clear difference in the manner in which the portal frames responded to the imposed deformations. The first observation was that the bending moment change was greatest for Frame (++) with the rigid structural elements. The frame also exhibited the greatest amount of moment redistribution as a result of greater excess stresses induced in the structural elements. The column moment response was much less for Frame (--) with the flexible structural elements. The frame also exhibited less redistribution of excess stresses. The column bending moments showed that the response of the frame was mainly localised to the areas where the deformation was imposed.

Frame (-+) exhibited minimal redistribution of bending moment which could be attributed to the flexible slab of the frame which resulted in a minimal build-up of excess bending moments. The frame, however, showed a greater response in bending moments to the imposed deformations which were attributed to the rigid columns, similar to the Frame (++). Frame (+-) on the other hand exhibited the lowest bending moment response to the imposed movement as well as the lowest redistribution of excess bending moments. There was minimal excess stresses in the slab, similar to Frame (-+), due to the relative column-slab stiffness. The flexible column also exhibited lower bending moment response compared to the rigid columns.

4.5.4 Slab Bending Moment Response

The final structural assessment parameter used to investigate the response of the frames was the slab bending moment response. Structural engineers utilise bending moments within slabs to design and size the slabs. As structures such as portal frames are designed for maximum allowable deformations it is assumed that the changes in bending moments due to deformations within these limits will be accounted for by the relevant safety factors (Lin et al., 2015). However, when excessive deformations caused by excessive ground movements such as those induced by groundwater extraction exceed the design limits, this could lead to the capacity of the slabs being exceeded, leading to damage and ultimately failure.

It was thus important to investigate the response of the slabs of the portal frames to the imposed deformations by assessing the change in bending moments at specific points during the tests. This would, furthermore, give an indication of how the stiffness of the frames affects the deformation of the slabs and in-turn the frames. The bending moments were determined at the points corresponding to those discussed in section 4.2 from the strain results for gauges 3, 4, 5, 6, 9 and 10 (see Figure 3-8). The sign convention used in this section is that an increase in bending moment at a point being discussed was taken as positive according to the bending moment diagrams. The results from preliminary tests where the frames were accelerated to 30 g while resting on dry soil are also presented.

4.5.4.1 Slab bending moment response: Frame (++)

Figure 4-42 presents the bending moment response for Frame (++). The first thing to note was the difference between the bending moments for the frame on stiffer dry soil (Frame Test 1), and the frame on the softer saturated soil (Start First Drawdown). The hogging moment reduced to the point where there was moment reversal and the sagging moment increased slightly. The difference between the two bending moments was as a result of the change in soil stiffness only as the edge columns, 1 and 3, rotated outwards reducing the bending moment diagram values.

When the first drawdown was initiated the bending moment of the slab at the connection with column 1 reduced more than that at the connection with column 3. This corroborates the results for the increase in column bending moments found in the previous section for this frame. The hogging moment also increased during this period, while more moment was transferred to column 2, as the hogging moment was greater for span 1 than it was for span 2. During the replenishing period, the hogging moment over column 2 reduced while the bending moments at the edge of the slabs increased. This, furthermore, shows that the frame could redistribute excess bending moments during this stage. During the final drawdown, the bending moments for span 1 reduced slightly while the hogging moment for span 2 increased and the edge bending moment reduced. This shows that the moment transferred to column 2 acted in the opposite direction as that after the first drawdown.

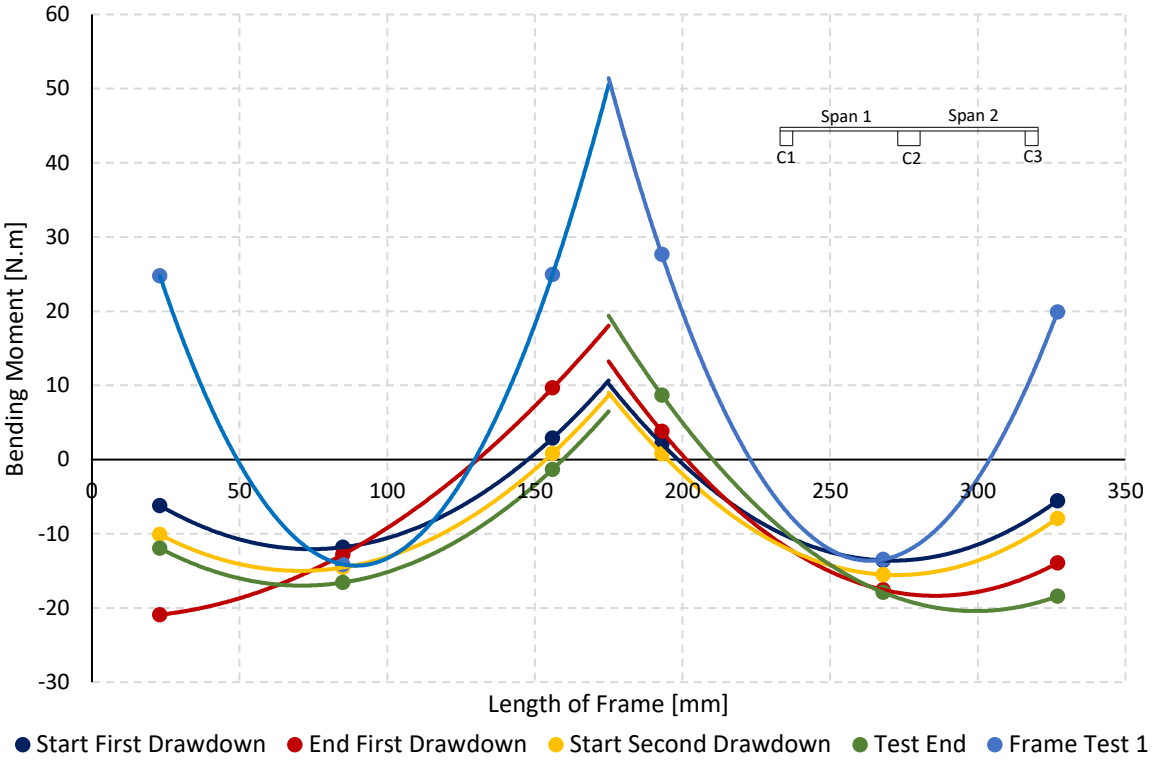

Figure 4-42: Frame (++) bending moments

4.5.4.2 Slab bending moment response: Frame (--)

Figure 4-43 presents the slab bending moments for Frame (--). As for Frame (++), there was a considerable difference in the bending moments between the dry and saturated soil tests. The change in bending moments throughout the test happened to a lesser degree for this frame compared to Frame (++). The deformation of the frame was also localised more to the part of the frame where the deformation was imposed as shown by the slab bending moments. During the first drawdown, the hogging moment reduced for span 2 while remaining unchanged for span 1. Although the magnitude in reduction of the slab edge bending moments were similar the frame relaxation induced increase in bending moment were only present for span 2 which was deformed the most during the first drawdown. Similar to the first drawdown the change in hogging moment was localised to the deforming bay of the frame (which was primarily span 1 for the second drawdown) while remaining relatively unchanged for span 2.

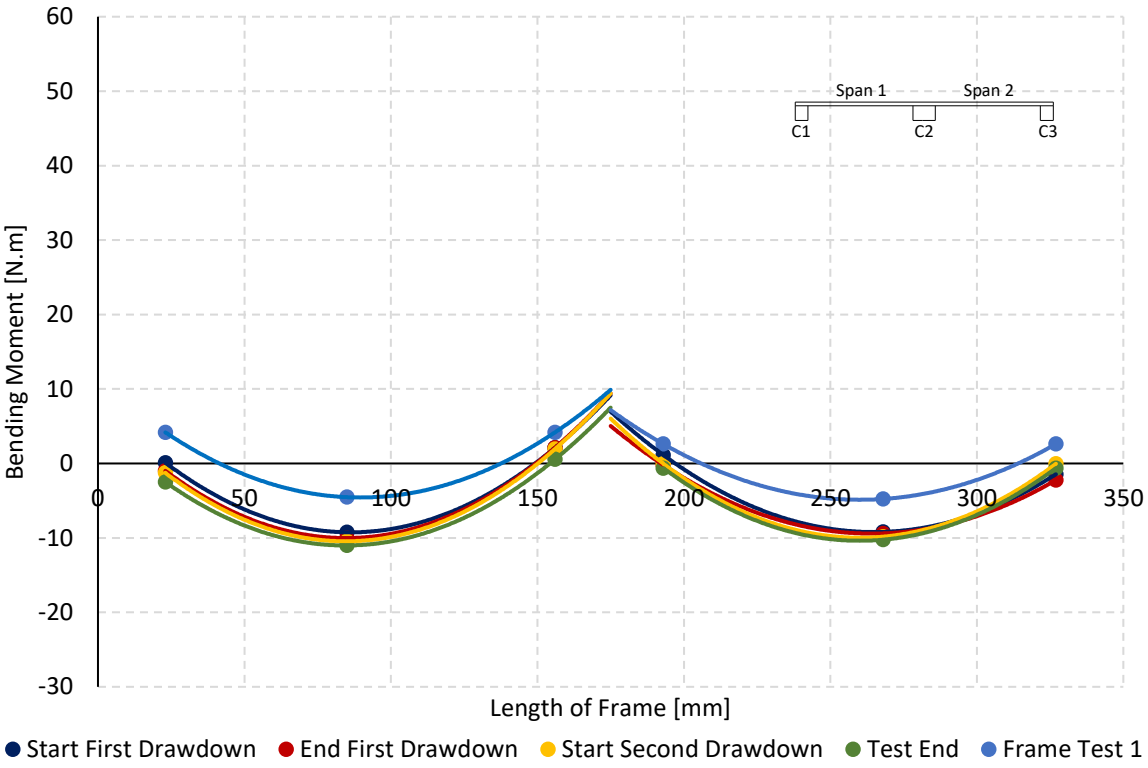

Figure 4-43: Frame (--) bending moments

4.5.4.3 Slab bending moment response: Frame (-+)

Figure 4-44 presents the slab bending moment response for Frame (-+). The two spans exhibited similar bending moment response for the groundwater drawdown during all the stages. The largest decrease in bending moment happened during the first drawdown while there was minimal relaxation of the slab during replenishing of the water table. The moment transferred to column 2 also reduced during this time. During the second drawdown, the reduction in bending moment were smaller compared to the first drawdown. This shows that the frames mostly deformed when loading was imposed onto the frame and less so during the replenishing phase.

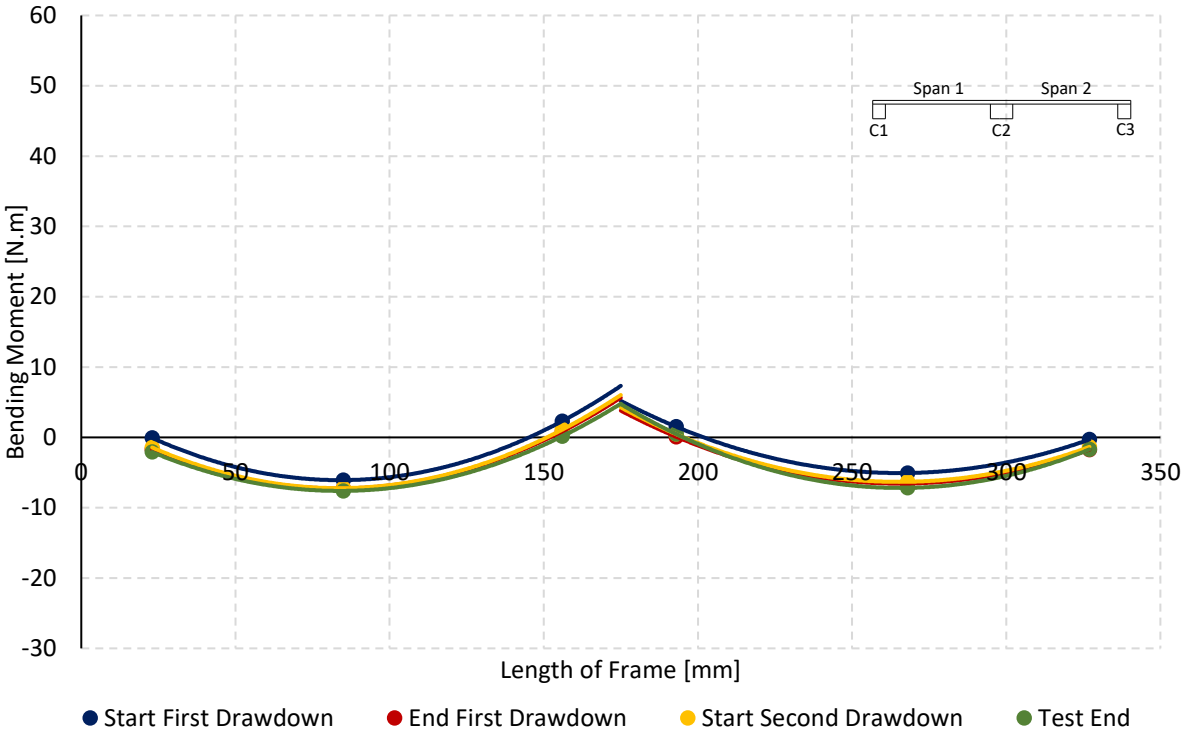

Figure 4-44: Frame (-+) bending moments

4.5.4.4 Slab bending moment response: Frame (+-)

Figure 4-45 presents the slab bending moment response for Frame (+-). The difference in bending moments between the dry and saturated soil tests was less for Frame (+-) than for the previous frames. The ground movement induced change in bending moment was also less for this test. There was a slight decrease in the bending moments for span 1 during the first drawdown. There was also no reversal in bending moment at the slab edges, as was the case for the previous frames, as the rotation of the flexible columns could not impose sufficient bending moment onto the slab for this to happen.

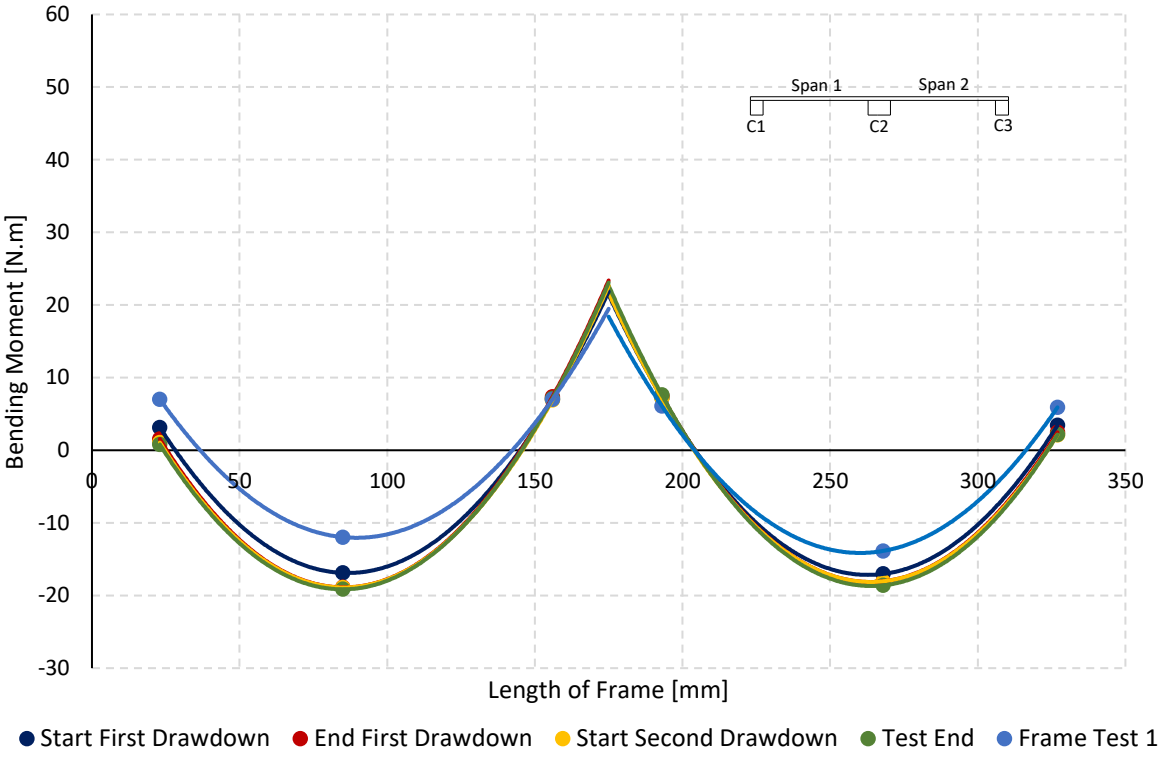

Figure 4-45: Frame (+-) bending moments

4.5.4.5 Summary of slab bending moment response

The slab bending moments show a clear distinction between the responses of the portal frames to the groundwater extraction induced deformation with a few exceptions. Frames (++) and (--) were the most sensitive to bending moment changes as the groundwater water table varied. The change in bending moments was, however, distributed throughout the frame for Frame (++) whereas it was more localised for Frame (--). This indicated that bending applied to one part of the frame was transferred throughout the frame to a greater degree for the rigid frame compared to the flexible frame.

The bending moments for Fames (-+) and (+-) on the other hand exhibited less variation throughout the water table fluctuation. The two frames, however, showed a similar change in bending moment throughout the slabs. Unlike for Frames (++) and (--), the bending moments decreased progressively for the frames meaning there was no relaxation induced changes in bending moments. This, furthermore, indicated that the slab bending moments for these frames were dictated primarily by the stiffer structural element. The change in bending moments was, however, greater for Frame (-+) than for Frame (+-).

Frame (++) showed the greatest change in bending moment compared to the rest of the frames. This corresponded with the largest relaxation, redistribution of excess stresses, for the frame as well. The minimal redistribution of column bending moments and column loads were, furthermore, corroborated by the slab bending moment response for Frames (--), (-+) and (+-). While the flexibility of Frame (--)

caused localised deformation of the frames as well as less build-up of excess stresses, the flexible structural elements contributed to this for Frame (-+). The flexible slab limited the build-up of excess stresses, and Frame (+-), where flexible columns could not transfer enough bending moment to induce excess stresses in the slab as shown by the slab bending moment response figures.

4.5.5 Discussion of Portal Frame Response

The data presented thus far focussed on the individual response of the portal frames to the induced ground movements with the differences in the response of the frames discussed. This section focusses on the comparative assessment of the response of the portal frames. There were differences in the amount of differential settlement imposed onto the frames which resulted from testing complications which were most prevalent for the test for Frame (+-) which had the least differential settlement. The comparative assessment was therefore carried out to the point where the frames experienced the same average slope, the differential settlement between columns 1 and 3 divided by the distance between the columns, which coincided with the maximum average slope for Frame (+-). The data was however presented in terms of differential settlement between column 1 and 3.

4.5.5.1 Column force response

Figures 4-46 to 48 presents the change in column forces for the portal frames for columns 3 to 1 respectively against the increase in differential settlement between columns 1 and 3. The data shows that the column force reduces for column 1 and 3 as the differential settlement increases while increasing for column 2. This shows that the pivoting effect about column 2 was present for all the portal frames for the range of differential settlement considered. As the water table was lowered column 3, closest to the extraction well, started to settle for all three frames resulting in a decrease in force for column 3 (see Figure 4-46). The reduction in column force was largest for Frames (++) and (+-) and the least for Frames (--) and (-+). The settlement of column 3 was resisted by the frame slabs and this resistance was greatest for the rigid slabs. The decrease in column force was, therefore, greatest for the frames with the rigid slabs (Frames (++) and (+-)). The pivoting effect of the frames would furthermore result in an increase in force for column 2 as presented in Figure 4-47. Frames (++) and (+-) experienced the largest increase in force as the rigid slab resulted in more force carried over to column 2 compared to the flexible slabs of Frames (--) and (-+) as a result of the frames pivoting around column 2. Figure 4-48 furthermore shows a reduction in force for column 1 as the differential settlement increased, which furthermore substantiates the pivoting effect of the frames in response to the imposed differential settlement. The column force response figures also show that the change in column force is almost instantaneous for Frame (++) while taking place gradually for the rest of the frames. This response further substantiates the rigid body rotation and greater transfer of forces throughout the frame, compared to the other frames, discussed in the previous sections for the frame.

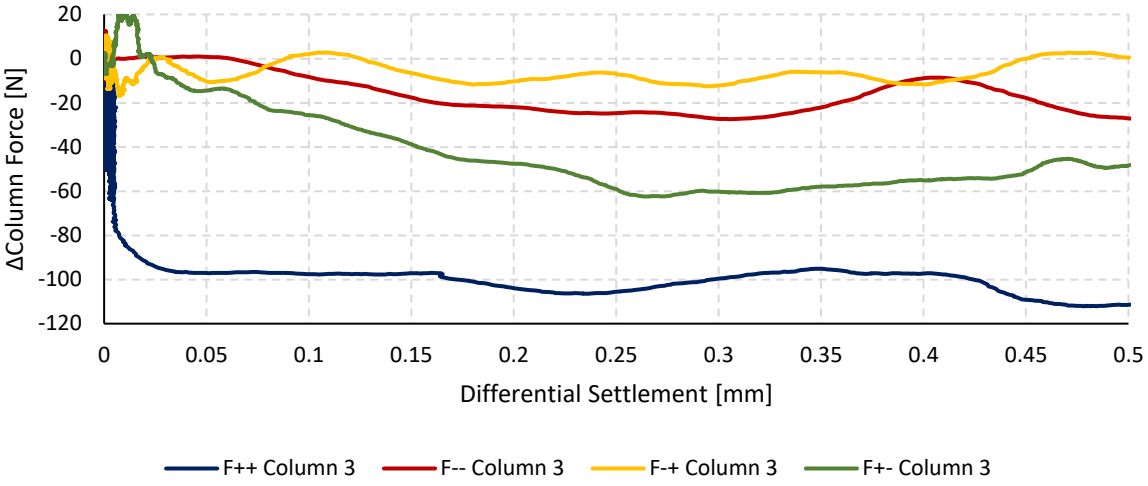

Figure 4-46: Column 3 axial force response

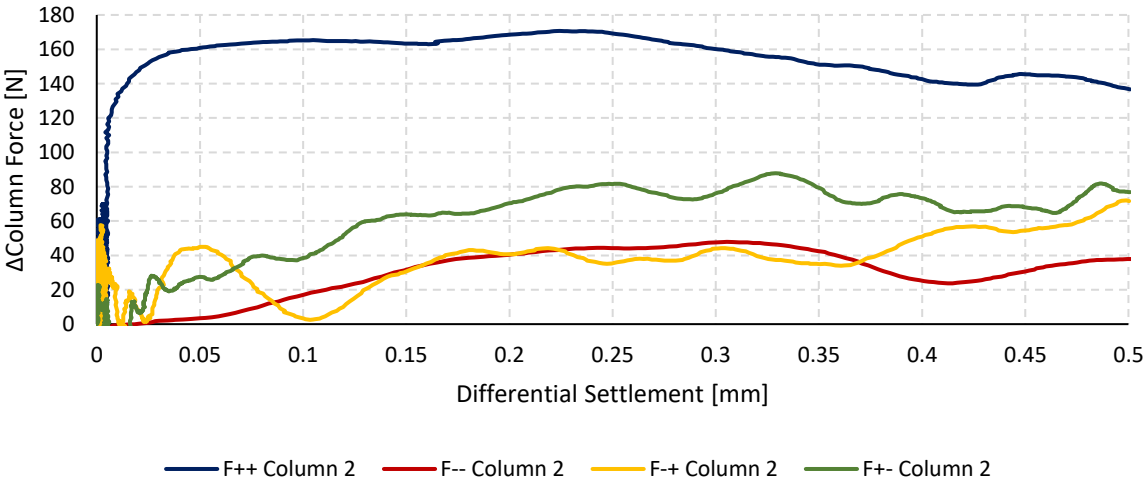

Figure 4-47: Column 2 axial force response

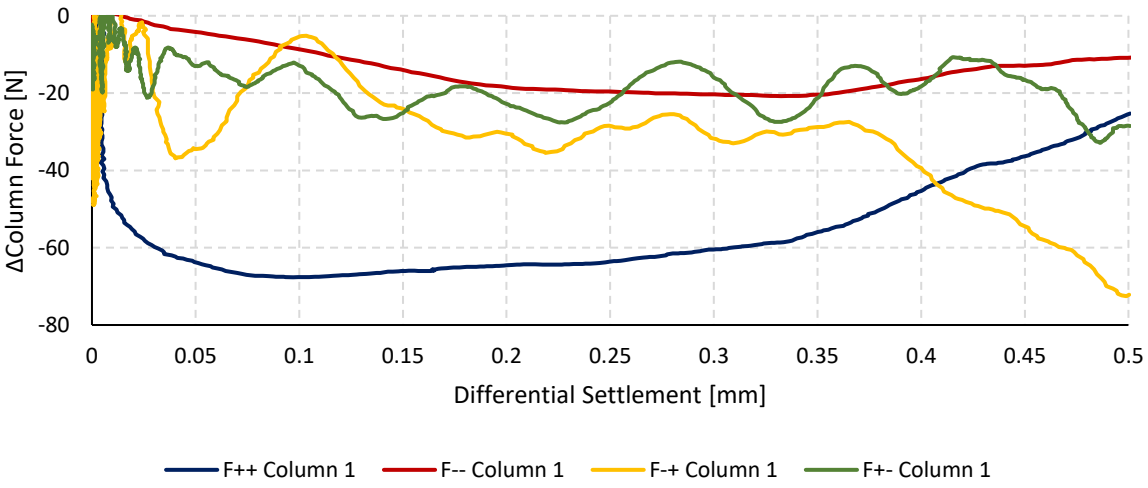

Figure 4-48: Column 1 axial force response

4.5.5.2 Column bending moment

The change in bending moments of the columns was primarily induced by the horizontal ground movement of the founding soil. The same sign convention adopted in section 4.5.3 was used in this section with a clockwise increase in bending moment taken as positive for column 1 and an anti-clockwise increase in bending moment positive for column 3. Figures 4-49 and 4-50 present the bending moment response for columns 3 and 1 plotted against the differential settlement. The increase in bending moment was greatest for Frames (++) and (-+) with the rigid columns. The rigid columns resisted the induced bending moments more than the flexible columns resulting in higher bending moments, however, the rigid slab of Frame (++) resisted the bending moment transferred to the slab to a greater degree resulting in greater bending moment in the column for this frame compared to Frame (-+) with the flexible slab.

Frames (--) and (+-) had lower bending moments which were due to the lower bending resistance of the flexible columns. The difference between column 1 and 3 at the end of the differential settlement range considered was similar for Frame (++) and Frame (--) at a difference of about 0.5 Nm while there was no difference between the two columns for Frame (+-). The difference between columns 1 and 3 for Frame (+-) could be attributed to the rigid slab which transferred the bending moments induced in column 3 to column 1 to a greater degree, compared to the rest of the frames. The opposite was true for Frame (-+) with the flexible slab which could not transfer the bending moment induced in column 3 to column 1, due to its lower bending resistance and therefore the difference between the column bending moments was the greatest.

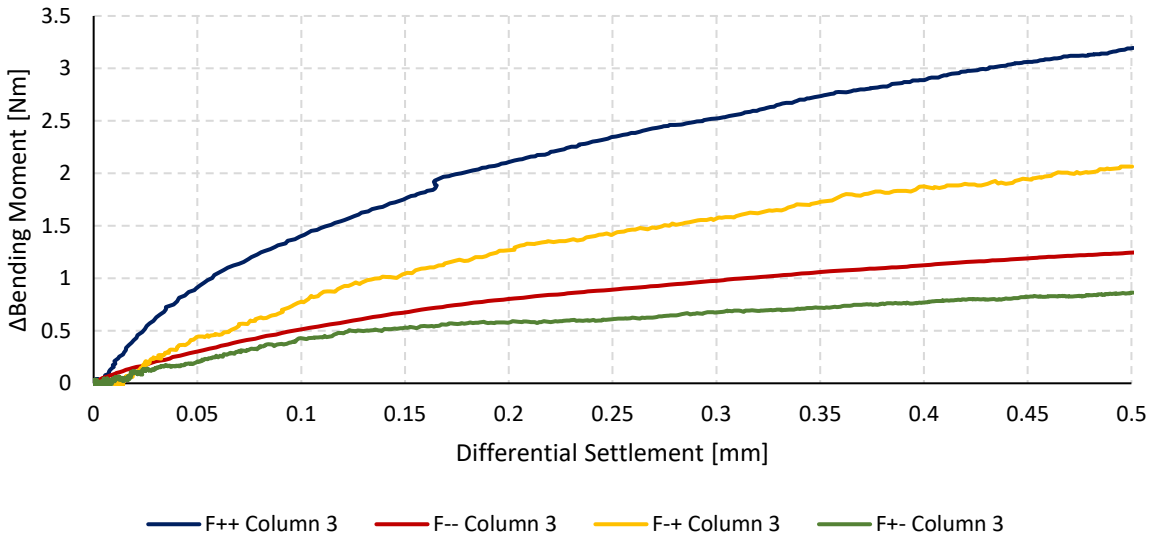

Figure 4-49: Column 3 bending moment response

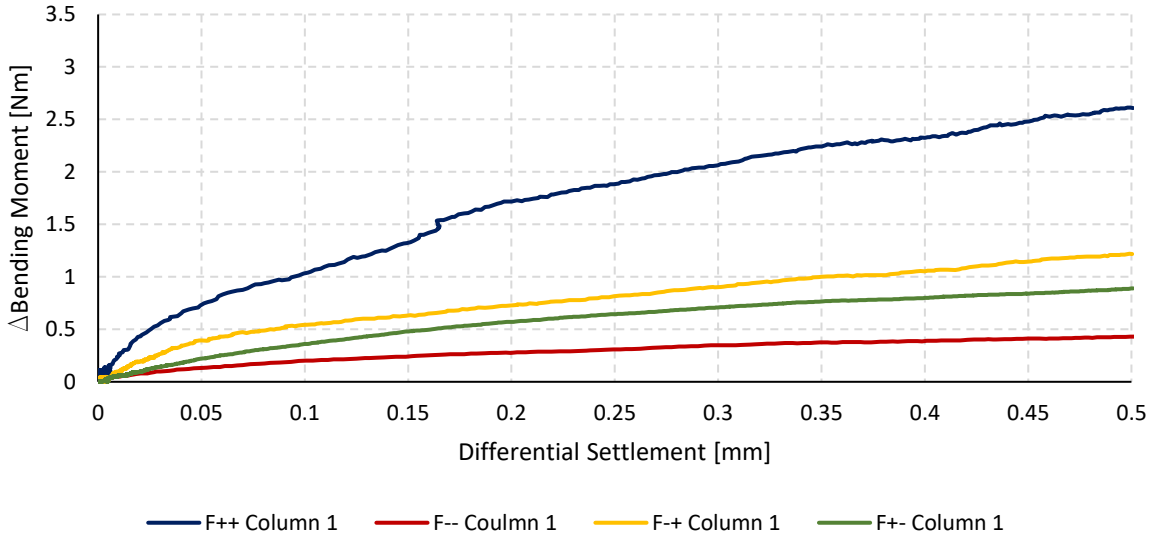

Figure 4-50: Column 1 bending moment response

4.5.5.3 Slab bending moment response

The slab bending moment change was determined at the end of the differential settlement range that was considered with the same sign convention adopted as in section 4.5.4. Figure 4-51 presents the slab bending moment response for the four frames. The change in bending moment was greatest for the Frame (++). This was as a result of the higher bending resistance of the rigid slab. Frame (-+) exhibited the second highest change in bending moment for the slab. This was, as a result, the greater increase bending imposed onto the slab by the rigid columns. The slabs showed different responses for the change in bending moments for gauge 5 and 6 which were at the slab connection with the middle column (column 2). The bending moment increased for the rigid slabs (Frames (++) and (+-)) while decreasing for the flexible slabs (Frames (--) and (++)). This was as a result of the rigid slabs resisting the imposed deformations more than the flexible slabs while the flexible slabs conformed more to the deformation.

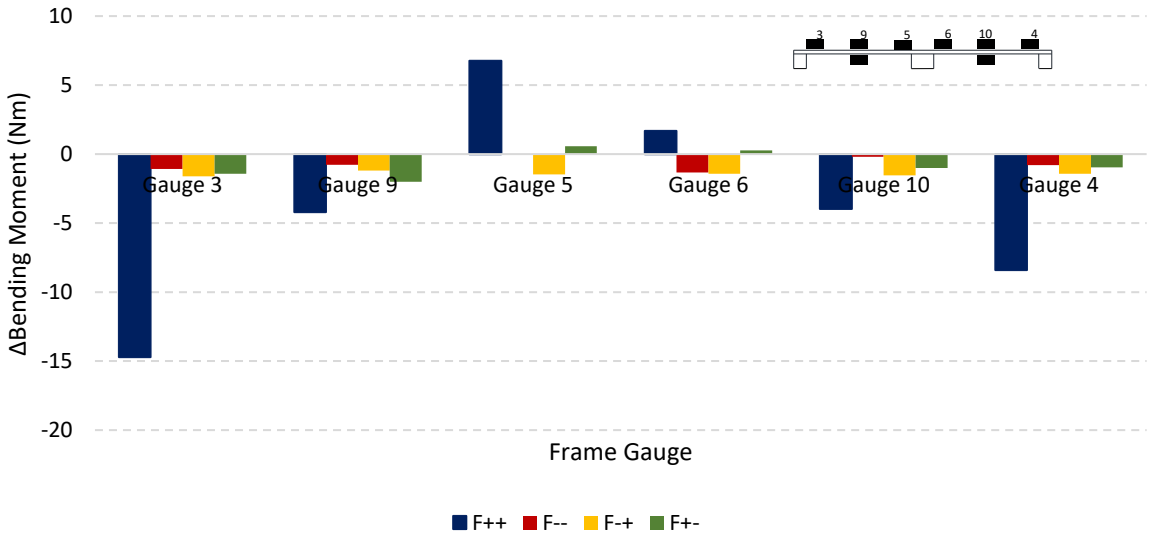

Figure 4-51 Slab bending moment response

4.5.6 Summary of Frame Test Results

The rigid frame (Frame ++) exhibited greater force and moment response due to the frame resisting the imposed deformations more than rest of the frames. The relative stiffness factor of 1 also meant that the imposed deformations were transferred more effectively through the frame. The frame resisted the deformations more as single structure compared to the other frames. The force and moment response was the lowest for the flexible frame (Frame --) as a result of the lower resistance of the flexible members. Although the frame had a relative stiffness factor of 1, the flexible slab and columns meant that the imposed deformations were transferred less effectively as the members deformed more. For the other two frames, the effectiveness of the transfer of imposed loading throughout the frames were hindered by the relative stiffness of 8 and 0.125 respectively. The more flexible members deformed more under the imposed loading reducing the resistance of the frames.

The rigid columns had the greatest change in bending moments. The slab bending stiffness, however, influenced the degree to which the column bending moment changed. The higher the bending stiffness the greater the increase in bending moment for the column, therefore, the increase in bending moment was greater for the rigid frame (Frame ++) than the frame with the with the relative stiffness of 0.125 (Frame -+).

The stiffness of the frames, furthermore, influenced the manner in which the frames deformed as a result of the imposed ground movements. Frames with a high global stiffness and a relative stiffness of 1 resisted the imposed ground movements mainly by rigid body rotation. Frames with a low global stiffness and a relative factor of 1, on the other hand, deformed in a more localised manner with the deformation localised to the area where the deformation is imposed. These frames also conformed more to the imposed ground movements.

Frames with a low vertical stiffness and a high horizontal stiffness (flexible slab and rigid columns) show a greater shear type deformation to imposed differential settlement. These frames also have a lower resistance to horizontal ground movements although they have rigid columns. This is a result of the flexible slab which can be bend by the rigid columns resulting in rotation of the columns about the slab-column connection in response to the imposed horizontal ground movement increasing the diagonal strain of the bay.

Frames with a high vertical stiffness and low horizontal stiffness (rigid slab and flexible column) showed a greater bending type deformation as a result of the imposed differential settlement of the foundations. These frames, similar to the high horizontal stiffness frames, have a low resistance to imposed horizontal

ground movements, but for a different reason. Whereas the columns rotated about the slab-column connection for the previous frame, the flexible columns cantilever about the connection as they fail to bend the rigid slab also increasing the diagonal strain of the bay.

The test results show that global and local (relative column-slab) frame stiffness influenced the manner in which the portal frames responded to groundwater extraction-induced ground movements and subsequent imposed deformations. This shows that the deformation of framed structures is not only governed by the bending stiffness of the slab of a structure but that the connection at the slab-column interphase, fixed or pinned, influences the deformation as well. In the case of a fixed column-slab connection, the stiffness of the columns has an influence on the response of framed structures to imposed deformations. Therefore, when assessing the response of framed structures to founding ground movement imposed deformations the relative stiffness between the slabs and columns should also be considered.

5 CONCLUSIONS AND RECOMMENDATIONS

Groundwater extraction from an unconfined aquifer was modelled in a geotechnical centrifuge while the pore-water pressure change, vertical surface settlement, and the resultant ground movements were monitored. Portal frames with varying global and relative column/slab stiffness were, furthermore, used to investigate the response of framed structures founded within the zone of influence to the resultant ground movements. This chapter summarises the conclusions reached for the geotechnical centrifuge modelled groundwater extraction-soil-structure interaction study. The chapter concludes with recommendations for future work and implementation of the results.

5.1 EFFECT OF GROUNDWATER EXTRACTION ON PORE-WATER PRESSURE CHANGE

The groundwater was extracted from the simulated aquifer through an extraction well while controlled in a control well. Lowering the water level in the extraction well resulted in the establishment of a hydraulic gradient facilitating groundwater flow towards the extraction well. The localised extraction results in a sloping water table throughout the soil mass causing a non-uniform reduction in pore-water pressure throughout the aquifer.

As the water table was lowered further, the distance of influence propagates away from the extraction well while the water table continues to lower differentially increasing the non-uniform reduction in pore-water pressure. This continues until the groundwater extraction is stopped or the distance of influence reaches the edge of the aquifer at which point the differential drawdown (slope of the water table) and therefore the non-uniform reduction in pore-water pressure is at a maximum.

Lowering the water table beyond the point where the distance of influence reaches the edge of the aquifer results in the water table lowering uniformly throughout the aquifer. However, as the phreatic surface moves towards the base of the aquifer the total reduction in pore-water pressure is greatest for the soil furthest from the extraction well. Replenishing the water table to the original position and increasing the pore-water pressures happens in a manner which replicates the reversal of the aforementioned process.

5.2 EFFECT OF PORE-WATER VARIATION ON SOIL SETTLEMENT

5.2.1 Vertical Soil Settlement

Pore-water pressure reduction within an aquifer causes an increase in the soil effective stresses. The increase in effective stresses is non-uniform throughout the aquifer due to the differential drawdown of the water table with the largest increase corresponding to where the pore-water pressure reduction is largest. Soil settlement is caused by an increase in the effective soil stresses, therefore, the soil settles as the effective soil stresses increase. The non-uniform increase in effective soil stresses, furthermore, results in differential settlement of the soil mass.

Soil settlement is, however, dependent on the stress history of the soil and, therefore, fluctuation of the water table causes progressively smaller increments in the settlement of the soil. If the water table is lowered to a point within the aquifer, replenished and then lowered throughout the aquifer, as was the case for this study, this would cause progressive reductions in the degree of soil settlement. Differentially lowering the water table throughout the aquifer would cause the soil closer to the extraction well, where the water table was lowered the most, to be at a higher stress state than the soil further from the extraction well. This would in-turn cause the soil closer to the extraction well to settle more than the soil further from the extraction well. During the second drawdown and lowering of the water table below the lowest level it had been, to the impermeable boundary at the base of the aquifer, will cause the soil closer to the point of extraction to settle less, as the total increase in effective soil stresses, from the highest it had been, will be lower for the soil closer to the extraction well.

5.2.2 Groundwater Extraction Induced Ground Movement

Groundwater extraction-induced ground movement has a component of vertical and horizontal ground movement. Groundwater extraction causes an increase in the rate of groundwater seepage which exerts greater forces on the soil particles inducing horizontal movement of the soil while also increasing the vertical settlement of the soil. Seepage forces are however greatest closer to the extraction well and, therefore, the seepage induced ground movements are greatest closer to the extraction well.

During the first drawdown, the movement of the soil further from the extraction well is predominantly vertical, with increasing horizontal movement in the direction of seepage closer to the extraction well. As discussed earlier soil deformation is dependent on the largest stress the soil had previously been loaded to. As the rate of seepage does not increase during the second drawdown, the horizontal movement of the soil closest to the extraction well is at its maximum after the first drawdown. During the second drawdown, the soil further from the extraction well moves in the direction opposing the seepage, while the settlement of the soil closest to the point of extraction well is predominantly vertical.

5.3 THE EFFECT OF SOIL SETTLEMENT ON PORTAL FRAME DEFORMATION

Groundwater extraction-induced soil settlement imposes deformations onto the portal frames founded within the distance of influence. The presence of the portal frames, however, also alters the soil settlement. The degree to which this happens is dependent on the mass and the stiffness of the frame. The mass of the frames causes an increase the effective soil stresses, greater than that of the soil in the absence of the frames. The soil, therefore, deforms less under the same increase in effective soil stresses induced by groundwater extraction for soil without the frames. This phenomenon increases as the mass of the frame increases.

The frame stiffness influences the manner in which frames deform due to imposed ground movements. Rigid frames with a relative stiffness of 1 deform by rigid body rotation and resist the imposed deformations while flexible frames with the same relative stiffness experience localised deformations and conform more to the imposed deformations. Frames with a low vertical stiffness and a high horizontal stiffness (flexible slab and rigid columns) show a greater shear type deformation to imposed differential settlement. Frames with a high vertical stiffness and low horizontal stiffness (rigid slab and flexible column) show a greater bending type deformation to the imposed differential settlement of the foundations. These frames have a low resistance to horizontal ground movements. The rigid columns rotate about the slab-column connection for the frame with the flexible slab while the flexible columns cantilever about the connection for the frame with the rigid slab and in both cases the diagonal strain is increased.

5.4 THE EFFECT OF PORTAL FRAME DEFORMATION ON STRAIN DEVELOPMENT IN THE PORTAL FRAMES

Rigid frames exhibit less strain increase and the strain increase in the frame is more uniform throughout the frame. Flexible frames, on the other hand, show greater and more localised strain increase for the imposed ground movements. The increase in strain is localised more to the flexible members for the remaining frames. The slab strained more as a result of the frame with the low vertical stiffness while the columns strained more for the frame with the low horizontal stiffness.

5.5 THE EFFECT OF FRAME STIFFNESS ON THE FORCE AND MOMENT RESPONSE OF THE FRAMES

The column forces were considered for assessing the force response of the frames. The forces increase or decrease as a result of the differential settlement of the frames, therefore, the frames with a higher vertical stiffness showed the greatest change in column forces. The rigid slabs resist the imposed differential settlement to a greater degree resulting in greater change in the column forces.

The bending response of the frames were assessed by means of the column and slab bending moment. The change in bending moments of the frames were primarily caused by the horizontal ground movements imposed onto the columns. The rigid columns, therefore, have the greatest change in bending moments. The bending stiffness of the slabs influenced the degree to which the column bending moment changed due to the imposed deformations. The higher the bending stiffness of the slab the greater the increase in bending moment for the column, therefore, the increase in bending moment was greater for the rigid frame (Frame ++) than the frame with the flexible slab (Frame -+).

5.6 RECOMMENDATIONS

The test results showed that the modelling and measuring of the soil response to groundwater extraction can be satisfactorily investigated in a centrifuge. The vertical soil settlement measured with the LVDTs and the ground movements tracked with DIC, together with the pore-water pressure measurements allowed the response of the soil to be comprehensively quantified. The following recommendations, therefore, pertain to the modelling of the portal frames and improving the ease with which the test data was analysed as well as recommendations for engineers.

5.6.1 Recommendations for Future Modelling

The study found that groundwater extraction induced non-uniform vertical and horizontal ground movements. The resultant differential settlement of the foundations induced tilt (rigid body rotation) of the frames as well as vertical differential distortion of the frame bays. The latter was the focus of the study, yet not explicitly measuring and or resisting the former resulted in numerous calculations to determine the forces and stresses arising only from the differential distortion of the bays of the frames. If the tilt was prohibited in the centrifuge tests, the resulting forces and stresses would be a function of the differential distortion only. Whereas, if the tilt was measured, formulae presented by Burland and Wroth (1974), Bosacrdin and Cording (1989) and Son and Cording (2005, 2007, 2010) could be used to determine the resultant forces and stresses as a function of bay distortion only. Therefore, it is recommended that one of the two methods be used in future tests.

Finally, during acceleration of the centrifuge, there was an interaction between the soil and structure taking place as the self-weight increased and the frames deforming in response. The non-uniform settlement and the indeterminacy of the frames would, therefore, result in some differential settlements and distortions being imposed onto the frames. It is, therefore, important to be cognisant of this and to measure the deformation of the frames as the models are accelerated to know how much the frames have distorted before testing commenced. Ritter et al., (2016) found similar findings.

5.6.2 Recommendations from Study Outcomes

If ground water is extracted from aquifers where compressible soils are present, engineers should be aware that a depression cone will develop where the largest settlement will be closest to the point of extraction. Therefore, the extraction systems and the points of extraction should be designed such that differential settlement is minimised.

Pore-water pressure and/or well water level at monitoring points as well as ground surface settlements during ground water extraction should be measured such that a zone of influence is determined. The zone of influence can be used to predict future settlement zones if ground water extraction is to be undertaken from the same aquifer.

It is also recommended that at greenfield sites, where aquifers with compressible soils are present, that are set out for future develops, that the water table within the aquifer is lowered to the lowest level it can be lowered to while considering the environmental impacts of such an undertaking. Lowering the water table within the aquifer will result in settlement of the compressible soil to a point that, further soil settlement will only take place if the water table is lowered beyond the lowest it had been lowered to. Therefore, seasonal and man-made fluctuations of the water table above the lowest point it had been, will only induce minimal settlement.

The study, furthermore, found that the presence of surface structures alter the degree to which soil will settle compared to greenfield sites. The alteration of the soil settlement by surface structures is influenced by the weight and the stiffness of the structure. The weight of surface structures is resisted by the soil which is in-turn loaded and therefore is at greater stress state compared to the same soil without surface structures. Groundwater extraction-induced soil settlement will, therefore, be less for the soil at a greater stress state. Structures, furthermore, resist imposed ground movements. Stiffer structures resist and alter ground movements to a greater degree compared to more flexible structures that conform to the ground movements. Greenfield sites where lightweight structures, flexible framed structures (Frame (--)) and framed structures with a low relative/Vertical shear stiffness (Frame (-+)) are to be erected can, therefore, be pre-loaded such that the resultant groundwater extraction-induced ground settlements (total and differential) can be reduced.

It is also recommend that flexible framed structures (Frame (--)), framed structures with a low relative/Vertical shear stiffness (Frame (-+)) and framed structures with a high relative/Vertical shear stiffness (Frame (+-)) be braced adequately such that the increase in diagonal strain of the structural bays induced by horizontal ground movements is reduced.

6 REFERENCES

Arapakou, A.E. and Papadopoulos, V.P. 2012. Factors Affecting Differential Settlements of Framed Structures. *Geotechnical and Geological Engineering*, Vol 30, No 6, pp 1323-1333.

Archer, A. 2014. *Using small-strain stiffness to predict the settlement of shallow foundations in sand.* Masters Dissertation. University of Pretoria.

ASTM Standard D2453-00. 2006. *Standard test method for maximum index density and unit weight of soils using a vibratory table*. Tech. Rep. ASTM International.

ASTM Standard D2454-91. 2006. *Standard test method for minimum index density and unit weight of soils and calculation of relative density*. Tech. Rep. ASTM International.

ASTM Standard D2487-11. 2011. *Standard Practice for Classification of Soils for Engineering Purpose (Unified Soil Classification System)*. Tech. Rep. ASTM International.

Baú, D. Ferronato, M. Gambolati, G. and Teatini, P. 2004. Surface flow boundary conditions in modeling land subsidence due to fluid withdrawal. *Ground Water,* Vol 42, No 4, pp 516-25.

Biot, M.A. 1941. General theory of three-dimensional consolidation. *Journal of Applied Physics.* Vol 12, No 2, pp 155-164.

Biot, M.A. 1955. Theory of elasticity and consolidation for a porous anisotropic solid. *Journal of Applied Physics,* Vol 26, No 2, pp 182-185.

Bjerrum, L. 1963. Allowable settlement of structures. *Proc. of the 3rd European Conference on Soil Mechanics and Foundation Engineering, Wiesbaden, Germany*, Vol 2, pp 135-137.

Boone, S.J. 1996. Ground-movement-related building damage. *Journal of Geotechnical Engineering,* Vol 122, No 11, pp 886-896.

Boscardin, M.D. and Cording, E.J. 1989. Building response to excavation-induced settlement. *Journal of Geotechnical Engineering,* Vol 115, No 1, pp 1-21.

Breysse, D. Niandou, H. Elachachi, S. and Houy, L. 2005. A generic approach to soil–structure interaction considering the effects of soil heterogeneity. *Geotechniqu,* Vol 55, No 2, pp 143-150.

British Standards Institution. 2004. *Eurocode 7: Geotechnical design: Part 1, General rules.* , BSI, London.

Budhu, M. and Adiyaman, I.B. 2010. Mechanics of land subsidence due to groundwater pumping. *International Journal for Numerical and Analytical Methods in Geomechanics*, Vol 34, No 14, pp 1459-1478.

Burkert, 2017, 20 October 2017, <https://www.burkert.com/en/type/6011>.

Burland, J.B. Broms, B.B. and de Mello, V.F. 1978. Behaviour of foundations and structures.

Burland, J. and Wroth, C. 1974. Settlement of buildings and associated damage in *SOA Review, Conf. Settlement of structures, Cambridge.* pp. 651-654.

Canon, 2017, 20 October 2017, <https://www.canon.co.za/for_home/product_finder/cameras/digital_slr/eos_100d/>.

Cashman, P.M. and Preene, M. 2013. *Groundwater lowering in construction : a practical guide to dewatering.* 2nd ed. ed., Taylor & Francis, Boca Raton, FL.

Charles, J. and Skinner, H. 2004. Settlement and tilt of low-rise buildings. *Proc. of the Institution of Civil Engineers-Geotechnical Engineering,* Vol 157, No 2, pp 65-75.

Cui, Z. Jia, Y. and Yuan, L. 2016. Distribution law of soil deformation caused by decompression of confined water. *Environmental Earth Sciences,* Vol 75, No 18, pp 1281.

Deck, O. and Harlalka, A. 2010. Numerical study of the soil-structure interaction within mining subsidence areas. *Computers & Geotechnics,* Vol 37, pp 802-816.

Díaz, E. and Tomás, R. 2016. A simple method to predict elastic settlements in foundations resting on two soils of differing deformability. *European Journal of Environmental and Civil Engineering,* Vol 20, No 3, pp 263-281.

Duncan, J.M. 1993. Limitations of conventional analysis of consolidation settlement. *Journal of Geotechnical Engineering,* Vol 119, No 9, pp 1333-1359.

Fahmi, A. Dabbagh, J. and Moezzi, M. 2015. FE Analysis and experimental validation of land subsidence due to ground water level variation. *International Journal of Engineering & Technology,* Vol 4, No 3, pp 451.

Fang, H. 1991. *Foundation engineering handbook.* 2nd ed., Van Nostrand Reinhold, New York :.

Frantziskoni, G. and Breysse, D. 2003. Influence of soil variabilty on differential settlements of structures. *Computers and Geotechnics,* Vol 30, No 3, pp 217-230.

Gambolati, G. and Teatini, P. 2015. Geomechanics of subsurface water withdrawal and injection. *Water Resources Research,* Vol 51, No 6, pp 3922-3955.

Gaudin, C. White, D. Boylan, N. Breen, J. Brown, T. De Catania, S. and Hortin, P. 2009. A wireless high-speed data acquisition system for geotechnical centrifuge model testing. *Measurement Science and Technology,* Vol 20, No 9, pp 095709.

Guan, Y. and Fredlund, D. 1997. Use of the tensile strength of water for the direct measurement of high soil suction. *Canadian Geotechnical Journal,* Vol 34, No 4, pp 604-614.

Grant, R. Christian, J.T. and Vanmarcke, E.H. 1974. Differential settlement of buildings. Extensive settlement and differential settlement data for a wide range of soils and structures are analyzed. *International Journal of Rock Mechanics and Mining Sciences & Geomechanics Abstracts,* Vol 11, No 12, pp 248.

Halim, D. and Wong, K.S. 2011. Prediction of frame structure damage resulting from deep excavation. *Journal of Geotechnical and Geoenvironmental Engineering,* Vol 138, No 12, pp 1530-1536.

HBM, 2017, 20 October 2017, <https://www.hbm.com/en/4561/ly-linear-strain-gauges-with-1-measurement-grid>

Hoffman, K. 1974. *Applying the wheatstone bridge circuit*. HBM.

Houy, L. Breysse, D. and Denis, A. 2005. Influence of soil heterogeneity on load redistribution and settlement of a hyperstatic three-support frame. *Geotechnique,*Vol 55, No 2, pp 163-170.

Jacobsz, S. 2013. Centrifuge modelling of a soil nail retaining wall. *Journal of the South African Institution of Civil Engineering,* Vol 55, No 1, pp 85-93.

Jacobsz, S. Kearsley, E. and Kock, J. 2014. The geotechnical centrifuge facility at the University of Pretoria. University of Pretoria.

Jardine, R.J. Potts, D. Fourie, A. and Burland, J. 1986. Studies of the influence of non-linear stress–strain characteristics in soil–structure interaction. *Geotechnique,* Vol 36, No 3, pp 377-396.

Kassimali, A. 2011. *Structural Analysis.* 4th ed., Standford: Cengage Learning.

Knappett, J. and Craig, R.F. 2012. *Craig's soil mechanics.* 8th ed. Spon Press, Abingdon, Oxon.

Laefer, D.F. Hong, L.T. Erkal, A. Long, J.H. and Cording, E.J. 2011. Manufacturing, assembly, and testing of scaled, historic masonry for one-gravity, pseudo-static, soil-structure experiments. *Construction and Building Materials,* Vol 25, No 12, pp 4362-4373.

Lemmen, H.E. 2015. *The influence of footing stiffness on the behaviour of surface strip foundations on sand.* Masters Dissertation. University of Pretoria.

Lesniewska, D. and Wood, D.M. 2009. Observations of stresses and strains in a granular material. *Journal of Engineering Mechanics,* Vol 135, No 9, pp 1038-1054.

Lin, L. Hanna, A. Sinha, A. and Tirca, L. 2015. Structural Response to Differential Settlement of Its Foundations. *Journal of civil engineering research,* Vol 5, No 3, pp 59-66.

Little, M., 1969, 'Discussion, Session 6' in *Proc. Symp. on Design for movement in buildings" The Concrete Society, London*.

Mair, R.J. Taylor, R.N. and Burland, J.B. 1996. Prediction of ground movements and assessment of risk of building damage due to bored tunnelling. *Proc. Geotechnical Aspects of Underground Construction in Soft Ground, London, 1996.*

Majumder, S. and Sundaram, N.S. 1991. The area of influence of groundwater pumping: determination by geostatistical method in a case study. *Mining Science and Technology,* Vol 13, No 3, pp 383-387.

Meilani, I. Rahardjo, H. Leong, E.C. and Fredlund, D.G. 2002. Mini suction probe for matric suction measurements. *Canadian Geotechnical Journal,* Vol 36, No 6, pp 1427-1432.

Meyerhof, G. 1956. Discussion on paper by AW Skempton and DH MacDonald: Allowable settlement of buildings. *Proc. Inst.Civ.Eng., Part,* Vol 2, No 5, pp 774-775.

Mitchell, J.K. and Soga, K. 2005. *Fundamentals of soil behavior*. Vol 3. New York: John Wiley & Sons.

Mitropoulou, C.C. Kostopanagiotis, C. Kopanos, M. Ioakim, D. and Lagaros, N.D. 2016. Influence of soil–structure interaction on fragility assessment of building structures. *Structures,* Vol 6, No 8, pp 85-98.

Mosley, W.H. Bungey, J.H. and Hulse, R. 2012. *Reinforced concrete design to Eurocode 2.* 7th ed. ed., Palgrave Macmillan, Basingstoke.

Noorzaei, J. Godbole, P. and Viladkar, M. 1993. Non-linear soil-structure interaction of plane frames—A parametric study. *Computers & Structures,* Vol 49, No 3, pp 561-566.

Noorzaei, J. Viladkar, M. and Godbole, P. 1995. Influence of strain hardening on soil-structure interaction of framed structures. *Computers & Structures,* Vol 55, No 5, pp 789-795.

Polshin, D.E. andn Tokar, R.A. 1957. Maximum allowable non-uniform settlement of structures. *Proc. 4th Int. Conf. on Soil Mechanics and Foundation Engineering, London: Butterworth's,* Vol 1, pp 402-405.

Potts, D.M. and Adenbrooke, T.I. 1997. A structure's influence on tunnelling-induced ground movements. *Proc. of the Institution of Civil Engineers: Geotechnical Engineering,* Vol 125, No 2.

Preene, M. and Brassington, R. 2003. Potential groundwater impacts from civil-engineering works. *Water and Environment Journal,* Vol 17, No 1, pp 59-64.

Preene, M. Roberts, T.O.L. Powrie, W and Dyer, M.R. 2000. *Groundwater control - design and Practice.* Construction Industry Research and Information Association, CIRIA Report C515, London.

Ridley, A. and Burland, J. 1993. A new instrument for the measurement of soil moisture suction. *Géotechnique,* Vol 43, No 2, pp 321-324.

Ritter, S. Giardina, G. DeJong, M.J. and Mair, R.J. 2016. Experimental challenges of modelling structures response to tunneling. University of Cambridge.

Ritter, S. Giardina, G. DeJong, M.J. and Mair, R.J. 2017(a). Centrifuge modelling of building response to tunnel excavation. University of Cambridge.

Ritter, S. Giardina, G. DeJong, M.J. and Mair, R.J. 2017(b). Influence of building characteristics on tunnelling-induced ground movements. University of Cambridge.

Roy, D. and Robinson, K.E. 2009. Surface settlements at a soft soil site due to bedrock dewatering. *Engineering Geology,* Vol 107, No 3, pp 109-117.

Schofield, A.N. 1980. Cambridge geotechnical centrifuge operations. *Geotechnique,* Vol 30, No 3, pp 227-268.

Shaqour, F.M. and Hasan, S.E. 2008. Groundwater control for construction purposes: a case study from Kuwait. *Environmental Geology,* Vol 53, No 8, pp 1603-1612.

Skempton, A.W. and MacDonald, D.H. 1956. The allowable settlements of buildings. *Proc. of the Institution of Civil Engineer,.* Vol 5, No 6, pp 727-768.

Smit, G. 2010. *The behaviour of modern flexible framed structures undergoing differential settlement*. PhD thesis. University of Southampton.

Smit, G. and Clayton, C.R.I. 2011. The behaviour of modern flexible framed structures undergoing differential settlement. *Proc. of Young Geotechnical Engineers Conference, 2011.*

Son, M. 2003. *The response of buildings to excavation-induced ground movements*. PhD thesis. University of Illinois.

Son, M. and Cording, E.J. 2005. Estimation of building damage due to excavation-induced ground movements. *Journal of Geotechnical and Geoenvironmental Engineering,* Vol 131, No 2, pp 162-177.

Son, M. and Cording, E.J. 2007. Evaluation of Building Stiffness for Building Response Analysis to Excavation-Induced Ground Movements. *Journal of Geotechnical and Geoenvironmental Engineering,* Vol 133, No 8, pp 995-1002.

Son, M. and Cording, E.J. 2010. Responses of buildings with different structural types to excavation-induced ground settlements. *Journal of Geotechnical and Geoenvironmental Engineering,* Vol 137, No 4, pp 323-333.

Take, W. and Bolton, M. 2003. Tensiometer saturation and the reliable measurement of soil suction. *Géotechnique,* Vol 53, No 2, pp 159-172.

Tarantino, A. and Mongiovi, L. 2003. Calibration of tensiometer for direct measurement of matric suction. *Géotechnique,* Vol 53, No 1, pp 137-141.

Tarantino, A. and Mongiovì, L. 2001. Experimental procedures and cavitation mechanisms in tensiometer measurements. *Unsaturated Soil Concepts and Their Application in Geotechnical Practic,*. Springer, Dordrecht, pp189-210 .

Taylor, R. 1995. Centrifuges in modelling: principles and scale effects. *Geotechnical centrifuge technology,* pp 19-33.

Terzaghi, K. 1935. *The actual factor of safety in foundations.*

Terzaghi, K. 1943. *Theoretical soil mechanics,* , J. Wiley and Sons, Inc. Chapman and Hall, Limited, New York, London,.

Timshenko, S. 1957. Strength of Materials -Part 1. Dvan Nostrand Co, Inc. London.

Toll, D.G. Lourenço, S.D. and Mendes, J. 2013. Advances in suction measurements using high suction tensiometers. *Engineering Geology,* Vol 165, pp 29-37.

University of Pretoria. 2014, 20 October 2017, <http://www.up.ac.za/civil-engineering/article/1914311/getechnical-centrifug-laboratory>

Vasco, D. Karasaki, K. and Kishida, K. 2001. A coupled inversion of pressure and surface displacement. *Water Resources Research,* Vol 37, No 12, pp 3071-3089.

Wahls, H.E. 1981. Tolerable settlement of buildings. *Journal of Geotechnical Engineering Division ASCE,* Vol 107, No 11, pp 1489-1504.

Wahls, H.E., 1994, 'Tolerable deformations' in *Vertical and Horizontal Deformations of Foundations and Embankments:*pp. 1611-1628.

Wang, S. Lee, C. and Hsu, K. 2015. A technique for quantifying groundwater pumping and land subsidence using a nonlinear stochastic poroelastic model. *Environmental Earth Sciences,* Vol 73, No 12, pp 8111-8124.

Weigel, T.A. Ott, K.J. and Hagerty, D.J. 1989. Load redistribution in frame with settling footings. *Journal of Computing in Civil Engineering*, Vol 3, No 1, pp 75-92.

White, D. Take, W. and Bolton, M. 2003. Soil deformation measurement using particle image velocimetry (PIV) and photogrammetry. *Geotechnique*, Vol 53, No 7, pp 619-631.

Yang, Y. Song, X.F. Zheng, F.D. Liu, L.C. and Qiao, X.J. 2015. Simulation of fully coupled finite element analysis of nonlinear hydraulic properties in land subsidence due to groundwater pumping. *Environmental Earth Sciences*, Vol 73, No 8, pp 4191-4199.

Zhang, L. and Ng, A. 2004. Probabilistic limiting tolerable displacements for serviceability limit state design of foundations. *Geotechnique*, Vol 55, No 2, pp 151-161.